ISTANBUL TECHNICAL UNIVERSITY ★ GRADUATE SCHOOL

DEVELOPMENT OF SELECTIVE IRON-BASED FISCHER-TROPSCH CATALYSTS TO LIGHT OLEFINS

Ph.D. THESIS

Yasemin FATİH AGHDAEI

Department of Chemical Engineering

Chemical Engineering Programme

AUGUST 2023

ISTANBUL TECHNICAL UNIVERSITY ★ GRADUATE SCHOOL

DEVELOPMENT OF SELECTIVE IRON-BASED FISCHER-TROPSCH CATALYSTS TO LIGHT OLEFINS

Ph.D. THESIS

Yasemin FATİH AGHDAEI
(506162021)

Department of Chemical Engineering

Chemical Engineering Programme

Thesis Advisor: Prof. Dr. Hüsnü ATAKÜL
Thesis Co-Advisor: Assoc. Prof. Dr. Alper SARIOĞLAN

AUGUST 2023

İSTANBUL TEKNİK ÜNİVERSİTESİ ★ LİSANSÜSTÜ EĞİTİM ENSTİTÜSÜ

HAFİF OLEFİNLER İÇİN SEÇİCİ DEMİR BAZLI FISCHER-TROPSCH KATALİZÖRLERİNİN GELİŞTİRİLMESİ

DOKTORA TEZİ

Yasemin FATİH AGHDAEI
(506162021)

Kimya Mühendisliği Anabilim Dalı

Kimya Mühendisliği Programı

Tez Danışmanı: Prof. Dr. Hüsnü ATAKÜL
Eş Danışman: Doç. Dr. Alper SARIOĞLAN

AĞUSTOS 2023

Yasemin FATİH AGHDAEI, a Ph.D. student of İTU Graduate School student ID 506162021, successfully defended the thesis/dissertation entitled "DEVELOPMENT OF SELECTIVE IRON-BASED FISCHER-TROPSCH CATALYSTS TO LIGHT OLEFINS", which she prepared after fulfilling the requirements specified in the associated legislations, before the jury whose signatures are below.

Thesis Advisor :	**Prof. Dr. Hüsnü ATAKÜL** Istanbul Technical University	.....
Co-advisor :	**Assoc. Prof. Dr. Alper SARIOĞLAN** Istanbul Technical University	.....
Jury Members :	**Prof. Dr. Ahmet SİRKECİOĞLU** Istanbul Technical University	.....
	Assis. Prof. Dr. Gamze GÜMÜŞLÜ GÜR Istanbul Technical University	.....
	Prof. Dr. İsmail BOZ Istanbul University -Cerrahpaşa	.....
	Prof. Dr. Ahmet KERIM AVCI Boğaziçi University	.....
	Prof. Dr. Şahika Sena BAYAZIT Istanbul University -Cerrahpaşa	.....

Date of Submission : 20 June 2023
Date of Defense : 29 August 2023

تقدیم به مادرم که عشقش همیشه با من است

To my mother whose love is always with me,

FOREWORD

I would like to express my deepest gratitude to my advisor Prof. Dr. Hüsnü ATAKÜL whom I learned a lot from him during my M.Sc. and Ph.D. I do appreciate his contribution to my Ph.D. experiments, thesis, and publication.

I am deeply grateful to my co-advisor Assoc. Prof. Dr. Alper SARIOĞLAN. This journey would not have been completed without his scientific contribution and moral supports.

Special thanks to Prof. Dr. Hasancan OKUTAN who provided the TÜBITAK project in which I could conduct my Ph.D. research and drove my research journey during my M.Sc. thesis.

My gratitude to Asst. Prof. Dr. Gamze GÜMÜŞLÜ GÜR who provided me the chance to work in "Development of Catalyst and Reactor Technology to Produce Lower Olefins from Clean Syngas" project.

Many thanks to my colleagues Utku BURGUN and Hadi RAHNAMAEI ZONOUZ who shared their experience with me at the beginning of my Ph.D. research and during PhD period.

I would like to express my deepest thanks and love to my patient husband who encouraged me continuously to finish the way I have started while the grief of my mother.

Lastly, I would like to mention that whatever I achieve and whoever I am, I owe to my lovely parents.

With the hope of peace and freedom everywhere around the world and in Iran.

June 2023

Yasemin FATİH AGHDAEI
(Chemical Engineer)

TABLE OF CONTENTS

Page

ABBREVIATIONS

AC : Activated Carbon
AH : Ammonium Hydroxide
AH-I : Ammonium Hydroxide-Impregnation
BET : Brunauer-Emmett-Teller
BJH :Barret–Joyner–Hallender
$C_2^=$-$C_4^=$:Light Olefins
C_2^o-C_4^o :Light Paraffins
FID : Flame Ionization Detector
FTIR : Fourier-Transform Infrared
FT-O : Fischer Tropsch to Olefins
FTS : Fischer Tropsch Synthesis
GC : Gas Chromatography
GHSV : Gas Hour Space Velocity
ICP-OES : Inductively Coupled Plasma-Optical Emission Spectrometry
N-doped AC : Nitrogen doped Activated Carbon
SC : Sodium Carbonate
SC-I : Sodium Carbonate-Impregnation
SEM : Scanning Electron Microscopy
TCD : Thermal Conductivity Detector
TGA : Thermogravimetric Analysis
TPD : Temperature Programmed Desorption
TPR : Temperature Programmed Reduction
WGS : Water Gas Shift reaction
XRD : X-Ray Powder Diffraction

SYMBOLS

E_1	: Adsorption heat for first layer (J)
E_c	: Condensation heat (J)
S_n	: Hydrocarbon Selectivity (Carbon base)
S_{BET}	: Specific Surface Area (m^2)
T	: Temperature
X_{CO}	: CO Conversion
θ	: Degree

LIST OF TABLES

Page

LIST OF FIGURES

Page

DEVELOPMENT OF SELECTIVE IRON-BASED FISCHER-TROPSCH CATALYSTS TO LIGHT OLEFINS

SUMMARY

Light olefins (alkenes) are among the key chemicals that are globally most produced from crude oil in amounts exceeding 200 million tons per year. They are hydrocarbons with at least one carbon - carbon double bond (C_2-C_4) namely, ethylene(C_2H_4), propylene(C_3H_6), and butylene(C_4H_8). Lower olefins (light olefins) are intermediates for the synthesis of a wide range of products such as solvents, polymers, drugs, detergents, and cosmetics. There are three types of olefins: alpha (also called ethylene molecules), beta, and gamma. Carbon-carbon double bond is located at the beginning, in the middle, and at the end of the olefin chain in alpha, beta, and gamma types, respectively. Currently, commercial light olefin production is mainly based on steam cracking of a broad range of hydrocarbon feedstock including naphtha, gas oil, condensates, ethane and propane. However, the production of lower olefins by steam cracking is one of the most energy-consuming processes of the chemical and petrochemical industry. The oil reserves are expected to be depleted at faster pace as the oil consumption surpasses the conventional oil production. As the conventional easy-reached oil reserves deplete, attempts are being made to use unconventional oil reserves for oil production. The extraction and upgrading of oil from unconventional oil reserves, however, may be expensive and involve release of higher amounts of CO_2 release in comparison to conventional reserves. CO_2, with its green-house effect, is widely claimed to be responsible for climate change and there is rapidly growing global awareness in this respect which leads to more and more stringent regulations about CO_2 emissions. Therefore, many countries are searching for alternatives to reduce their reliance on imported crude oil and refined products and to comply with CO_2 regulations. The new alternative fuels for olefin production are coal, natural gas and biomass. Light olefins may be produced from the synthesis gas (CO/ H_2) obtained from gasification of these fuels by direct Fischer-Tropsch-to-Olefins (FTO) process. FTO is a catalytic process and the most crucial and critical issue of this process is using proper and effective catalyst(s). Although there are plenty of research available in literature focusing on FTO process, there still exists lack of a proper catalytic process to be used commercially in FTO.

In this work, the aim was to make an effort to produce light olefins in direct unconventional way via FTS by synthesizing iron-based catalysts with different promoters and supports that can show high FTO performance, means high CO conversion and stability with time on stream, high selectivity to light olefins, and low selectivity to methane and CO_2. In other words, the aim was to narrow the wide hydrocarbon range produced by FTS to C_2-C_4 olefins.

To reach the goal of study, the catalysts have been synthesized in different routes and with promoters. Their performance has been evaluated via catalytic tests and catalytic activity-structure relation have been investigated. In this term, iron-based catalysts

have been prepared both by precipitation and impregnation techniques. Precipitation route has been tuned as well by changing the alkalinity of the precipitation environment. To synthesize the first set of bulk catalysts, nitrate salt solutions of iron and zinc as prepared in a stoichiometry of Fe:Zn=2 have been co-precipitated with NH_4OH (AH). Sodium has been incorporated to Fe.Zn precipitate by different routes; use of sodium nitrate during co-precipitation reaction (AH route) or its subsequent impregnation on co-precipitated Fe.Zn catalyst (AH-I route). Alternatively, Na_2CO_3 (SC) was employed instead of NH_4OH (AH) for the initial precipitation to investigate the role of the precipitant and its effect on catalyst surface basicity in terms of Fischer-Tropsch activity. The basicity of the precipitate Fe.Zn (SC) has been altered by changing the number of washing cycles as well and impregnated with a sodium precursor for further basicity. The last route has been called as SC-I. In addition to Na, Cu and K promoters have been impregnated to Fe.Zn precipitate as well.

For the impregnation route, activated carbon (AC) and nitrogen-doped AC have been used as support material. Fe:Zn of 2 with alkali promoters has been chosen since it resulted in high olefin selectivity for unsupported catalysts. Activated carbon (AC) and its nitrogen doped form have been used as support. Activated carbon has been treated with N-containing chemicals namely, HNO_3, NH_3 and urea in order to create nitrogenous surface functional groups over AC (Chemical modification of surface). The so-formed supports were denoted as AC-N_1, AC-N_2, and AC-N_3, respectively upon treatment with HNO_3, NH_3, and urea. Co-impregnation has been applied as by first dissolving the metal salts in stoichiometric amounts in a minimum amount of water and then by wetting AC support with the metal salt solutions.

All catalysts have been calcined, reduced and tested in a high pressure fixed-bed reactor to investigate their catalyst activity and performance in Fischer-Tropsch synthesis to light olefins (FTO). Test results were interpreted together with the characterizations such as BET surface areas via N_2 adsorption, crystal phase identification by x-ray diffraction (XRD), elemental analysis by inductively coupled plasma (ICP-OES), thermal stability of supports using (TGA) analysis, morphological investigation by scanning electron microscopy (SEM), reducibility characteristics of active phases using H_2-TPR , the basicity of Na promoted bulk catalysts by CO_2-TPD, and SEM-EDS mapping to observe metal distribution in Na promoted catalysts and a carbon supported catalyst.

As total alkalinity of precipitation affects hydrolysis and influences the composition of the intermediate hydrolytic complexes, the final features of metal hydroxide precipitates might be induced with the precipitation conditions. This was proved by the observed change on the textural properties of zinc ferrites such as total surface area, crystal size and morphology under different alkaline precipitation environment. Improved conversion due to the facilitated CO dissociation over basic sites and concomitant deactivation possibly through fouling might be interpreted as both the number of basic sites and strength were determinant on the final catalytic behavior. Na provides a surface with high electron density that leads to intensification of CO dissociation and adsorption. However, although this is a favorable effect, it has limitation in terms of alkali content of the catalyst and its dispersion. As mentioned before, there is an optimum basicity which ensures a balance between CO conversion to CH_x and the rate of hydrocarbon chain growth and its termination. If this balance alters, long chain hydrocarbon may form and cover the catalyst surface which can block the active sites. Depleted surface vacancies might suppress the rate of CO dissociation with time on stream and result in high deactivation. In this case, the

hydrocarbon distribution does not change significantly but deactivation dominates. When surface is covered with high C content, surface H deficiency may result in a decrease in hydrogenation activity that might end up with poor paraffin and methane selectivity. Alkali metals may also improve re-adsorption of olefinic intermediates which may further polymerize to C_{5+} species. Therefore, both C_2-C_4 olefin light olefin and C_{5+} selectivity increase in the presence of alkali promoter, sodium or potassium. However, potassium as with more alkalinity strength led to more coke formation over the catalytic surface, e.g. a total carbon content of 17% on the spent ~3%K-2Fe.Zn(SC) catalyst and thereby, a fast decrease in CO conversion from 88% to 55% has been observed. Copper (Cu) is a widely accepted promoter for facilitated reduction of iron oxides and it improves the catalyst stability when the reduction occurs at lower temperatures. Temperature programmed reduction (TPR) profile of the catalysts have shown the improved dispersion upon copper addition.

AC and N-doped AC supported Fe.Zn catalysts have shown high and satisfactory FTO performance. High surface area of AC whether in N-doped form or not has provided improved catalytic stability. Supported catalysts in the same Fe:Zn ratio seemed to be less deactivated in comparison to the bulk catalysts. For all supported catalysts in Fe: Zn: P=2:1:0.2 molar ratios where P=Na and K, high olefin selectivity of ~ 45-50% and high CO conversion of ~89-93%(stability) have been achieved. Using AC as the support of the catalyst, dispersion and hence the number of active sites have been increased and accessibility to each single active site has been improved as compared to the case in bulk catalysts.

In conclusion, the hydrocarbon product distribution in the presence of alkali has been altered towards high C_2-C_4 olefin and C_{5+} selectivity values. The strength and homogeneity of surface basicity seemed effective in case of bulk catalysts. Highly active and selective bulk catalysts can be prepared by changing the precipitation conditions. Copper was seen to stabilize the catalytic activity by improving the dispersion and reducing the reduction temperatures of metal oxides. Activated carbon appeared as a suitable support for well dispersion of active sites. Its surface nature has been modified with nitrogen and slight changes in catalytic performance has been noticed. Improved thermal stability upon nitrogen doping was the only point to be remarked. All in all, Fe to Zn ratio of 2 as in zinc ferrite spinel crystals were active catalysts for Fischer-Tropsch reaction and reaction selectivity have been directed to light olefins when appropriately doped with alkali metals.

HAFİF OLEFİNLER İÇİN SEÇİCİ DEMİR BAZLI FISCHER-TROPSCH KATALİZÖRLERİNİN GELİŞTİRİLMESİ

ÖZET

Hafif olefinler (alkenler), yılda 200 milyon tonu aşan miktarlarda ham petrolden dünya çapında en çok üretilen temel kimyasallar arasındadır. Bu ürünler, yani etilen (C_2H_4), propilen (C_3H_6) ve bütilen (C_4H_8), en az bir karbon - karbon çift bağına (C_2-C_4) sahip hidrokarbonlardır. Hafif olefinler; çözücüler, polimerler, ilaçlar, deterjanlar ve kozmetikler gibi çok çeşitli ürünlerin sentezi için ara ürünlerdir. Üç tür olefin vardır: alfa (etilen molekülleri olarak da adlandırılır), beta ve gama. Karbon-karbon çift bağı, olefin zincirinin alfa, beta ve gama tiplerinde sırasıyla başında, ortasında ve sonunda bulunur. Mevcut durumda, ticari hafif olefin üretimi temel olarak nafta, gaz yağı, kondensatlar, etan ve propan dahil olmak üzere çok çeşitli hidrokarbon hammaddelerinin buharla parçalanmasına dayanmaktadır. Bununla birlikte, buharla parçalama yoluyla düşük olefinlerin üretimi, kimya ve petrokimya endüstrisinin en çok enerji tüketen süreçlerinden biridir. Petrol tüketiminin konvansiyonel petrol üretimini aşması nedeniyle petrol rezervlerinin daha hızlı tükenmesi beklenmektedir. Geleneksel kolay ulaşılabilen petrol rezervleri tükenirken, petrol üretimi için geleneksel olmayan petrol rezervlerinin kullanılması için girişimlerde bulunulmaktadır. Bununla birlikte, konvansiyonel olmayan petrol rezervlerinden petrolün çıkarılması ve yükseltilmesi pahalı olabilir ve konvansiyonel rezervlere kıyasla daha yüksek miktarlarda CO_2 salınımını içerebilir. Sera etkisine sahip CO_2'nin iklim değişikliğinden sorumlu olduğu yaygın bir şekilde iddia edilmektedir ve bu konuda hızla artan küresel farkındalık CO_2 emisyonları konusunda giderek daha sıkı düzenlemelere yol açmaktadır. Bu nedenle, birçok ülke ithal ham petrol ve rafine ürünlere bağımlılığını azaltmak ve CO_2 düzenlemelerine uyum sağlamak için alternatifler aramaktadır. Olefin üretimi için yeni alternatif yakıtlar kömür, doğal gaz ve biyokütledir. Hafif olefinler, bu yakıtların gazlaştırılmasıyla elde edilen sentez gazının (CO / H_2) doğrudan Fischer-Tropsch-olefin (FTO) prosesi ile üretilebilir.FTO katalitik bir süreçtir ve bu sürecin en önemli ve kritik konusu uygun ve etkili katalizör(ler) kullanmaktır. Literatürde FTO sürecine odaklanan pek çok araştırma olmasına rağmen, FTO'da ticari olarak kullanılacak uygun bir katalitik proses hala mevcut değildir.

Bu çalışmada amaç, yüksek FTO performansı gösterebilen, yüksek CO dönüşümüne, stabilitiye, hafif olefinlere yüksek seçicilik ve metan ile CO_2'ye düşük seçiciliğe. sahip, demir bazlı katalizörleri farklı promotörler ve destek malzemeleriyle sentezleyerek FTS aracılığıyla doğrudan, geleneksel olmayan, bir şekilde hafif olefinler üretmeye çalışmaktır. Başka bir deyişle, amaç FTS tarafından üretilen geniş hidrokarbon aralığını C_2-C_4 olefinlere daraltmaktır.

Çalışmanın amacına ulaşmak için katalizörler farklı yollarda ve promotörlerle sentezlenmiştir. Performansları katalitik testler ile değerlendirilmiş ve katalitik aktivite-yapı ilişkisi incelenmiştir. Bu açıdan demir bazlı katalizörler hem çöktürme hem de emdirme teknikleri ile hazırlanmıştır. Çöktürme ortamının alkalinitesi

değiştirilerek çöktürme rotası da ayarlanmıştır. Destek malzemesiz ilkkatalizör setini sentezlemek için, demir ve çinkonun Fe:Zn=2 stokiyometrisinde hazırlanan nitrat tuzu çözeltileri, NH_4OH (AH) ile birlikte çöktürülmüştür. Sodyum, Fe.Zn çökeltisine farklı yollarla katılmıştır; birlikte çökeltme reaksiyonu (AH yolu) sırasında sodyum nitratın kullanımı veya bunun ardından birlikte çöktürülmüş Fe.Zn katalizörü üzerine emdirme edilmesi (AH-I yolu). Alternatif olarak, çökelticinin rolünü ve bunun Fischer-Tropsch aktivitesi açısından katalizör yüzey bazikliği üzerindeki etkisini araştırmak için ilk çökeltme için NH_4OH (AH) yerine Na_2CO_3 (SC) kullanılmıştır. Fe.Zn (SC) çökeltisinin bazikliği, yıkama döngülerinin sayısı da değiştirilerek değiştirilmiş ve daha fazla baziklik için bir sodyum öncüsü emdirilmiştir. Son rota SC-I olarak adlandırılmıştır. Fe.Zn çökeltisine Na'nın yanı sıra, Cu ve K promotörleri de emdirilmiştir.

Emdirme yolu için destek malzemesi olarak aktif karbon (AC) ve nitrojen katkılı AC kullanılmıştır. Desteksiz katalizörler için yüksek olefin seçiciliği sağladığı için alkali promotörlü Fe:Zn 2 seçilmiştir. Aktif karbon (AC) ve nitrojen katkılı formu destek olarak kullanılmıştır. Aktif karbon, AC üzerinde nitrojenli yüzey fonksiyonel grupları oluşturmak için N-içeren kimyasallar, yani HNO_3, NH_3 ve üre ile muamele edilmiştir (Yüzeyin kimyasal modifikasyonu). Bu şekilde oluşturulan destekler, sırasıyla HNO3, NH_3 ve üre ile işlendikten sonra AC-N_1, AC-N_2 ve AC-N_3 olarak gösterilmiştir. Birlikte-emdirme, stokiyometrik miktarlardaki metal tuzlarının minimum miktarda suda önce çözülmesi ve ardından AC desteğinin metal tuzu çözeltileri ile ıslatılması şeklinde uygulanmıştır.

Tüm katalizörler, katalizör aktivitelerini ve hafif olefinlere (FTO) Fischer-Tropsch sentezindeki performanslarını araştırmak için kalsine edilmiş, indirgenmiş ve yüksek basınçlı sabit yataklı bir reaktörde test edilmiştir. Test sonuçları, N_2 adsorpsiyonu yoluyla BET yüzey alanları, x-ışını kırınımı (XRD) ile kristal faz tanımlaması, endüktif olarak eşleşmiş plazma (ICP-OES) ile element analizi, (TGA) analizi kullanılarak desteklerin termal stabilitesi, , taramalı elektron mikroskobu (SEM) ile morfolojik araştırma, H2-TPR kullanılarak aktif fazların indirgenebilirlik özellikleri, CO_2-TPD ile Na promotörlü desteksiz katalizörlerin bazikliği ve Na promotörlü ve karbon destekli katalizörlerde metal dağılımını gözlemlemek için SEM-EDS haritalamasıkarakterizasyonları ile birlikte yorumlanmıştır..

Çökeltmenin toplam alkaliliği hidrolizi ve ara hidrolitik komplekslerin bileşimini etkilediğinden, metal hidroksit çökeltilerinin son özellikleri çökeltme koşullarıyla etkilenebilmektedir. Bu durum, farklı alkali çökeltme ortamları altında çinko ferritlerin toplam yüzey alanı, kristal boyutu ve morfoloji gibi yapısal özelliklerinde gözlemlenen değişimle kanıtlanmıştır. Bazik bölgeler üzerinde kolaylaştırılmış CO ayrışması ve muhtemelen birikme yoluyla eşzamanlı deaktivasyon nedeniyle iyileştirilmiş dönüşüm, hem bazik bölgelerin sayısı hem de kuvvetinin nihai katalitik davranış üzerinde belirleyici olduğu şeklinde yorumlanabilir. Na, CO ayrışmasının ve adsorpsiyonunun yoğunlaşmasına yol açan yüksek elektron yoğunluğuna sahip bir yüzey sağlar. Ancak bu olumlu bir etki olmakla birlikte katalizörün alkali içeriği ve dispersiyonu açısından sınırlamaları vardır. Daha önce bahsedildiği gibi, CO'nun CHx'e dönüşümü ile hidrokarbon zincirinin büyüme hızı ve sonlanması arasında bir denge sağlayan optimum bir baziklik vardır. Bu denge değişirse, uzun zincirli hidrokarbon oluşabilir ve katalizör yüzeyini kaplayarak aktif bölgeleri bloke edebilir. Tükenmiş yüzey boşlukları, CO ayrışma hızını zamanla bastırabilir ve yüksek düzeyde deaktivasyonla sonuçlanabilir. Bu durumda, hidrokarbon dağılımı önemli ölçüde değişmez, ancak deaktivasyon baskındır. Yüzey yüksek C içeriği ile kaplandığında,

yüzey H eksikliği, zayıf parafin ve metan seçiciliği ile sonuçlanabilecek hidrojenasyon aktivitesinde bir azalmaya neden olabilir. Alkali metaller, ayrıca C_{5+} türlerine polimerize olabilen olefinik ara ürünlerin yeniden adsorpsiyonunu da arttırabilir. Bu nedenle, hem C_2-C_4 olefin hafif olefin hem de C_{5+} seçiciliği, alkali promotör, sodyum veya potasyum, varlığında artar. Bununla birlikte, daha fazla alkalilnite gücüne sahip olan potasyum, katalitik yüzey üzerinde daha fazla kok oluşumuna yol açmıştır; örneğin. harcanan ~3%K-2Fe.Zn(SC) katalizöründe toplam karbon içeriğinin %17'ye ulaşmış ve böylece CO dönüşümünde %88'den %55'e hızlı bir şekilde düşüş gözlenmiştir. Bakır (Cu), demir oksitlerin kolaylaştırılmış indirgenmesi için yaygın olarak kabul edilen bir promotördür ve indirgeme daha düşük sıcaklıklarda gerçekleştiğinde katalizör stabilitesini arttırır. Katalizörlerin sıcaklık programlı indirgeme (TPR) profili, bakır ilavesiyle iyileştirilmiş dağılım göstermiştir.

AC ve N-katkılı AC destekli Fe.Zn katalizörleri, yüksek ve tatmin edici FTO performansı göstermiştir. AC'nin yüksek yüzey alanı, N-katkılı formda olsun ya da olmasın, gelişmiş katalitik stabilite sağlamıştır. Aynı Fe:Zn oranında desteklenen katalizörler, desteksiz katalizörlere kıyasla daha az deaktive olduğu görülmüştür. Destekli tüm katalizörler için Fe: Zn: P=2:1:0.2, P=Na ve K, molar oranlarında, ~ %45-50 yüksek olefin seçiciliği ve %~89-93 yüksek CO dönüşümü ve stabilite elde edilmiştir. Katalizör desteği olarak AC kullanıldığında, yığın katalizörlerdeki duruma kıyasla dağılım ve dolayısıyla aktif bölgelerin sayısı artmış ve her bir aktif bölgeye erişilebilirlik iyileştirilmiştir.

Sonuç olarak, alkali varlığında hidrokarbon ürün dağılımı yüksek C_2-C_4 olefin ve C_{5+} seçicilik değerlerine doğru değişmiştir. Yüzey bazikliğinin gücü ve homojenliği, yığın katalizörler durumunda etkili görünüyordu. Çökeltme koşulları değiştirilerek oldukça aktif ve seçici toplu katalizörler hazırlanabilir. Bakırın, dağılımı iyileştirerek ve metal oksitlerin indirgeme sıcaklıklarını düşürerek katalitik aktiviteyi stabilize ettiği görülmüştür. Aktif karbon, aktif bölgelerin iyi dağılması için uygun bir destek olarak ortaya çıkmıştır. Yüzey yapısı azot ile modifiye edilmiş ve katalitik performansta hafif değişiklikler fark edilmiştir. Azot katkısı ile termal kararlılığın artması, dikkat edilmesi gereken tek noktadır. Sonuç olarak, çinko ferrit spinel kristallerinde olduğu gibi Fe: Zn = 2 oranına sahip katalizörler Fischer-Tropsch reaksiyonu için aktiftirve alkali metallerle uygun şekilde katkılandığında reaksiyon seçiciliği hafif olefinlere yönlendirilmiştir.

1. INTRODUCTION

Hydrocarbons are extracted from the nature in different forms such as coal, crude oil, biomass, and natural gas. These raw hydrocarbon chains should be broken down into simpler intermediate compounds that could be recombined to produce value added products. Light olefins (alkenes) are among the intermediate chemicals that are globally most produced from crude oil in amounts exceeding 200 million tons per year. They are hydrocarbons with at least one carbon - carbon double bond (C_2-C_4) namely, ethylene(C_2H_4), propylene(C_3H_6), and butylene(C_4H_8). Light olefins (lower olefins) are used for the synthesis of a wide range of products including solvents, polymers, lubricants, fibers, drugs, detergents, and cosmetics. There are three types of olefins: alpha (also called ethylene molecules), beta, and gamma based on the position of double bond. Currently, the commercial light olefin production is mainly based on steam cracking of a broad range of hydrocarbon feedstock including naphtha, gas oil, condensates, ethane and propane. However, the production of light olefins by steam cracking is one of the highest energy-intensive processes of the chemical and petrochemical industry. The oil reserves are expected to be depleted at faster pace as its consumption surpasses its production. As the conventional and accessible oil reserves deplete, attempts will be given to the use of unconventional oil reserves in depth. The extraction and upgrading of oil from unconventional oil reserves, however, may be expensive and leads much more CO_2 emissions in comparison to the case in conventional reserves. CO_2 as a greenhouse gas is widely claimed to be responsible for the climate change and global warming. There is a rapidly growing global awareness in this respect which leads to more and more stringent regulations on CO_2 emissions. Therefore, many countries are vigorously searching for green alternatives to reduce their reliance on imported crude oil and refined products and to comply with CO_2 regulations. In this respect, one way is methanol to olefin process on zeolite catalysts which is at a certain maturity. However, catalyst deactivation is the major concern in spite of high yields of ethylene and propylene. The second alternative route is syngas to olefins in a direct or indirect way. The first step is the production of syngas via reforming or gasification of alternative feedstock such as biomass, biooil or biogas

together with the conventional ones, namely coal and natural gas. Fischer-Tropsh Synthesis (FTS) is required for both of the direct or indirect routes. In indirect way of olefin production, first synthetic fuels are produced then conventional steam cracking is applied on synfuel. In the other side, light olefins can directly be produced by tuning the FTS selectivity and the reaction is called as Fischer-Tropsch-to-Olefins (FTO). If an active and selective catalyst can be developed, FTO seems more economical route than the others. Therefore, the most crucial and critical issue of this process is the catalyst. Numerous efforts have been devoted to increasing the $C_2^= - C_4^=$ selectivity of the catalysts by investigating the catalytic active sites, alternative catalyst supports, and promoters. Up to now, iron carbides, especially χ-Fe_5C_2, are widely accepted to be the active species in Fischer Tropsch to Olefin synthesis (FTO).

Basically in FTO process, first, the CO and H_2 should be activated on the catalytic surface to produce CH_x monomers. Then surface polymerization reactions occur for chain growth through propagation. Then surface species terminate to olefins, paraffins or oxygenated compounds. There are different CO activation mechanisms such as carbide and CO insertion. In the carbide mechanism, the reaction starts with the formation of CH_x intermediates. The CH_x intermediate is formed by dissociation of the C–O bond of the surface CO compound. In the CO insertion mechanism; chain growth occurs in two separate steps. After the initial dissociation of a CO molecule, another CO is added to the generated CH_x intermediate. Then the C-O bond of the added CO is broken and the first C_2H_y intermediate is formed. Chain growth continues with successive steps of addition of CO to the surface hydrocarbon fragments followed by cleavage of the C-O bond. Carbon formation, in other words coking, is related with the relative rates of CO activation and chain growth rates. So this is a challenge for applicability of FTO catalyst that limits carbon deposition while preserving activity and selectivity under reaction conditions.

The objective of this thesis is to develop an active Fischer-Tropsch Synthesis (FTS) catalyst which is selective to light olefins. The scope is to elucidate the activity-structure relationship for bulk and carbon supported iron-zinc catalysts for FTO. Within this framework, the effect of precipitant and precipitation conditions has been investigated for zinc ferrite catalysts in bulk. Bulk zinc ferrites have been prepared by co-precipitation method by using NH_4OH (AH) as precipitant. Then sodium cation has been incorporated into the Fe.Zn precipitate by different routes; use of sodium nitrate

during co-precipitation (AH route) or its subsequent impregnation on co-precipitated Fe.Zn catalyst (AH-I route). Alternatively, Na_2CO_3 (SC) was employed instead of NH_4OH (SC route). Finally, the ultimate surface basicity of the catalyst, Fe.Zn (SC), has been changed by applying different numbers of washing cycles after precipitation. Precipitates washed with different amount of water were subsequently impregnated by sodium after calcination (SC-I route). In order to investigate the effect of promoters, 2Fe.Zn precipitate has been impregnated with potassium and copper nitrate together or individually as well.

In the second section of the thesis, commercial activated carbon (AC) has been used to support the same type of zinc ferrite catalysts in order to improve their catalytic stability. Promoter choice and amount have been decided in the light of the previous results on bulk catalysts. The efforts have been devoted to suppress coke formation while keeping high olefin selectivity and CO conversion. Since AC support provides high surface areas and better metal dispersions, the presence of Na and K promotors have been expected to give high CO dissociation as the initiation of the reaction with less coking. Due to the importance of carbon support features, AC has been doped with nitrogen precursors such as nitric acid (HNO_3), ammonia (NH_3) and urea. All catalysts have been characterized extensively and tested in a high pressure fixed bed reactor for their Fischer-Tropsch to olefin (FTO) performances.

2. LIGHT OLEFINS

Olefins are aliphatic hydrocarbons with at least one C=C double bond with C_nH_{2n} general chemical formula. As they are unsaturated hydrocarbons, they are highly reactive to synthesis a variety of chemicals. Light olefins are namely, ethylene (C_2H_4), propylene (C_3H_6), and butylene(C_4H_8). Olefin production is reported more than 400 million tons per year via steam cracking (SC) of a wide range of hydrocarbon feedstock, fluid catalytic cracking(FCC) and other routes. The cracking products of large molecules include kerosene, gasoline, and a wide range of hydrocarbons. Olefins are also produced conventionally by the steam cracking (SC) of hydrocarbons that mainly originated from fossil resources (such as ethane, naphtha, etc.) [1]. In Europe and Asia, ethylene is mainly made from cracking of gasoil, naphtha, and condensates. However, in Canada, US, and Middle East, ethylene is made from cracking of ethane and propane. Though naphtha cracking is the most route worldwide, gas cracking has been common in 2000 decade.

For breaking of the C–C bonds in the cracking process, heat is required that makes steam cracking one of the most energy consuming processes. It is still the most common and commercial method for olefin production [2]. Steam cracking plants are reported to produce 30% of global emissions of chemical plants [3].

Ethylene is the simplest alkene. It is colorless and flammable gas with a sweet odor. Polymerization of ethylene gives polyethylene which is used abundantly in packaging films, coatings, and bottles and as a starting material for production of ethanol, ethylene glycol, etc. Ethylene has the largest production volume in petrochemical industry. It is an intermediate for production of ethylene oxide, ethyl benzene and ethylene dichloride. The ethylene derivatives are illustrated in Figure 2.1 [4]. Ethylene is mostly needed for plastic sector. In western European countries, nearly 60% of ethylene is consumed for polyethylene production. Ethylene derivatives find use in construction, textile, and packaging industry for polyethylene terephthalate (PET), polystyrene (PS), and polyvinyl chloride (PVC). Ethylene demand and production capacity from 2015-2022 is illustrated in Figure 2.2 [5].

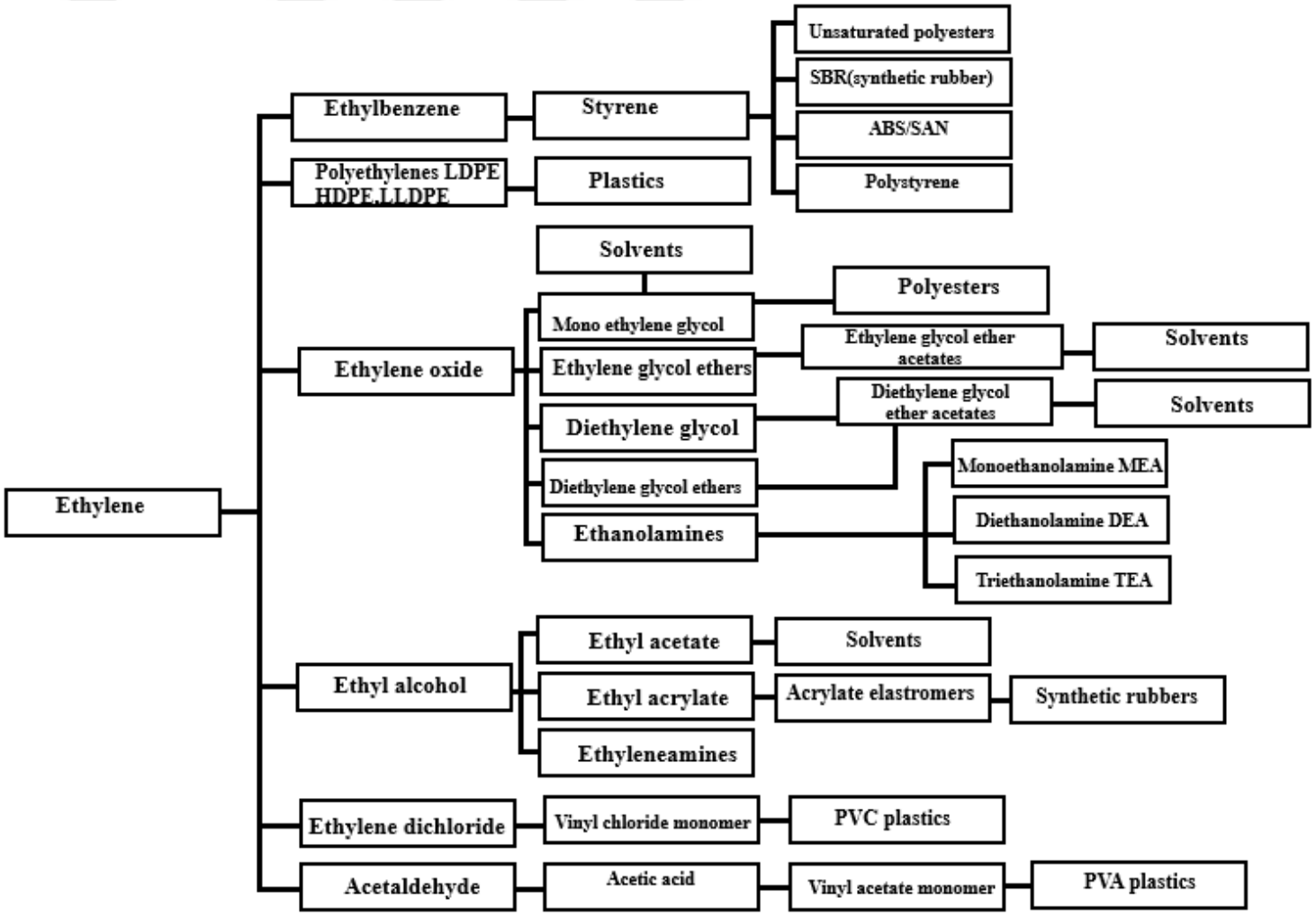

Figure 2.1 : Derivatives of ethylene.

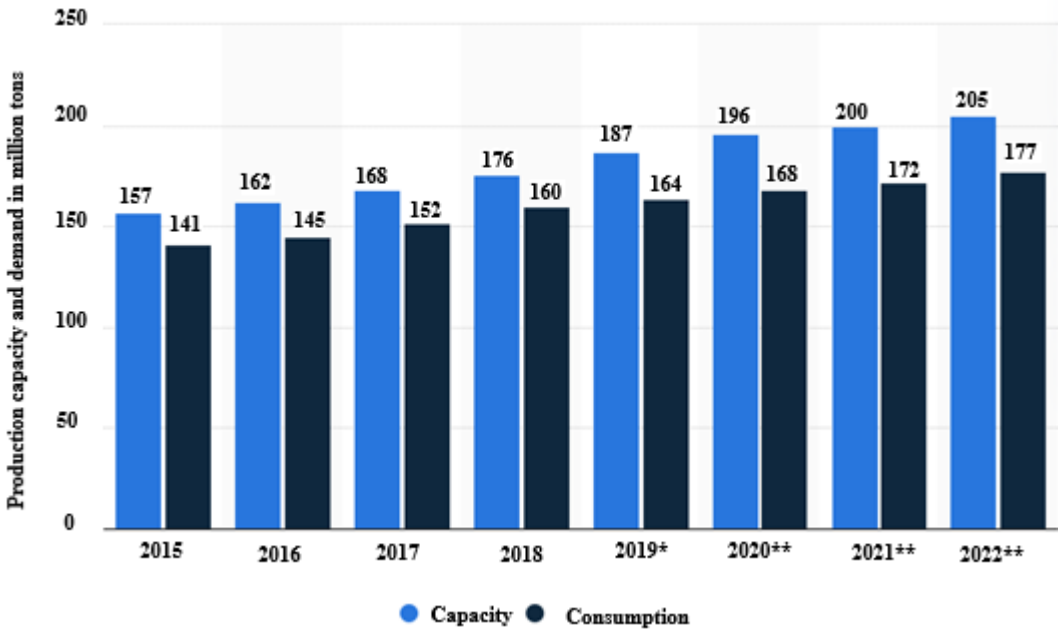

Figure 2.2 : Ethylene demand and production capacity worldwide from 2015-2022 [5].

Propylene(propene) is needed in large production volumes for resins, elastomers, fibers, and chemicals such as propyl alcohol. Propylene has more derivatives than ethylene. At Western European countries, 55% of propylene is consumed for polypropylene production. 13% of propylene find use for the production of propylene oxide towards propylene glycol and polyols synthesis. The rest of propylene around 32% is needed in acrylonitrile, cumene, and isopropyl alcohol productions. Propylene is traditionally manufactured as the byproduct during ethylene production or it is recovered from fluid catalytic cracking (FCC). The severity of the steam cracking (SC) process alters the ethylene/propylene ratio so process selectively may be changed to increase ethylene or propylene yield. Mild conditions favor less ethylene and more propylene yields. However, at conventional SC condition, sever cracking occurs to increase the ethylene yield. In the other side, ~30 % of global supply of propylene come from FCC process. The third route for propylene production is the dehydrogenation of propane (PDH) when propane supply is economic from shale gas[4].

Butylene has four isomeric compounds namely, 1-butene, cis-2-butene, trans-2-butene, and isobutylene[6]. Butadiene, isobutylene and n-butenes are the other C_4 olefin fractions. Butadiene is the raw material in the production of synthetic rubber (SBR, polybutadiene rubber). Synthetic rubber has high demand in electronics and

automotive sectors. Other usages of butadiene are in the production of SB (styrene-butadiene) copolymer latex and block copolymers, ABS (acrylonitrile-butadiene-styrene), and nitrile rubbers (NBR). ~85% of the butylene is blended with gasoline by the fuel industry. Ethyl tert-butyl ether (ETBE) and methyl tert-butyl ether (MTBE) as octane enhancers are produced from isobutylene. Among C_4 olefins, n-butenes have less demand as a comonomer for polyethylene. Sec-butyl alcohol, which is a raw material in the synthesis of methyl ethyl ketone(MEK) is obtained from this comonomer as well [4].

2.1 Indirect Processes

The applications of olefins are numerous and increasing demands for plastics necessitates sustainable olefin supply. There are two major issues to be concerned. One is sustainability issue due to the limited fossil fuel based feedstock. Second and the most important issue is that there is an urgent need to cut CO_2 emissions to bate with global warming from the environmental point of view. The route from syngas and its conversion to synfuels can be one alternative when syngas is obtained from non-petroleum sources such as biomass, waste and biogas gas. Then the existing infrastructure can be used to crack synfuel into olefins after its supply via Fishcer-Tropsch Syntheis (FTS) [2–5]. In indirect processes, methanol or dimethyl ether can be the other major alternatives to synfuel since there is commercial Methanol-to-Olefins process technology (MTO) [6, 7]. Generally, zeolite such as ZSM-5 and SAPO-34 are used as the catalyst in MTO process. When SAPO-34 catalyst is used, the main product is ethylene. MTO UOP/Hydro process produces up to 90 % C_2-C_4 but the problem is high deactivation of the catalyst by carbon deposition. In response to coking problem, Liu et al.[12] used two reactors in a MTO pilot plant. The first reactor contained γ-Al_2O_3 to dehydrate methanol to dimethyl ether (DME) and in the second reactor, ZSM-5 was used for the conversion of DME to light olefins. In their study, 85 wt% C_2-C_4 was attained with 100% methanol conversion during 1500 hour of reaction with a reasonable catalyst stability. The second indirect process is Dimethyl ether-to- Olefins process (DMTO) or SDTO (Syngas-via-Dimethyl Ether-to-Olefins). DME is thermodynamically favorable in comparison to methanol. At first stage, a metal-acid bifunctional catalyst and in the second stage, SAPO-34 catalyst is used for DME conversion to olefins. Liu et al.[12] reported 90 wt% C_2-C_4 with 100% DME

conversion over Cu-Zn/ZSM-5(syngas to DME) and a metal-modified SAPO-34 type of molecular sieve (DME to light olefins). However, regeneration is required to prevent excessive coking in case of SAPO type catalysts [4].

2.2 Direct Processes

Fischer-Tropsch Synthesis is a catalytic process that allows the production of synthetic fuels and chemicals from a carbon monoxide-hydrogen mixture called as syngas. When biomass is the feedstock for syngas generation, the whole process is counted to be sustainable and green. Although Fischer-Tropsch synthesis is a well-known process for about a century there exist still important research questions that remain up to date e.g. direct production of light olefins. Fischer-Tropsch to Olefins (FTO) process is a direct conversion of syngas to light olefins. The number of research and patent of FTO changed with the crisis in oil. It reached maximum values after the oil embargo of 1973 and the second oil crisis in 1979. The high cost of oil for the production of C_2-C_4 derived research into new alternative routes to produce these high demanded chemicals. After those crisis years, research and scientific publications went on mostly focused on the effect of supports and promoters on FTO performance as well as maximizing the activity.

Different FTS plants and their capacity that are currently active are given in Table 2.1 [1].

Table 2.1 : Currently active FTS plants.

Company	Carbon Source	Capacity (bpd)	Commissioning Date
Sasol	Coal	2500	1955
Sasol	Coal	85000	1980
Sasol	Coal	85000	1982
MossGas	Natural gas	30000	1992
Shell	Natural gas	12500	1993
Sasol/Qatar Petroleum	Natural gas	34000	2006
Sasol Chevron	Natural gas	34000	2007
Shell	Natural gas	140000	2009
Sasol/USA	Natural gas	96000	2018
Sasol/Canada	Natural gas	96000	2020

All direct and indirect processes for transformation of CO-rich synthesis gas into lower olefins are depicted in Figure 2.3 [8]. Herein after, more details will be given on FTO process.

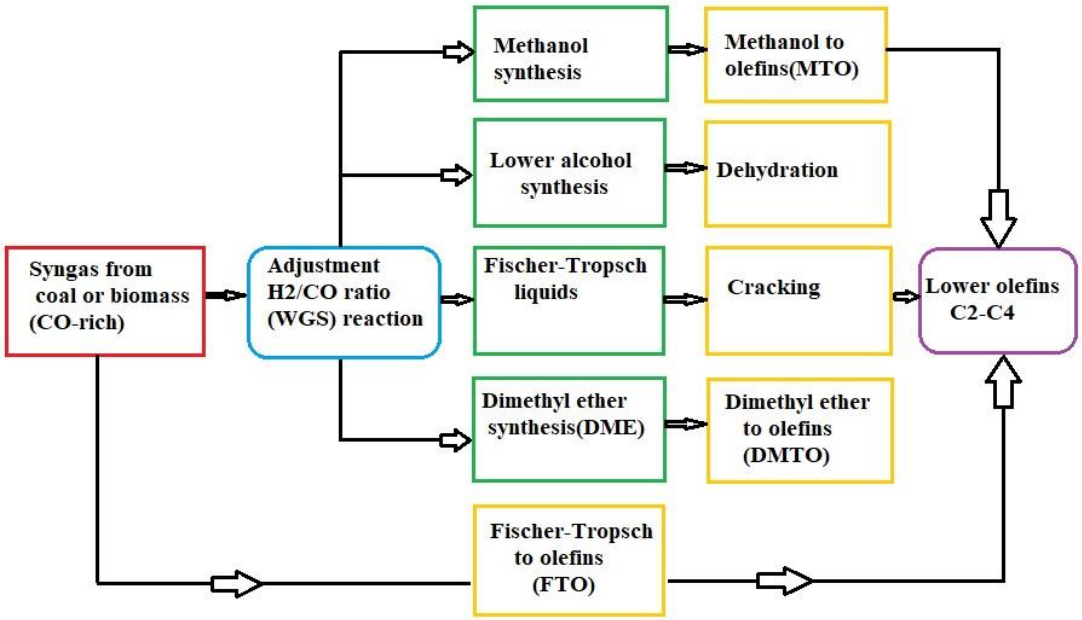

Figure 2.3 : Processes for transformation of CO-rich synthesis gas into light olefins.

3. FISHER-TROPSCH SYNTHESIS

As described in previous section, FTS is an alternative route for the production of a wide range of hydrocarbons(C_1-C_{20+}) that can be limited and tuned to favorable targets using catalysts. The reactions occurring during FT synthesis, in which alkanes and alkenes are favorite products, are as:

$$Alkane: (2n+1)H_2 + nCO \rightarrow C_nH_{2n+2} + nH_2O \quad (3.1)$$

$$\text{Alkene: } 2nH_2 + nCO \rightarrow C_nH_{2n} + nH_2O \quad (3.2)$$

$$Water - gas\ shift\ reaction: \quad CO + H_2O \leftrightarrow CO_2 + H_2 \quad (3.3)$$

In the cases where syngas is obtained from gasification of coal and biomass (H_2 lean), Water-gas shift (WGS) reactions contributes to H_2 production and can alter the H_2/CO ratio. In addition to the mentioned reactions, there are side reactions as follows:

$$Alcohols: \quad 2nH_2 + nCO \rightarrow C_nH_{2n+2}O + (n-1)H_2O \quad (3.4)$$

$$Boudouard\ reaction: \quad 2CO \rightarrow C + CO_2 \quad (3.5)$$

Boudouard reaction or carbon deposition is an unwanted reaction that may occur during FTS. FT is a polymerization reaction.

3.1 FTS Reaction Mechanism

There are many proposed mechanistic pathways but all include the polymerization reaction steps (initiation, chain propagation, and chain termination). Two proposed FTS reaction mechanism are 1-surface carbide mechanism and 2-CO insertion mechanism. In any case, via adsorption of an adsorbed C_1 reaction intermediate having one carbon atom, the adsorbed hydrocarbon intermediate grows. In carbide mechanism, chain initiates with dissociative adsorption of CO on metal atoms and carbide phase forms. Dissociated hydrogen is adsorbed to the carbide to produce CH_2 active intermediate. Then the chain propagates and n number of -(CH_x)- forms. Finally,

the alkyl chain desorbs from metal after hydrogenation (paraffin) or without secondary hydrogenation (olefins) [13]. The surface carbide mechanism is illustrated in Figure 3.1 [8]. However, in CO insertion mechanism, the chain grows in two steps. Firstly, CO is inserted to the adsorbed CH_x intermediate, then the C-O bond of the inserted one breaks and C_2H_y is formed. By consecutive insertion of CO to hydrocarbon intermediates followed by C-O cleavage of the inserted CO, the chain grows. Both mechanisms are schematically shown in Figure 3.2 [14].

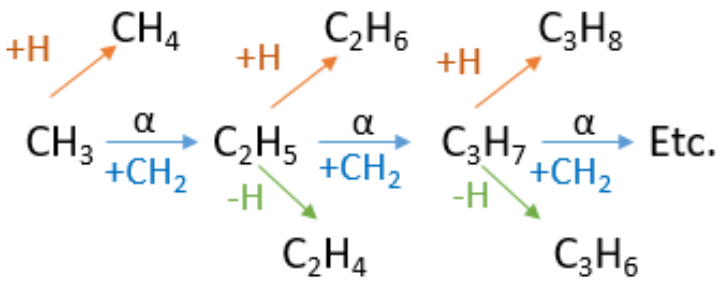

Figure 3.1 : Surface carbide mechanism of Fischer-Tropsch reaction [8].

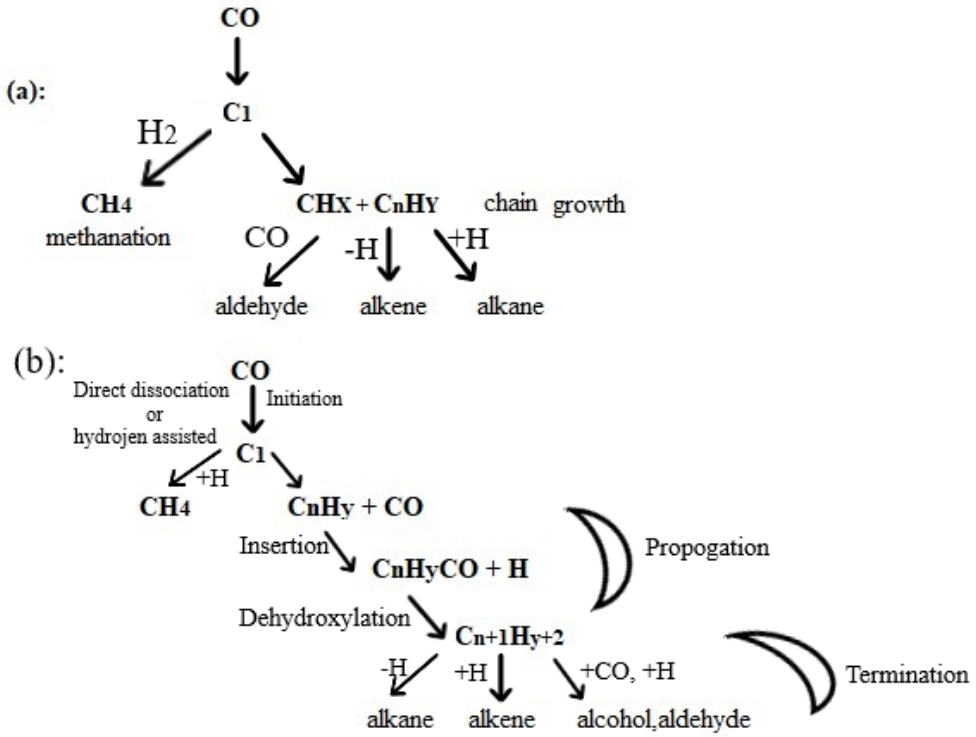

Figure 3.2 : Schematic of FT reaction mechanism a: Carbide mechanism , b: CO insertion chain growth [14].

Considering thermodynamic analysis of CO hydrogenating via FT synthesis, there are many serial-parallel reactions. These reactions have different enthalpy of reaction (ΔH_R) that suggests the formation of methane and considerable carbon deposition both as most unwanted products. Potential Gibbs free enthalpies of reactions vs temperature

is illustrated in Figure 3.3. The reactions named equation (3.6)-(3.10) are as follows [15]:

$$CO + 2H_2 \leftrightarrow (-CH_2-) + H_2O \quad \Delta H_R = -164.7\ KJ(227\ C, n-Hexane) \tag{3.6}$$

$$CO + H_2O \leftrightarrow CO_2 + H_2 \quad \Delta H_R = -39.7\ KJ(227\ C) \tag{3.7}$$

$$2CO + 2H_2 \leftrightarrow (-CH_2-) + CO_2 \quad \Delta H_R = -204.4\ KJ(227\ C, n-Hexane\ ) \tag{3.8}$$

$$CO + 3H_2 \leftrightarrow CH_4 + H_2O \quad \Delta H_R = -214.4\ KJ(227\ C) \tag{3.9}$$

$$CO \leftrightarrow C + CO_2 \quad \Delta H_R = -133.8\ KJ(227\ C) \tag{3.10}$$

Equation (3.8) is obtained from the summation of reaction (3.7) and (3.6). It can be concluded from Figure 3.3 that methane and carbon deposition formation are thermodynamically favorable between 200-400 ^{o}C. This issue explains one of the concerns being faced in FTS.

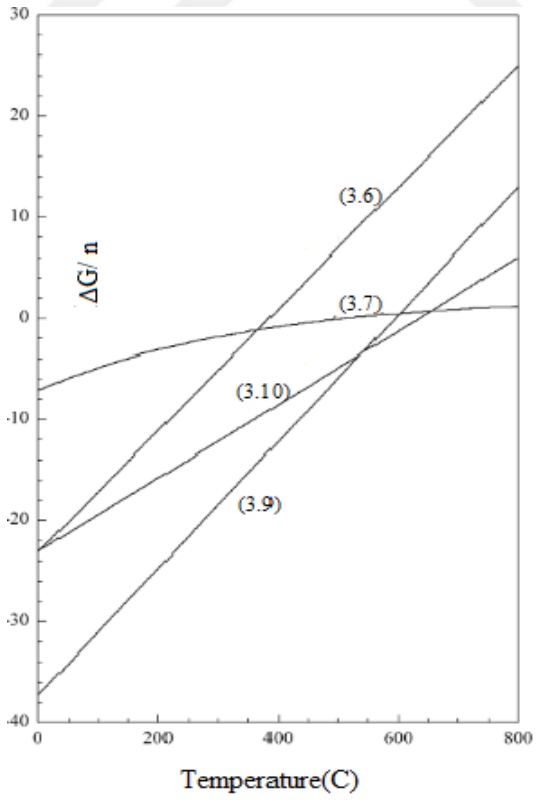

Figure 3.3 : Variation of enthalpy of FT reactions with temperature during the formation of hexane (ΔG: kj).

3.2 Fischer-Tropsch Synthesis Catalysts

In FTS, catalyst is the most critical component for an efficient and commercial scale light olefin production. Catalysts are required to tune the selectivity towards light olefins by altering the chain growth and limiting the secondary hydrogenation reactions. Fe, Co, Ni, Ru and Os are used as the most widely catalytic materials in FTS. It is reported that Re and Rh also show acceptable catalytic activity for FTS [13]. Fe, Co, Ni, and Ru are accepted as suitable transition metals to be used in FTS due to high rates of CO dissociation and subsequently high rate of chain growth. Ru is not considered a proper choice because it has limited resources and high price. However, Fe-based and Co-based catalysts are the most used ones. Fe-based catalysts are more reactive to water-gas shift (WGS) reaction making them ideal for low H_2 to CO ratios. In addition, Fe-based catalysts are more tolerant to sulfur impurities than Co based catalysts recommending to be used for coal and biomass derived syngas. Moreover, iron exhibits lower hydrogenation activity to Co resulting in high selectivity to olefins [10–12]. Available literature on iron-based catalysts that have been used in FTS for light olefin production, supports and promoters that have been used, synthesis method, active phase, and catalytic activity all are summarized in Table 3.1 [1].

The catalytic behavior of iron catalysts can be improved by the use of transition (Zn, Cu, Ru) and alkali (K, Na, Cs, Rb) metals added as promoters. A summary of the promoters and reaction conditions used in iron-based catalysts to increase the olefin selectivity in FT reaction are presented in Table 3.2 [1].

Table 3.1 : Iron-based catalysts used for FTO [1].

Active metal	Support	Promoter	Synthesis Method	Active Phase	$C^{=}_{2}$-$C^{=}_{4}$ Sel.(%)	CO Conv.(%)
Fe	CNTs	Mn/K	Impregnation	$FeMn_2O_4$ before reduction	51.7	30.1
Fe	CNTs	Bi	Impregnation	Hägg χ-Fe_5C_2 or ε-Fe_2C	60.9	10.0
Fe	CNTs	Pb	Impregnation	Hägg χ-Fe_5C_2 or ε-Fe_2C	57.7	18.6
Fe	CNTs	Bi	Impregnation	χ-Fe_5C_2	45–62.4	25.5–25.6
Fe	CNTs	Pb/K	Impregnation	χ-Fe_5C_2	52.6–62	40.7–76.2
Fe	CNTs	Mn/K	Impregnation	Hägg χ-Fe_5C_2	50.3	22.7
Fe-Zn-Cu	-	-	Co-precipitation	-	35	45
Fe	CNTs	K	Deposition-precipitation	-	42	16
Fe	N- CNTs [a]	K	Impregnation	χ-Fe_5C_2	54.6	14.4
Fe	NMCs [b]	-	Ultrasonic-impregnation	Fe_5C_2 and Fe_2C	33.9	92.6
Fe-Cu	Graphite	-	Co-precipitation	Fe_7C_3	37.8	44.9
Fe	AC	K	Impregnation	χ-Fe_5C_2 and ε'-$Fe_{2.2}C$	21.7	32.2
Fe	$CSiO_2$[c]	K			26.5	16.5
Fe	$CSiO_2$[c]	K/S			51.7	11.8
Fe	SiC	Na/S			51.4	10.3
Fe	SiC	K			19.7	57.1
Fe	γ-Al_2O_3	-	Impregnation	χ-Fe_5C_2 and ε'-$Fe_{2.2}C$	16.1	10.0
Fe	SiO_2	-			19.5	16.7
Fe	TiO_2	K			17.3	67.7
Fe	$mSiO_2$[d]	-	Impregnation	χ-Fe_5C_2 is dominant - (above 36%), Fe_3C & ε-$Fe_{2.2}C$ (less than 14%)	12.8	15.4
Fe	SiO_2	-			15.22	28.5
Fe	SiO_2-CO [e]	-			18.3	76.9
Fe	SiO_2-H_2[e]	-			14.1	51.6
Fe	SiO_2-E [f]	Mn	Impregnation	-	54.6	50.5

Table 3.1 (Continued) : Iron-based catalysts used for FTO [1].

Active metal	Support	Promoter	Synthesis Method	Active Phase	$C^{=}_{2}$-$C^{=}_{4}$ Sel.(%)	CO Conv.(%)
Fe	SiO_2	-	Impregnation		10.1	23
Fe-Cu	SiO_2	-	Co-impregnation	χ-Fe_5C_2	15.2	33.9
Fe	SiO_2	K	Impregnation		18.7	29.9
Fe-Cu	SiO_2	K	Co-impregnation		18.1	34.3
Fe	SiO_2	Bi	Impregnation	χ-Fe_5C_2	53	17
Fe	SiO_2	Pb			32	55
Fe	SiO_2-GC [g]	-	Hydrothermal deposition	Hägg χ-Fe5C2	12.9	40.6
Fe_2O_3	SiO_2	-	Hydrothermal deposition	Hägg χ-Fe_5C_2	17.4	40.6
Fe-Mn	SiO_2	Cu	Co-precipitation, Impregnation	Hägg χ-Fe_5C_2	40.1	96.9
Fe	Si-CO [e]	-	Co-precipitation	Fe_7C_3, χ-Fe_5C_2 ε-Fe_2C, χ-Fe_5C_2 χ-Fe_5C_2	30.8	50.8
Fe	Si-H_2[e]	-			15.0	33.1
Fe	Si-Syngas [e]	-			17.1	22.3
Fe	α-Al_2O_3	S/Na	Impregnation	-	50	66
Fe-Ni	Al_2O_3	K_2S	Co-precipitation	-	77.8	64.6
Fe	MgO-NS [h]		Impregnation Deposition-		14.6	55.6
Fe	MgO-NS		precipitation Ultrasonic		15.5	38.0
Fe	MgO-NS		Impregnation Ultrasonic		29.6	35.5
Fe	MgO cubes		Impregnation		21.5	35.7
Fe	MnO_x	Ag	Impregnation	χ-Fe_5C_2	35.4	50.3
Fe	-	Na/S	precipitation	-	66	30
Fe	-	-	Solvothermal	-	19.3	91.0
Fe	-	Na		-	23.3	93.2
Fe	-	K			22.1	97.1
Fe	-	Zn	Solvothermal	-	18.1	98.3
Fe	-	Mn			34.1	37.4
Fe	-	Zn/Na	Co-precipitation		42.7	97.16
Fe	-	Zn/K	Co-precipitation		37.19	5.02
Fe	-	Zr	Co-precipitation		57	40.6

[a] Nitrogen-doped CNTs; [b] Nitrogen-rich mesoporous carbon-supported Fe catalyst; [c] Carbon-coated SiO_2; [d] Mesoporous silica; [e] Fe-Si calcined catalyst treated with CO, H_2, and syngas; [f] Ethylene glycol pretreated silica support; [g] Silica-graphitic carbon encapsulated iron; [h] Nanosheet.

Table 3.2 : Iron-based catalysts, their FT reaction conditions, light olefin selectivity and catalyst activity [1].

Catalyst	Promoter	T(^{o}C)	P(bar)	GHSV ($Lh^{-1}g^{-1}$)	H_2/CO	C_2-C_4 Sel.(%)	CO Conv.(%)
Fe/α-Al_2O_3	S/Na	340	20	3	1	50	60-66
Fe/α-Al_2O_3-H[a]	S	350	1	9	1	68	0.9
Fe-Ni/Al_2O_3	K_2S	340	1	3	2	77.8	64.6
Fe/CNTs	Mn/K	270	20	30	1	51.7	30.1
Fe/CNTs	Bi	350	1	3.4	1	60.9	10
Fe/CNTs	Pb	350	1	3.4	1	57.7	18.6
Fe/CNTs-Confined[b]	Bi	350	10	17	1	45	60.2
Fe/CNTs-Confined	Bi	350	1	3.4	1	62.4	25.6
Fe/CNTs-Confined	Pb/K	350	10	17	1	52.6	76.2
Fe/CNTs-Confined	Pb/K	350	1	3.4	1	62	40.7
Fe/CNTs[c]	Mn/K	270	20	30	1	50.3	22.7
Fe/N-doped CNTs	-	300	1	4.2	1	46.7	14.4
Fe/N-doped CNTs	K	300	1	4.2	1	54.6	16.5
Fe/NMCs[d]	-	340	10	-	1	33.9	92.6
Fe/CNTs	K	270	20	18	1	42.2	28.8
Fe/CNF	Na/S	350	1.85	12-24	10	50	10
Fe/AC	K	300	10	2.2	1.1	21.7	48.9
Fe/$CSiO_2$[e]	K	300	10	2.2	1.1	26.5	32.2
Fe/SiC	Na/S	300	2	2.2	1.1	51.4	10.3
Fe/SiO_2-E[f]	Mn	300	10	-	1	54.6	50.5
Fe/SiO_2	-	300	20	16	2	10.1	23
Fe/SiO_2	Cu	300	20	16	2	15.2	33.9
Fe/SiO_2	K	300	20	16	2	18.7	29.9
Fe/SiO_2	Cu/K	300	20	16	2	18.1	34.3
Fe/SiO_2	Bi	350	1	3.4	1	53	17
Fe/SiO_2	Pb	350	1	3.4	1	32	55
Fe/MnO_x	Ag	340	10	7.4	1.1	35.4	50.3
Fe/MnO_x	Ag	320	10	7.4	1.1	34.3	55

Table 3.2 (continued) : Iron-based catalysts, their FT reaction conditions, light olefin selectivity and catalyst activity [1].

Catalyst	Promoter	T(^{o}C)	P(bar)	GHSV ($Lh^{-1}g^{-1}$)	H_2/CO	C_2-C_4 Sel.(%)	CO Conv.(%)
Fe/MgO nanosheets	-	300	10	8	1	14.6-29.6	35.5-55.6
Fe/MgO cubes	-	300	10	8	1	21.5	35.7
Fe-Cu/Graphite	-	260	20	-	1.1	37.8	44.9
Fe	Na/S	330	20	12.9	4	64.24	25
Fe	-	280	20	3	1	19.3	91
Fe	Na	280	20	3	1	23.3	93.2
Fe	K	280	20	3	1	22.1	97.1
Fe	Zn	280	20	3	1	18.1	98.3
Fe	Mn	280	20	3	1	34.1	37.4
Fe	Zn/Na	350	20	3	2.2	42.7	95.09
Fe	Zn/K	350	20	3	2.2	37.19	95.02
Fe	Zr	280	1	-	1	57	40.6
Mo/γ-Al_2O_3	K	300	10	6	2	21.8	4.2

[a] Hierarchical α-Al_2O_3 support; [b] Iron nanoconfinement inside carbon nanotubes; [c] Supercritical hexane with hexane/syngas ratio of 3; [d] Nitrogen-rich mesoporous carbon-supported Fe catalyst; [e] Carbon-coated SiO_2; [f] Ethylene glycol pretreated catalyst

The transition/alkali metals can act as structural or chemical promoters to enhance the metal dispersion and facilitate the iron oxide reduction by stabilization of iron against oxidation [13,14]. It is believed that alkali metals could affect the catalytic performance by decreasing the strength of C-O bonds leading to an increase in CO dissociation. Alkali promoters make the iron catalyst gain additional features such as suppression of the secondary hydrogenation, facilitated light olefins desorption and increased chain growth probability all that brings high olefin to paraffin ratio and C_{5+} selectivity at the expense of low carbon paraffin. Among alkali metals in group I, effect of K and Na have been investigated widely in literature[15 - 19]. Iron carbides are believed to be the most catalytic active phase in FTS [24]. Alkali metals, e.g. Na, extend the carburization of iron oxides. However, an optimum alkali concentration exists and coking dominates beyond that [17, 20, 25]. Apart from the need for active iron carbide formation, preserving the active surface area is the other concern for an acceptable light olefin selectivity. Transition metals are employed as a structural promoter of iron carbide. In this context, the effect of Zn on Fe-based catalysts have been investigated [20, 16-26]. Their use in an appropriate amount may inhibit sintering [31].

The effect of Zn, Cu and K on the structure and catalytic behavior of iron-based Fischer–Tropsch synthesis catalyst were studied by E. Iglesia et al.[26]. In case of Zn, it was shown that spinel-type zinc ferrite structure appears along with hematite. They have argued the structural promoter effect alters at changing Zn concentrations. In their discussions, the inhibited sintering of Fe_2O_3 was ascribed to the formation of small $ZnFe_2O_4$ crystallites at low Zn concentration while $ZnFe_2O_4$ crystallites at high Zn concentration was seen as a matrix for the isolation of Fe_2O_3. As it was reported by Y. H. Choi that Na-promoted spinel zinc ferrite was highly selective to liquid hydrocarbons, up to 58% and a high olefin/paraffin ratio up to 11 was achieved for CO_2 hydrogenation[27]. In a study of bimetallic interactions of iron and zinc by H. Wang et al., it was found that when $ZnFe_2O_4$ was formed, the stability and activity of the catalyst were increased due to the enhanced dispersion of active sites [32].

The type of the precipitant and the precipitation method are the other primary concerns which determines the final catalytic activity since they may change the nature of iron oxy-hydroxides formed during precipitation [33] . The effect of various precipitants on FTO performance of Fe/Zn catalysts have been investigated by Zhao et al. [34].

The catalysts precipitated with sodium carbonate displayed higher selectivity towards light olefins compared to those precipitated with potassium carbonate and ammonium carbonate. They reported a 95% CO conversion and a 53% light olefin selectivity for the Fe.Zn catalyst with Fe/Zn molar ratio = 1 and 1.86 wt% Na. Na-promoted $FeZn_{1.2}Ox$ catalysts have been synthesized and investigated for their FTS performance at 340 ^{o}C and 2.0 MPa by Yang et al. [23]. It was claimed that the presence of Na retards the reduction of $Fe_1Zn_{1.2}Ox$ while facilitating Fe_5C_2 formation. A CO conversion of 76.7 % and olefin selectivity of 29.2 % were obtained with Na0.2/ $Fe_1Zn_{1.2}Ox$ which was calcined at 400 °C.

All in all, structural effect of Zn and electronic effect of Na on iron catalyst might be utilized in order to get high activity and selectivity towards light olefins [17, 24]. Previous studies revealed that presence of Zn and Na can influence the structure and electronic configuration of the catalyst, respectively. Therefore, these elements may be used to increase the activity and selectivity of the catalyst towards light olefins. However, their optimum combinations and incorporation routes into catalyst matrix still needs further investigation.

Apart from the bulk catalysts prepared by precipitation and co-precipitation, supported iron-catalysts are well known in FT reaction. In order to increase iron dispersion, different supports have been used in FTO including metal oxides such as Al_2O_3 [35] , TiO_2[36], SiO_2 [37], Zeolites, MgO, and mesoporous materials. However, strong metal-support interaction is believed to form a metal (Fe/Co) and support compound for instance Co_2SiO_2, Co_2AlO_4, and $CoTiO_4$ as well as forming hardly reducible iron mixed oxides [32, 33]. Carbonaceous materials as catalyst supports have shown weak interaction between metal and support due to the inertness of support. Carbonaceous materials include metal–organic frameworks (MOFs) [40], activated carbon (AC), carbon nanofibers (CNF's), carbon nanotubes (CNT's), and carbon spheres (CS's) [41].

Carbonaceous materials have been widely used as the support of Fe(metal) catalysts in FT synthesis as depicted in Figure 3.4 [42].

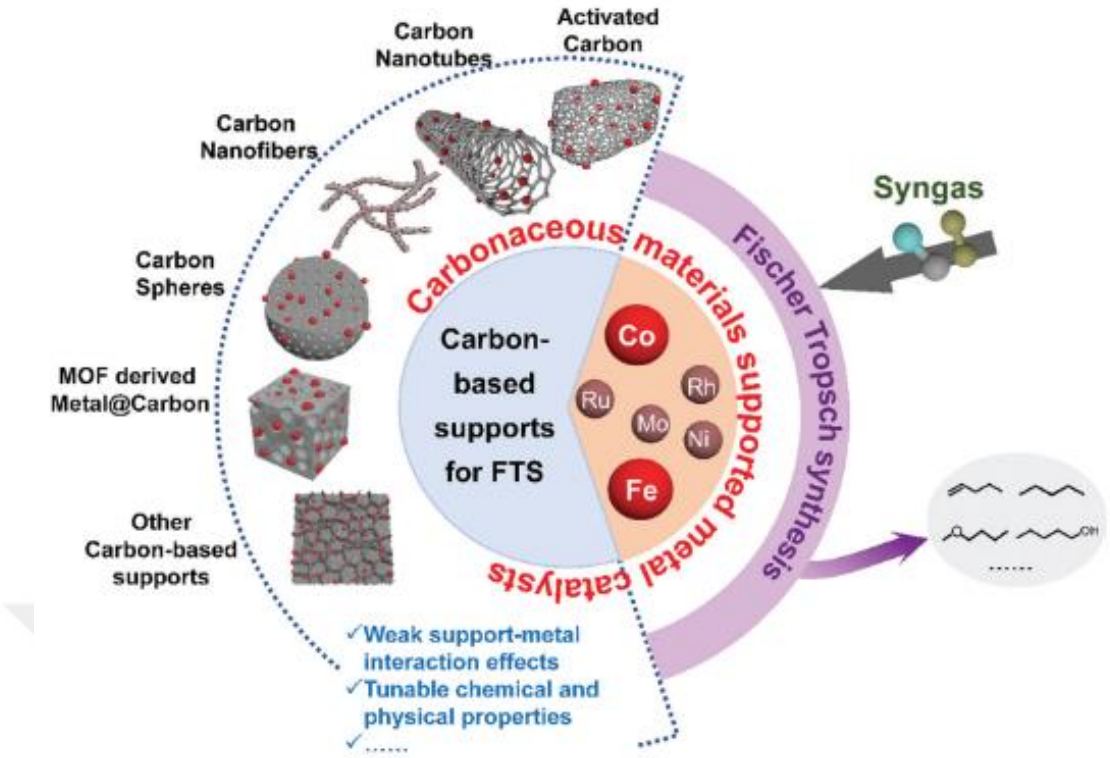

Figure 3.4 : Catalysts with carbonaceous material supports used in FTS [42].

In between, CNT's are vastly applied. As an example, Haifeng Xiong et al. have investigated the effect of Na, K, and Li as promoters on CNT's supported iron based Fischer–Tropsch synthesis (FTS) [20]. It is reported that alkali metals in group I increased iron oxide crystallite size and decrease the surface area. Alkali metals effect on hindering the reduction was the highest in K, and no effect for Li was observed. Na and K has shown decrease in CH_4 selectivity, enhancement in olefin selectivity and shifted the product to higher molecular weights.

Between carbonaceous materials, activated carbon (AC) can be obtained from low cost wastes and biomass. The surface functionality and textural properties (porous structure) of AC has the potential to be tuned during pyrolysis and subsequent activation treatment. The surface functional groups of AC resulting from chemical or thermal treatments, may affect the acidity–basicity of the carbon surface and in adsorption and catalysis, these acid-base sites could be considered as potential active sites [43].

In catalytic reactions, AC is known as an excellent sorbent and support for nanoparticles thanks to its properties such as high surface area, large pore volume, high thermal conductivity, hydrophilicity, low cost, and surface modification potentials

such as heteroatom doping. Activated carbons with acidic surfaces mainly include oxygen-containing functional groups such as carboxylic, chromene, lactone, phenol, quinone, pyrone, carbonyl and ethers. Basicity of AC is provided by two routes, namely, delocalized π-electrons of fused aromatic structures (resonating π-electrons in the carbon matrix) and basic surface groups that can bind protons groups (e.g., nitrogen-enriched functionalities) [44]. The functional groups of AC can be altered for specific needs for instance N-containing groups can be added to AC matrix [38].

Nitrogen-doped porous carbon (NPC) materials have gained large interest and have been used in many research areas as like supports in heterogeneous catalysis [31, 32, 36–42]. N-doped carbon materials have shown special properties by creating the anchor of active sites and electron donation due to the N incorporation.

Two methods are commonly used for N-doping into NPC materials. Post treatment and direct synthesis. Nitrogen- containing reagents (e.g. amines and NH_3) are added through reactions to NPC's which is called post treatment. However, carbonization of nitrogen dopants with nitrogen-rich carbon precursors is considered direct synthesis. Figure 3.5 [38] illustrates the possible nitrogen functionalities in NPC's.

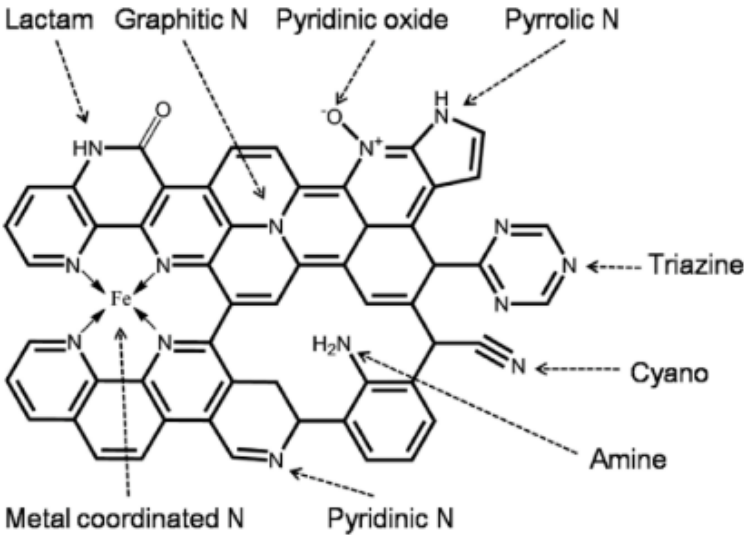

Figure 3.5 : Nitrogen functionalities noticed in nitrogen-doped porous carbon [38].

As Xiong et al. [52] reported, N-CNT's were prepared by post N-doping of CNT's at 700-900 °C while acetonitrile is passed over CNT's in a CVD tube in a way that N (and C) deposit on the CNT surface. Spherical carbon was formed when T≥850 °C. Therefore, the morphologies have changed. N-content enhanced linearly with Temperature (0.7 % at 700 °C to 6.54% at 900 °C). However, surface area of CNT's

decreased after N-doping due to the tube cavity shrinkage and the deposition of spherical carbon with increase in temperature. Pyridinic N atoms, quaternary N atoms and N atoms from pyridinic oxide as given in Figure 3.6 were showed to be homogeneously dispersed on the N-CNT's applying XPS and TEM-EELS. The N-CNT's prepared under both mild and harsh acid conditions were used as the support of Fe catalysts in Fischer–Tropsch synthesis (FTS). Harsh conditions resulted in smaller Fe oxide particle size. Moreover, Fe/ N-CNT's were less reducible. The activity had significantly increased by N-doping regardless of pretreatment conditions [52].

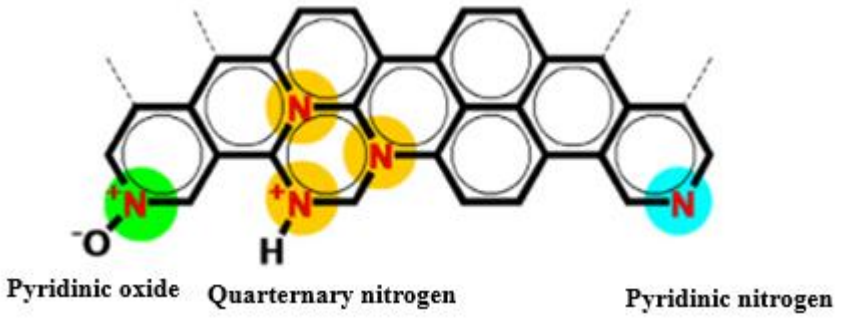

Figure 3.6 : Nitrogen species formed by post doping of CNT's [52].

In the study of Zhenhua Li et al. [39], different nitric acid concentration as nitrogen source have been doped on CNT's followed by Fe impregnation and FTS performance have been investigated. Adding nitric acid increased the oxygen-containing functional groups, graphitization degree, and iron dispersion on the nitrogen-doped carbon nanotubes (NCNT's).

In another work, Guoguo Liu a et al.[46], high Fe loading (40%) on nitrogen-rich mesoporous carbons with high porosity and 11.3% N-content was achieved. N-containing groups suppressed CH_4 (11.6%), improved CO conversion (92.6%), and olefin selectivity (33.9%) in FTS reaction.

Considering literature in FTO, in this work, two type of catalysts have been synthesized and tested for FTS. First, Fe.Zn bulk catalysts prepared by co-precipitation synthesis method using two precipitants, ammonium hydroxide and sodium carbonate in which the methods are denoted as (AH) and (SC), respectively. Type of precipitant has been changed to investigate its effect on FTO performance of the bulk catalysts. Other applied methods were co-precipitation and subsequent impregnation using both of the precipitants in which synthesis methods were denoted as (AH-I) and (SC-I). Na

as promoter has been incorporated to Fe.Zn structure using synthesis methods namely, (AH-I), (SC), and (SC-I) . Moreover, Cu and K promoters have been added to Fe.Zn precipitate as promoter with post impregnation methods, namely, (AH-I) and (SC-I). In the second step, a metal combination resulted in high olefin selectivity was selected from bulk catalysts and added to the determined supports. The metals were co-impregnated to the supports with the aim of increasing metal dispersion and reducing carbon deposition (deactivation). Activated carbon(AC) has been used as the support of the catalysts. Moreover, N-containing sources namely, HNO_3, NH_3 and urea have been applied in order to add N-containing functionalities to the surface of AC (Chemical modification of surface). The obtained catalyst supports after N-doping were denoted as AC-N_1, AC-N_2, and AC-N_3, respectively. All the catalysts have been tested in a high pressure fixed-bed reactor to investigate the catalyst activity and hydrocarbon distribution of the product gas. Test results were interpreted together with the characterizations such as BET surface areas via N_2 adsorption, crystal phase identification by x-ray diffraction (XRD), elemental analysis by inductively coupled plasma (ICP-OES), morphological investigation by scanning electron microscopy (SEM), elemental mapping by energy dispersive spectroscopy (EDS), reducibility characteristics of active phases using H_2-TPR and finally the basicity of Na promoted bulk catalysts by CO_2-TPD.

4. EXPERİMENTAL

In this study, two types of catalysts have been synthesized and further tested at high pressure fixed-bed reactor for their FTO performance. First, bulk catalysts were prepared using ammonium hydroxide and sodium carbonate as precipitants and Na, K, and Cu as promoters which were incorporated to Fe.Zn precipitate via different synthesis routes namely, AH route, AH-I route, SC route, and SC-I route. Furthermore, with the aim of decreasing coke deposition by providing activated carbon(AC) with high surface area, Fe, Zn and a promoter was co-impregnated to the supports. In addition to AC, in order to investigate the effect of nitrogen doping to the support on the FTO performance of the catalysts, AC's where exposed to N-sources namely, nitric acid, ammonia, and urea as dopants. These chemically surface modified AC's where also used as the support in this work.

4.1 Materials and Methods

4.1.1 Materials

Chemicals used in the synthesis of the catalysts are given Table 4.1.

Table 4.1 : Chemicals used in synthesis of catalysts.

Chemical names	Chemicals	Provider/Grade
Ferric nitrate nonahydrate	$Fe(NO_3)_3.9H_2O$	Merck, ACS grade
Zinc nitrate hexahydrate	$Zn(NO_3)_2.6H_2O$	Sigma, ACS grade
Sodium nitrate	$NaNO_3$	Sigma, ACS grade
Ammonium hydroxide	NH_4OH	Sigma, 25-30%NH_3basis
Sodium carbonate	Na_2CO_3	Sigma, ACS grade
Quartz	SiO_2	Sigma
Potassium nitrate	KNO_3	Merck, ISO-Reag
Ammonia	NH_3	Elite, %5 Ammonia-Balance He
Nitric acid	HNO_3	Merck, 65%
Urea	CH_4N_2O	Carlo Erba, %99
Activated carbon	Activated carbon	Acid washed, commercial
Copper(II) nitrate trihydrate	$Cu(NO_3)_2.3H_2O$	Merck, %99.5

4.1.2 Synthesis of catalysts

In this study, two types of catalysts (bulk and supported catalysts) have been synthesized and tested for their FT performance. First, nine Na-promoted bulk catalysts have been synthesized. In addition to Na-promoted bulk catalysts, Cu- and K- promoted bulk catalysts have been prepared. Finally, supported catalysts were prepared by impregnation of metal salt precursors on activated carbon (AC) and N-doped activated carbon. The metal combination used in the supported catalysts has been selected from the first part (bulk catalysts) of the study considering the highest olefin selectivity. Synthesis of the bulk catalysts and supported catalysts will be discussed in different sections as follows.

4.1.2.1 Synthesis of bulk catalysts

In this part, iron-based bulk catalysts have been synthesized. Zinc and the third metal namely, Na, K, and Cu have been used as promoter. Two precipitants have been used to investigate the effect of precipitant on the FTO performance of the catalysts. AH and SC denote the used precipitants, NH_4OH and Na_2CO_3, respectively. Synthesis routes used in precipitation are denoted as AH route, AH-I route, SC route, and SC-I route. First, Na promoted catalysts are discussed. Afterward, K and Cu promoted catalysts have been introduced in the second part.

Synthesis of Na promoted bulk catalysts

A series of Na promoted Fe bulk catalyst were synthesized by AH route, AH-I route, SC route, and SC-I route. In this group, nine catalysts have been synthesized.

a) AH route

In AH route, Fe /Zn / Na / NH_4 / H_2O molar ratios are given in Table 4.2. For the precipitation synthesis, the mixture of metal salts ($Fe(NO_3)_3.9H_2O$, $Zn(NO_3)_2.6H_2O$, $NaNO_3$) have first been dissolved in deionized water and kept at 80 ^oC under continuous stirring at 400-500 rpm. Then, ammonium hydroxide (AH) as in 30% NH_3 solution was added into the stirred solution at 80 °C in dropwise until the pH of the solution was stabilized between 7 and 8. Dropwise addition of AH was complete in 20 minutes. Then the precipitate was filtered with a filter paper, MN 640 DE Ø 125 mm. The filtering pore size of the filter paper was 2–4 μm. The precipitate was washed by deionized water for several times and dried in an oven at 80 ^oC overnight. Dried

catalysts were calcined under dry air flow of 35 ml/min at 400 ^{o}C for 2 h. Heating ramp to calcination temperature was 5 °C/min. So-prepared catalysts were denoted as 2Fe.Zn(AH), 2Fe.Zn0.2Na (AH), and 2Fe.Zn0.4Na(AH).

Table 4.2 : Fe /Zn / Na / NH_4 / H_2O molar ratios of the catalyst prepared by AH route.

catalysts	Fe /Zn / Na / NH_4 / H_2O molar ratios
2Fe.Zn(AH)	2 / 1 / 0 / 9.6 / 246
2Fe.Zn0.2Na (AH)	2 / 1 / 0.2 / 9.9 / 252
2Fe.Zn0.4Na (AH)	2 / 1 / 0.4 / 10.1 / 259

b) AH-I route

In AH-I route, the base catalyst 2Fe.Zn(AH) was impregnated with $NaNO_3$ solution. Upon impregnation with Na, the catalysts were dried in an oven at 80 ^{o}C overnight. Then, the catalysts were calcined at 400 ^{o}C for 2 h under dry air flow of 35 ml/min. So-prepared catalysts were labelled with 2Fe.Zn0.1Na (AH-I), and 2Fe.Zn0.2Na (AH-I) based on the sodium content of the starting impregnation batch (molar ratios of 2Fe.ZnxNa, x=0.1 and 0.2).

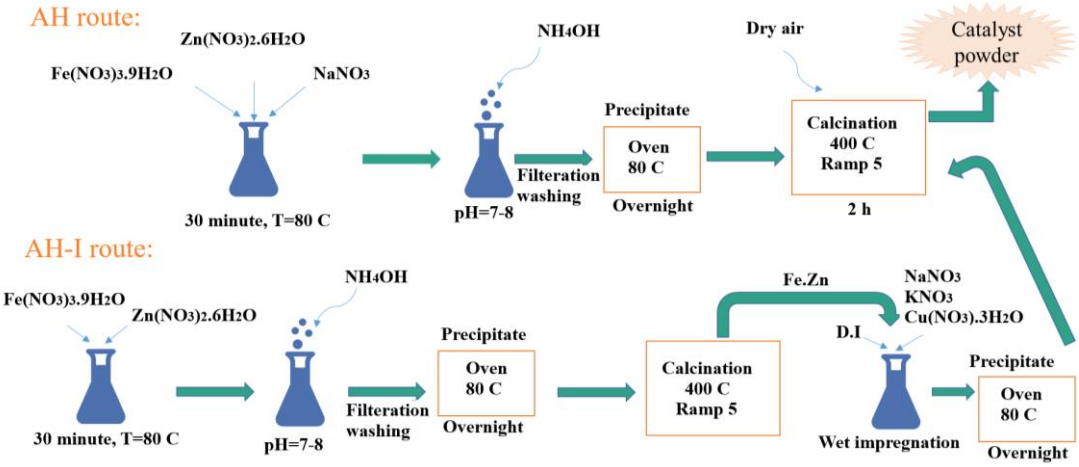

Figure 4.1 : Schematics of AH and AH-I synthesis methods.

c) SC route

In SC method, sodium carbonate (SC) was used in place of ammonium hydroxide (AH) in order to the synthesis of another group of catalysts. The method is schematically shown in Figure 4.2. First a base 2Fe.Zn catalyst was co-precipitated with sodium carbonate. For the synthesis via SC route, Fe / Zn /Na / NH_4 / H_2O molar ratio of the precipitation was 2 / 1 / 10.6 / 369. It took 30 minutes to complete the dropwise addition of SC. Then the precipitate was filtered and washed with deionized

water as in the same way with AH route. Washing becomes a critical step for the sodium based precipitants since the amount of residual sodium in the catalysts decreased with the increasing washing cycles. The high level of washing is required to bring the residual Na left over the base catalysts to trace amounts. The criteria to decide whether the washing was effective or complete were pH of the resulting solutions of the precipitate's washing. It was targeted to attain a pH = 6-7 to ensure the complete removal of sodium cations. To investigate the effect of washing efficiency on residual sodium content, three sets of base catalysts with changing washing levels were prepared. For the thoroughly washing case, that was expected to have the least sodium content, the catalyst was washed with 1800 ml water and denoted as 2Fe.Zn (SC). For the latter cases, 1200 ml and 600 ml of water were used for washing to obtain precipitates with moderate and high residual sodium contents, respectively.

d) SC-I route

In the SC-I method, the same amount of sodium salt promotor was subsequently impregnated on each of the base catalysts prepared by the SC method. The thoroughly washed base catalyst, 2Fe.Zn (SC), was impregnated with sodium nitrate in an amount corresponding to an initial Fe/Zn/Na molar ratio of 2/1/0.2 and denoted as 2Fe.Zn0.2Na $(SC\text{-}I)_1$. The catalysts prepared from two and three times less final washing steps were impregnated with the same amount of sodium and denoted as 2Fe.Zn0.2Na $(SC\text{-}I)_2$ and 2Fe.Zn0.2Na $(SC\text{-}I)_3$, respectively. The SC-I method is schematically shown in Figure 4.2. Finally, in order to investigate the structural promotion effect of Zn for 2Fe.Zn catalyst, Fe without Zn is precipitated by ammonium hydroxide and denoted as Fe (AH).

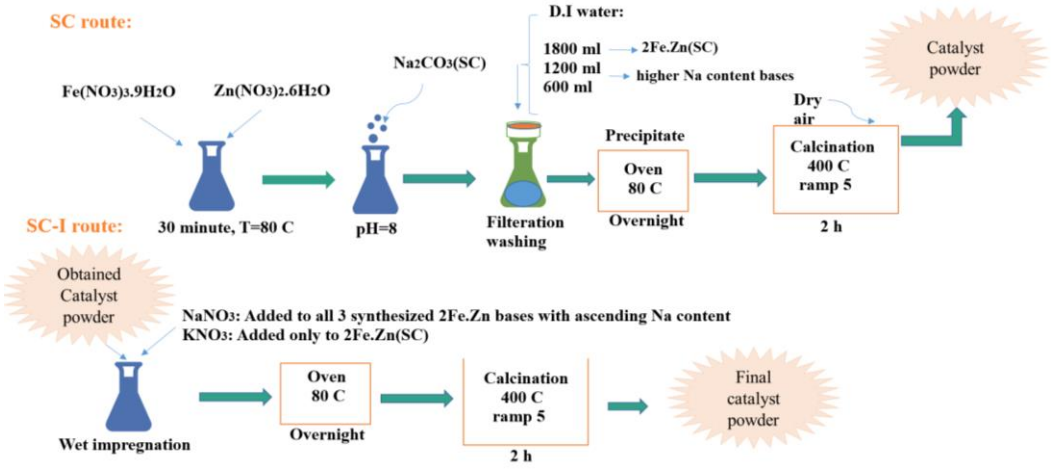

Figure 4.2 : Schematics of SC and SC-I synthesis methods.

All Na promoted iron bulk catalysts are shown in Table 4.3.

Table 4.3 : Prepared Na-promoted bulk catalysts.

Code	Catalyst	Synthesis route	Precipitant	Na addition methods
S1	2Fe.Zn (AH)	AH	NH_4OH	No
S2	2Fe.Zn0.1Na (AH-I)	AH-I	NH_4OH	subsequent impregnation
S3	2Fe.Zn0.2Na (AH-I)	AH-I	NH_4OH	subsequent impregnation
S4	2Fe.Zn0.2Na (AH)	AH	NH_4OH	co-precipitation
S5	2Fe.Zn0.4Na (AH)	AH	NH_4OH	co-precipitation
S6	2Fe.Zn (SC)	SC	Na_2CO_3	Residual Na from co-precipitation
S7	2Fe.Zn0.2Na (SC-I)$_1$	SC-I	Na_2CO_3	Residual Na + subsequent impregnation
S8	2Fe.Zn0.2Na (SC-I)$_2$	SC-I	Na_2CO_3	Residual Na + subsequent impregnation
S9	2Fe.Zn0.2Na (SC-I)$_3$	SC-I	Na_2CO_3	Residual Na + subsequent impregnation

Synthesis of K- and Cu -promoted bulk catalysts

Cu- and K- promoted catalysts were also synthesized by (AH-I) and (SC-I) methods. The totally 4 catalysts have been synthesized according the procedure given in Figure 4.1 and Figure 4.2 and labeled as given in Table 4.4. In the first step, Fe.Zn catalyst was co-precipitated with AH. $Fe(NO_3)_3.9H_2O$, $Zn(NO_3)_2.6H_2O$, and deionized water with Fe: Zn=2:1 molar ratios were stirred at 80 °C. Then, ammonium hydroxide (AH) as precipitant was added to form precipitate. The washed cake from co-precipitation was dried in oven at 80 °C overnight followed by calcination in air at 400 °C for 2 h at heating rate of 5 °C min-1. In order to be able to investigate the promotional effect of Cu and K, the base catalysts 2Fe.Zn (AH) and 2Fe.Zn (SC) are also included in Table 4.4.

Table 4.4 : Catalyst identification of K- and Cu-promoted bulk catalysts.

Code	Catalyst
S1	2Fe.Zn (AH)
L1	2Fe.Zn0.2Cu (AH-I)
L2	2Fe.Zn0.2K (AH-I)
L3	2Fe.Zn0.2Cu0.05K (AH-I)
S6	2Fe.Zn (SC)
L4	2Fe.Zn0.2K (SC-I)

The base catalyst 2Fe.Zn (AH) is the same as Table 4.3. At the second step, Cu and K were post impregnated onto the as prepared 2Fe.Zn(AH) catalyst by 2Fe.Zn.xCu.yK where (x,y) = (0.2,0), (0,0.2), (0.2,0.05) . The obtained catalysts were dried and calcined with the same conditions mentioned in the preparation of 2Fe.Zn(AH). From this stage, 2Fe.Zn0.2Cu (AH-I), 2Fe.Zn0.2K (AH-I), and 2Fe.Zn0.2Cu0.05K (AH-I) catalysts were achieved. In order to check the effect of precipitant in FT performance

of the catalysts, Na_2CO_3 (SC) was replaced with AH. The synthesis procedure was the same as for AH. The base catalyst 2Fe.Zn (SC) was the same as Table 4.3. Consequently, potassium was post impregnated onto 2Fe.Zn(SC) and 2Fe.Zn0.2K(SC-I) catalyst was obtained.

4.1.2.2 Synthesis of activated carbon and nitrogen-doped activated carbon supported catalysts

In this part, the synthesis of activated carbon (AC)-supported iron catalysts will be explained. The supported catalysts were prepared by both active carbon and the nitrogen-modified active carbon. Activated carbon was chemically modified by using different sources of nitrogen namely, HNO_3, NH_3, and urea. The procedure applied for the synthesis is given below.

Chemical modification of activated carbon

Activated carbon (AC) was nitrogen-doped using 3 dopants, namely, nitric acid (HNO_3), ammonia (NH_3), and urea. HNO_3 (65%) was added to activated carbon 10:1 (wt%), stirred for 3 h at 80 °C. Afterwards, the solution was filtered. While filtering, continuously deionized water was added from the top to wash the sample till pH: 6-7 was reached. Residue on the filter paper was put in oven overnight. Further, it was heat treated with N_2 (0.3 L/h) to 600 °C by heating ramp of 6 °C min^{-1} and kept at 600 °C for 2 h. Then the catalysts were cooled to the room temperature under N_2 atmosphere. Obtained catalyst support was labeled as AC-N_1.

Activated carbon in a fixed-bed reactor was exposed to NH_3 (0.3 L/h) while temperature was increased to 700 °C by heating ramp of 6 °C min^{-1}, kept 2 h at 700 °C, and cooled under N_2 atmosphere to the room temperature. The treated sample was labeled as AC-N_2.

Urea was dissolved in deionized water and added to activated carbon by mass ratio of urea /AC: 2/1. Then, the mixture was stirred, put in Teflon-lined stainless-steel autoclave and maintained at 180 °C under autogenous pressure overnight. Afterward, it was dried at 80 °C. Urea-doped catalyst was heat treated under N_2 (0.3 L/h) atmosphere at 600 °C by heating ramp of 6 °C.min^{-1} and kept at 600 °C for 2 h followed by cooling to the room temperature under N_2. Obtained sample was labeled as AC-N_3.

Synthesis of promoted supported Fe.Zn catalysts

The promoted supported Fe.Zn catalyst were prepared according to procedure shown in Figure 4.3. Bulk catalysts (section 4.1.2.1) with molar ratio of Fe/Zn/P= 2/1/0.2 (where P is promotor) were wet co-impregnated on AC and modified AC supports. The resulting catalysts were consisted of 25% metal and %75 support material. The catalysts prepared by co-precipitation and with this composition in previous part of the study displayed a high olefin selectivity. That is why the promoted supported catalysts prepared by using same metal composition. The aim of this step of the work was to decrease or eliminate the deactivation which occurred during FTS reaction of bulk catalysts by enhancing the metal dispersion using carbon supports/modified carbon supports. After co-impregnation of the metals, the samples were dried overnight at 80 °C and heat treated with N_2 (0.3 L/h) at 500 °C for 2 h. Catalysts are coded as in Table 4.5. Fe.Zn.Na/AC-N_3 has been investigated by another member of the group and is not included in Table 4.5.

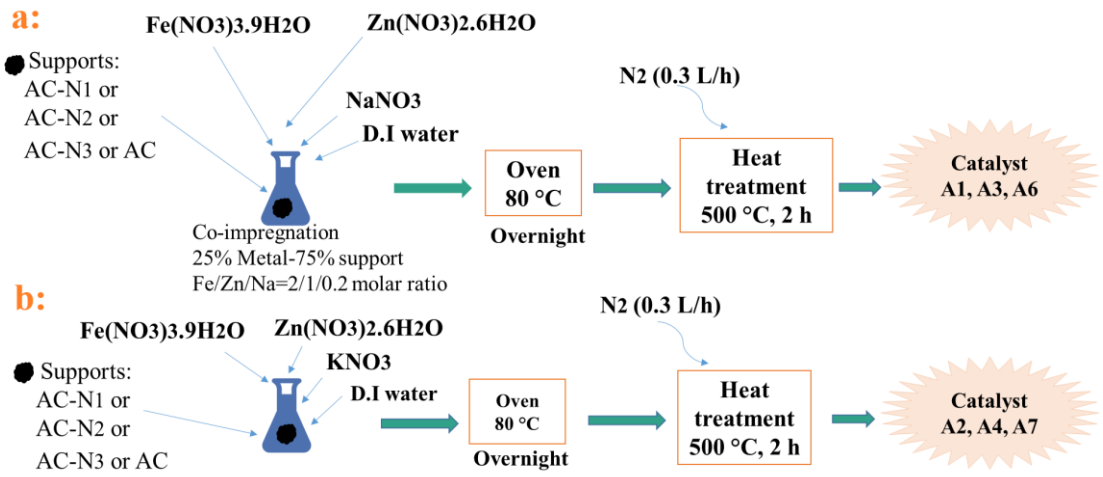

Figure 4.3 : a)Synthesis of Na promoted AC/N-doped AC supported catalysts, b) Synthesis of K promoted AC/N-doped AC supported catalysts.

Table 4.5 : Synthesized AC and modified AC supported catalyst.

Code	Catalyst	Synthesis method	Promoter	Support	Initial Fe/Zn/P ratio(molar)
A1	Fe.Zn.Na/ AC-N_1	co-impregnation	Na	AC-N_1	2/1/0.2
A2	Fe.Zn.K/ AC-N_1	co-impregnation	K	AC-N_1	2/1/0.2
A3	Fe.Zn.Na/ AC-N_2	co-impregnation	Na	AC-N_2	2/1/0.2
A4	Fe.Zn.K/ AC-N_2	co-impregnation	K	AC-N_2	2/1/0.2
A5	Fe.Zn.K/ AC-N_3	co-impregnation	K	AC-N_3	2/1/0.2
A6	Fe.Zn.Na/AC	co-impregnation	Na	AC	2/1/0.2
A7	Fe.Zn.K/AC	co-impregnation	K	AC	2/1/0.2

4.1.3 Characterization of catalysts

The catalysts have been characterized by the BET surface areas via N_2 adsorption, by the X-ray diffraction (XRD) for crystal phase identification, by inductively coupled plasma (ICP-OES) for the elemental analysis, by scanning electron microscopy (SEM-EDS) for morphological investigation and elemental mapping, by using H_2-TPR for reducibility characteristics of active phases and finally by CO_2-TPD to determine the basicity of Na-promoted bulk catalysts.

4.1.3.1 Brunauer-Emmett-Teller (BET) analysis

Surface area was performed by Brunauer-Emmett-Teller analysis (BET) following N_2-adsorption at 77 K in a Micromeritics 3 Flex analyzer, after the samples were degassed at 150 °C for 24 h under vacuum condition. BET surface area was estimated in relative pressure range of 0.05 to 0.30, over five adsorption points. The pore volume and average pore size distribution were calculated by Barret–Joyner–Hallender (BJH) method. The equation used in BET is as follows:

$$\frac{1}{\vartheta\left[\left(\frac{P_0}{P}\right)-1\right]} = \frac{C-1}{\vartheta_m C}\left(\frac{P}{P_0}\right) + \frac{1}{\vartheta_m C} \tag{4.1}$$

P_o and P are saturation and equilibrium pressure of nitrogen molecule, respectively, at a specific temperature. ϑ_m and ϑ are the monolayer adsorbed and adsorbed gas, respectively, in volumetric units. C constant in BET equation is defined by equation (4.2).

$$C = \exp\frac{E_1 - E_C}{RT} \tag{4.2}$$

where, E_1 is the first layer heat of adsorption and E_c is the heat of condensation.

From plotting θ vs p the adsorbed gas in monolayer is obtained from the y-intercept of the equation. Total surface area and BET surface areas are defined by Equation (4.3) and Equation (4.4).

$$Total\ surface\ area(S_{Total}): \qquad = \frac{\vartheta_m N s}{V} \tag{4.3}$$

$$BET\ Surface\ area(S_{BET}):\ \frac{S_{Total}}{a} \quad (4.4)$$

where a is molar weight of adsorbed species, N is Avogadro number, s is the adsorption cross section which for N_2 is 0.16 nm^2 , and V=22.4 L/mole [53].

4.1.3.2 Inductively coupled plasma optical emission spectrometer

Inductively coupled plasma optical emission spectrometer (ICP-OES, Optical 2100 DV) was used to determine the chemical composition of the catalysts. For chemical analysis, the catalysts samples were first digested into the solution of HNO_3 and HCl by microwave instrument (Multiwave PRO, Multiwave 3000). The effect of washing cycles on residual alkali content for the catalysts prepared by 2Fe.Zn(SC-I) route was checked by chemical analysis as well.

4.1.3.3 X-ray diffraction

The bulk crystalline structures of the fresh and the spent catalysts were determined by X-ray diffraction (XRD), (PANanalytical/X pert Pro) at 40 kV and 30 mA in range of 10-70^o with a step size of 0.0167^o using CuKα radiation(λ=0.15405 nm). Crystallite size of fresh catalysts were calculated by Scherrer equation $D=(K.\lambda)/(d*\cos\theta)$, where, K=0.9, λ = 0.15406, 2θ=35.5^o and d=Full Width at Half Maximum(FWHM) based on the strongest diffraction peak at 35.5°. XRD patterns of Na-promoted bulk catalysts were also taken by Co anode and are given in Figure C.1.

4.1.3.4 Elemental analysis

The amounts of carbon deposited on the spent catalysts and the N content of the N-doped activated carbon samples were determined by Vario MACRO cube Analyzer using ASTM D 4239-12 method.

4.1.3.5 H_2-temperature programmed reduction (H_2-TPR) analysis

The reducibility behavior of catalysts was determined by H_2-temperature programmed reduction (H_2-TPR) with two methods by using a fixed bed reactor and TGA. First, for sodium promoted bulk catalysts and AC supported catalysts, in a fixed bed reactor, 0.15 g of catalyst was preheated in N_2 flow at 350 ^{o}C for 30 minutes. Then the reactor temperature was decreased to 50 ^{o}C and a hydrogen mixture of 10v% H_2 in balance N_2 (80 mL h^{-1}) were flown over the catalyst by raising the temperature again from 50 to

800 ^{o}C at a rate of 10 ^{o}C min^{-1}. Data were collected by both a micro GC (Inficon, micro GC Fusion) equipped with a thermal conductivity detector (TCD) and a mass spectrometer (MS) (Stanford Research Systems, RGA 200).

4.1.3.6 Temperature programmed reduction (TPR) by TGA

TPR measurements of K and Cu promoted bulk catalysts were carried out on thermal gravimetric analyzer (DTG-60H, SHIMADZU) from ambient to 900 °C with a heating rate of 15°C/min. In the measurements, ~10 mg sample and a gas mixture of 20% H_2 and 80% N_2 were used.

4.1.3.7 Scanning electron microscopy (SEM) analysis

Scanning electron microscopy (SEM) images were taken by TESCAN VEGA 3 SBH to probe the morphological changes of the samples. Prior to each analysis, all catalyst samples were pretreated by coating with Au-Pd.

4.1.3.8 Scanning electron microscopy energy dispersive spectroscopy (SEM-EDS) analysis

SEM-EDS images of Na-promoted bulk catalysts and also Fe.Zn.Na/AC-N_2 were taken by Thermofisher ChemiSEM Axia to probe the morphological changes of the samples with no pre-coating.

4.1.3.9 CO_2-temperature programmed desorption (CO_2-TPD) analysis

The surface basicity of the Na-promoted bulk catalysts was determined by CO_2-temperature programmed desorption in the system used for H_2-TPR analysis. In the CO_2-TPD measurements, a 0.15 mg catalyst was thermally treated and reduced under H_2 flow (53 mL min^{-1}) for 2 hours at 350 ^{o}C. It was then purged by passing N_2 flow (100 mL min^{-1}) through the catalyst bed for 30 minutes at 350 ^{o}C. Afterwards, temperature was reduced to 50 ^{o}C. Upon completion of the purging step, CO_2 adsorption took place by flowing a mixture of 5%CO_2 and 95% He (100 mL min^{-1}) at 50 °C for 30 minutes. Then physisorbed CO_2 was swept away by N_2 (100 mL min^{-1}) for 30 minutes. To conduct the temperature programmed desorption of chemisorbed CO_2, the temperature was increased from 50 ^{o}C to 800 ^{o}C with a ramp of 10 ^{o}C min^{-1} under N_2 flow (100 mL min^{-1}). The CO_2 desorption profiles were driven by detecting

the desorbed amount of CO_2 at corresponding desorption temperature by micro GC and MS.

4.1.4 Experimental Set-Up

The Fischer-Tropsch synthesis (FTS) performance tests of catalysts were s conducted in a high pressure test system equipped with a fixed bed reactor (i.d.: 10 mm; length: 800 mm). A schematic flow diagram and a photograph of the reactor system are shown in Figure 4.4 and Figure 4.5, respectively. The temperature of the reactor was monitored by a thermocouple which was in direct contact with the catalyst bed. Output lines of the reactor are heat traced to prevent any condensation.

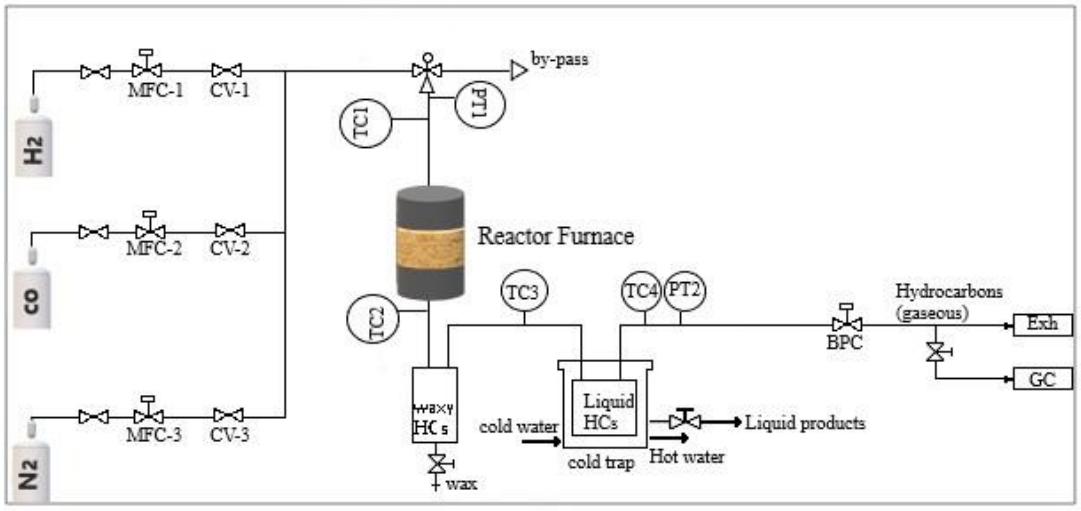

Figure 4.4 : The schematic flow diagram of the FTS performance system.

Figure 4.5 : A photograph of FTS performance test system.

4.1.5 Procedure of running performance tests

Catalytic activity tests of catalyst were performed by using 1 g catalyst in a particle size distribution of 50-150 microns. It was diluted with quartz particles with the same particle size range and in equivalent volume to prevent hot spots. Prior to the reaction, calcined catalyst was reduced with a gas mixture composed of 50v%H_2 -50v%N_2 at 350 ºC for 2 hours at atmospheric pressure. Subsequently, the reactor was set to FT

reaction conditions, namely 310 °C and 10 bar. The FT reaction was performed with a 50 mL min^{-1} flow of 60v% H_2 / 30v% CO / 10v% N_2. The product gas was quantitatively analyzed in every 30 minutes by an online gas chromatography (Agilent, 7820A GC). The amounts of H_2, CO, CO_2, and N_2 were detected by thermal conductivity detector (TCD) with a Carboxen column. C_1-C_{5+} hydrocarbons were measured by a flame ionization detector (FID) with Alumina S column. On average, reaction lasted for 30-35 h. During reaction periods samples were taken from the reactor effluent to analyze product components at a 30 minute time interval.

4.1.6 Evaluation of catalyst performance

Performance of catalyst performance were determined based on the CO conversion (X_{CO}), the CO_2 free hydrocarbon selectivity on carbon basis (Scn), the CO_2 selectivity on carbon basis (X_{CO2}). These parameters are described by the equations (4.5-4.10). The olefin/paraffin molar ratio(Ɓ) is defined by equation (4.10).

Inlet flow rate of CO:

$$CO_{in} = F_{in} \times CO_{entry} \tag{4.5}$$

Outlet flow rate of CO:

$$CO_{out} = F_{out} \times CO_{exit} \tag{4.6}$$

Conversion of CO:

$$X_{CO} = \frac{(CO_{in} - CO_{out})}{(CO_{in})} \times 100 \tag{4.7}$$

Hydrocarbon Selectivity (C basis): $S_{cn} = \frac{n_C \times F_{out} \times x_n(\mathrm{HC})}{(CO_{in} - CO_{out}) - CO_{2\,\mathrm{out}}} \times 100$ (4.8)

$$X_{CO_2} = \frac{CO_{2_{out}}}{(CO_{in} - CO_{out})} \times 100 \tag{4.9}$$

$$\text{Olefin/ paraffin}(Ɓ) = \frac{\sum_2^4 C^=}{\sum_2^4 C^0} \tag{4.10}$$

where F_{in} is the molar flow rate of feed gas stream(mole/h), F_{out} is the molar flow rate of product gas stream (mole/h), CO_{in} is molar flow rate of CO at inlet(mole/h) and

CO_{out} is molar flow rate of CO at outlet (mole/h), X_n (HC) is the mole fraction of the hydrocarbon in the product stream, n_C is the carbon number of the hydrocarbon whose selectivity is calculated and CO_{2out} denotes the molar flow rate of CO_2 at outlet (mole/h). “in” and “out” denote inlet and outlet of the reactor.

5. RESULTS AND DISCUSSION

In this section, characterization results of all synthesized catalysts, namely iron based bulk catalysts (precipitated) and promoted supported catalysts is given.

5.1 Catalyst Characterization

In this study, catalysts have been synthesized as bulk catalysts with different promoters and supported catalysts. The characterization of each group is given separately in the following section.

5.1.1 Characterization of bulk catalysts

Bulk catalysts prepared by co-precipitation synthesis and promoted by Na, K, and Cu have been characterized both before and after FT reaction. The BET surface areas via N_2 adsorption, crystal phase identification by x-ray diffraction (XRD), metal concentration by inductively coupled plasma (ICP-OES), texture observation by scanning electron microscopy (SEM), reducibility of catalysts using H_2-TPR and basicity of the catalysts by CO_2-TPD, and elemental analysis by MACRO cube Analyzer using ASTM D 4239-12 have been applied to characterize the fresh and spent catalysts.

5.1.1.1 Na promoted bulk catalysts

The elemental analysis of each catalyst sample and actual Fe/Zn/Na molar ratios of the catalysts calculated are given in Table 5.1. All the catalysts were precipitated initially with the same synthesis batch in which iron and zinc salts existed in stoichiometric amounts for zinc ferrite structure (Fe to Zn molar ratio of 2). However, the precipitation bath contained different precipitant ions of NH_4^+, OH^-, Na^+, NO_3^-, CO_3^{2-} and in different concentrations. Therefore, ionic strength might affect the ultimate Fe/Zn ratio of the catalysts since concentration dependent interactions between ions bring non-ideality by moving from dilute solutions to concentrates. In this term, concentrations can be substantially different depending on the ionic equilibria as a

feature of ionic strength of the solution. The electrolyte precipitate solution attained different ionic strength and ionic radius in each case which led to altered solubility and precipitation phenomenon. As it is shown in Table 5.1, when ammonium hydroxide(AH) was used as precipitant, the ultimate Fe/Zn ratios of the catalysts changed between ~2.3-3.0. On the other hand, when sodium carbonate(SC) was used as precipitant, the Fe/Zn ratio decreased to a level of ~ 1.85-1.89 which was much closer to the stoichiometric ratio of zinc ferrite structure. These results can be interpreted as iron oxide compounds can be found in the 2Fe.Zn(AH) catalyst composition, apart from the zinc ferrite structure depending on the type of the precipitant.

When Na contents of the catalysts precipitated with sodium carbonate were examined, it was noticed that ~0.5% of sodium came to the final catalyst 2Fe.Zn (SC) composition due to the sodium content of the precipitant. Depending on washing level, the concentration of the residual sodium left over the precipitate changes. For example, while 2Fe.Zn0.2Na $(SC\text{-}I)_1$, 2Fe.Zn0.2Na $(SC\text{-}I)_2$, and 2Fe.Zn0.2Na $(SC\text{-}I)_3$ all have the same amount of sodium impregnation, their final sodium contents were quite different. Well washed sample, 2Fe.Zn0.2Na $(SC\text{-}I)_1$, has shown the least sodium content, namely 2.59%. However, much higher sodium content of 5.6% were measured over the catalyst, 2Fe.Zn0.2Na $(SC\text{-}I)_3$, when the washing step was quite poor. As long as the washing step eliminates all the residual sodium content coming from the precipitant, the more the sodium content of the catalyst get close to the actual amount of sodium impregnated on it. The comparison of 2Fe.Zn0.2Na (AH-I) and 2Fe.Zn0.2Na $(SC\text{-}I)_1$ has verified the effect of washing on the residual sodium content. 2Fe.Zn0.2Na (AH-I) and 2Fe.Zn0.2Na $(SC\text{-}I)_1$ catalysts were precipitated in the absence and presence of sodium cation, respectively. Thanks to a good washing process, sodium content of 2Fe.Zn0.2Na $(SC\text{-}I)_1$ was mostly due to impregnation.

The second point that should be remarked here is that if sodium is incorporated to the precipitation batch instead of impregnation, less sodium is fixed to the final catalyst matrix. For example, the sample 2Fe.Zn0.2Na (AH) had less sodium than their counterpart catalyst sample, 2Fe.Zn0.2Na (AH-I). This is reasonable since most of the sodium was lost within the sol during the filtration of the precipitate. However, since ionic medium of iron hydrolysis was shown to have an influence on the composition of the hydrolytic complexes, initially formed unstable products such as $Fe(OH)^{2+}$,

$Fe(OH)_2^+$, $Fe_3(OH)_4^{5+}$, and $Fe_2(OH)_2^{2+}$ might end up with the precipitation of a basic salt of probably polymeric nature[54]. These might change the morphology and size of the precipitates.

Table 5.1 : Iron, zinc, and sodium contents and Fe/Zn/Na ratios of fresh catalysts and carbon content of spent catalysts.

		Fresh catalyst				Spent catalyst
	Catalyst	Fe (%wt)	Zn (%wt)	Na (%wt)	Actual molar ratio of Fe/Zn/Na	C (%wt)
S1	2Fe.Zn (AH)	46.0	18.2	0	2.95/1/0	2.2
S2	2Fe.Zn0.1Na (AH-I)	49.9	20.1	1.55	2.90/1/0.21	14.0
S3	2Fe.Zn0.2Na (AH-I)	53.3	20.2	2.33	3.08/1/0.32	15.7
S4	2Fe.Zn0.2Na (AH)	46.5	23.6	0.42	2.30/1/0.05	5.5
S5	2Fe.Zn0.4Na (AH)	45.7	19.4	0.16	2.75/1/0.02	1.5
S6	2Fe.Zn (SC)	45.1	28.4	0.50	1.85/1/0.05	3.5
S7	2Fe.Zn0.2Na $(SC\text{-}I)_1$	39.2	24.3	2.59	1.88/1/0.30	2.2
S8	2Fe.Zn0.2Na $(SC\text{-}I)_2$	40.0	24.7	3.04	1.89/1/0.35	9.6
S9	2Fe.Zn0.2Na $(SC\text{-}I)_3$	39.7	24.5	5.60	1.89/1/0.64	19.8

XRD patterns of calcined fresh catalysts are given in Figure 5.1. In case of calcined fresh catalysts, diffraction peaks at 2θ= 30.37º, 35.5º, 42.9º, 53.6º, 57.09º, and 62.62º, assigned to a cubic spinel phase of $ZnFe_2O_4$ (JCPDS card No. 22-1012), were observed for all catalysts[55]. The formation of $ZnFe_2O_4$ phase with a cubic franklinite spinel-type structure for Fe_2O_3–ZnO precursors with Zn/Fe atomic ratios of > 0.2 has been reported by Li et al.[26]. XRD patterns of all samples had broad peaks due to their small crystallite size. The poor diffraction peaks, one with a 2θ value of 33° and the other at a 2θ value of 20° were observed for some catalysts, the former for 2Fe.Zn0.2Na (AH-I), 2Fe.Zn (SC), and 2Fe.Zn0.2Na $(SC\text{-}I)_3$ and the latter for 2Fe.Zn0.2Na (AH-I). These peaks were characteristics of α-Fe_2O_3 and ZnO crystal phases, respectively[50,51]. It is clear that these phases out of the zinc ferrite spinel phase might exist depending on the preparation routes.

XRD patterns of spent catalysts are given in the Appendix B. Obviously there are some low intensity peaks in the XRD patterns of the spent catalysts that might be attributed to carbide species. As frequently reported in the literature, iron carbide is characterized by many peaks of low intensity. For example, Abbas et al. [58] labeled the noise-like peaks between ~39-46° 2θ in the spent zinc ferrite catalysts as Hagg iron carbide

(Fe_5C_2) phases. In an another study by Yang et al.[59], the diffraction peaks at 2θ = 39.31°, 40.83°, 43.40°, 44.08°, and 47.18° were assigned to Fe_5C_2 phase (JCPDS, NO. 51-0997). Janbroers et al.[60] gave insights into the nature of iron-based Fischer–Tropsch catalysts from in situ XRD, a poorly crystalline iron carbide phase was characterized by diffraction lines at 2θ = 39.2°, 41.0°, 43.5° 46.8°, 58.5°, and 67.7°. Therefore, XRD did not seem to be an adequate technique for the accurate identification of iron carbide compounds in spent catalysts. Supplementary surface or in-situ characterization techniques like XPS, Mossbauer spectroscopy or in-situ XRD are needed to resolve this matter. The final point that should be remarked here that XRD peaks of zinc ferrite weakened upon reaction that might be due to the formation of amorphous carbon layer or change of iron phases.

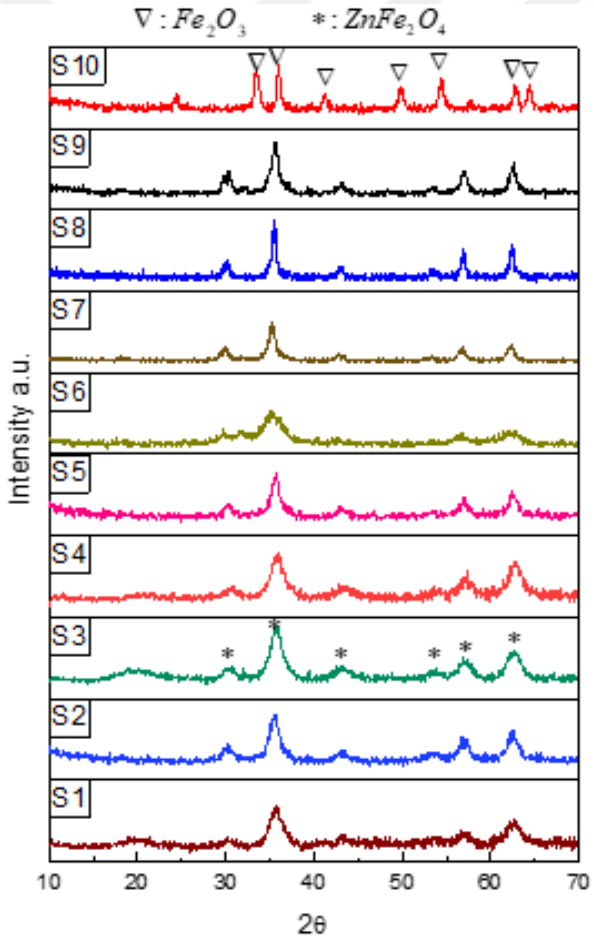

Figure 5.1 : XRD patterns of Na-promoted fresh calcined catalysts .S1= 2Fe.Zn (AH), S2= 2Fe.Zn0.1Na (AH-I), S3= 2Fe.Zn0.2Na (AH-I), S4= 2Fe.Zn0.2Na (AH), S5= 2Fe.Zn0.4Na (AH), S6= 2Fe.Zn (SC), S7= 2Fe.Zn0.2Na (SC-I)$_1$, S8= 2Fe.Zn0.2Na (SC-I)$_2$, S9= 2Fe.Zn0.2Na (SC-I)$_3$, S10=Fe(AH).

Crystallite size of the fresh catalysts calculated by Scherrer Equation were given in Table 5.2. Textural properties such as pore size and surface area and Fe/Zn ratios of the catalysts calculated by elemental mapping using energy dispersive spectroscopy (EDS) were reported in the same Table. It is noteworthy that the precipitation agent has a significant effect on the crystal size of zinc ferrite. In this context, it was clear that sodium carbonate gave zinc ferrite with smaller crystal size than ammonium hydroxide when the crystallite sizes of 2Fe.Zn(AH) and 2Fe.Zn(SC) were compared. The crystal growth can be induced by the precipitation agent in the solution where the size of nanoparticles can be modified by alkali concentration and ionic strength of aqueous medium [59]. Another thing worth mentioning is that when XRD pattern of iron oxide was compared with that of zinc ferrite, smaller crystal size of zinc ferrite than iron oxide was noticed. This suggests that zinc is a suitable structural promoter that could inhibit the growth of the iron oxide crystallite[54]. In the co-precipitation of zinc and iron salts, several parameters, such the counter ions, the ionic strength, pH, and precipitation temperature all might affect the ultimate physicochemical properties of zinc ferrites [48,49], i.e., smaller aggregates are formed at high pH values due to the high nucleation rates compared to the crystals formed at a lower pH [60] . This was further supported by Knight and Sylva [61], in their study increased basicity was directed the precipitation towards getting smaller crystallites during the synthesis of catalysts.

In this study, the type of the precipitant and ionic medium of hydrolysis were seen to impact the total surface area of zinc ferrite samples. The effect of ionic strength in the precipitation medium on the final zinc ferrite surface area was evident. For example, zinc ferrite with a higher surface area of 102 m^2/g was obtained as a result of precipitation with sodium carbonate, 2Fe.Zn (SC). For catalysts, 2Fe.Zn0.2Na (AH) and 2Fe.Zn0.4Na (AH), precipitated in the presence of both sodium and ammonium ions, a significant increase in surface area was observed compared to the catalyst, 2Fe.Zn (AH) which was precipitated only in the presence of ammonium ions. While surface area of 2Fe.Zn (AH) was 77 m^2/g, incorporation of sodium ion to the precipitation bath has led to an increase in surface area to 113 m^2/g for 2Fe.Zn0.2Na (AH).

On the other hand, the total surface area of the catalysts decreased and their crystal size increased upon sodium impregnation. This phenomenon was well observed for

the samples 2Fe.Zn (SC), 2Fe.Zn0.2Na $(SC\text{-}I)_1$, 2Fe.Zn0.2Na $(SC\text{-}I)_2$, and 2Fe.Zn0.2Na $(SC\text{-}I)_3$. Surface area and pore volume of the sample, 2Fe.Zn (SC), decreased from 102 m^2/g and 0.18 cm^3/g to 25 m^2/g and 0.06 cm^3/g, respectively when its sodium content increased from 0.5% to 5.6% via impregnation.

Table 5.2 : Textural properties and crystallite size of the catalysts and Fe/Zn ratios.

	Catalyst	Surface area (m^2/g)	Pore volume (cm^3/g)	Crystallite size (nm)	Fe/Zn calculated by EDS analysis
S10	Fe(AH)	72.3	0.23	17.4	-
S1	2Fe.Zn (AH)	77	0.10	4.7	3.2/1
S2	2Fe.Zn0.1Na (AH-I)	55	0.09	4.5	2.54/1
S3	2Fe.Zn0.2Na (AH-I)	52	0.06	7.8	2.88/1
S4	2Fe.Zn0.2Na (AH)	113	0.14	4.8	2.39/1
S5	2Fe.Zn0.4Na (AH)	91	0.17	6.2	2.99/1
S6	2Fe.Zn (SC)	102	0.18	2.9	1.75/1
S7	2Fe.Zn0.2Na (SC-I)1	41	0.11	7.9	1.72/1
S8	2Fe.Zn0.2Na (SC-I)2	39	0.11	7.2	1.23/1
S9	2Fe.Zn0.2Na (SC-I)3	25	0.06	10.7	na

The SEM images, elemental mappings and EDS analysis for 2Fe.Zn(AH) and 2Fe.Zn(SC) were used for comparison whereas those for remaining were provided in Appendix A. Figure 5.2 shows SEM micrographs of 2Fe.Zn (AH) and 2Fe.Zn (SC) catalysts together with elemental mappings for iron and zinc. A rough zinc ferrite surface was distinguished, which was not plate-like. Although the effect of the precipitation agent on the surface morphology was not very obvious, it was noticed that sample 2Fe.Zn(SC) looks like somewhat similar to an eroded sponge with some small holes and cavities. On the other hand, smoother surfaces were more prominent for 2Fe.Zn (AH) catalyst. All catalysts with or without sodium based precipitant were calcined at 400 °C to avoid agglomeration. This is probably why smaller grains in less spherical morphology were obtained due to incomplete reaction between iron hydroxide and zinc hydroxide to give zinc ferrite. When the bulk and EDS chemical analysis were evaluated together, it was apparent that the samples precipitated without sodium has an iron content more than the stoichiometric amount of zinc ferrite structure. For example, Fe/Zn ratio of 2Fe.Zn(AH) were calculated as 2.95-3.2 based on ICP or EDS analysis however, those values for 2Fe.Zn(SC) were 1.75-1.85. These results were interpreted as iron oxide compounds can be found in the 2Fe.Zn(AH) catalyst composition, apart from the zinc ferrite structure. Elemental mapping confirmed that the lumps observed in the SEM images were predominantly iron and zinc species.

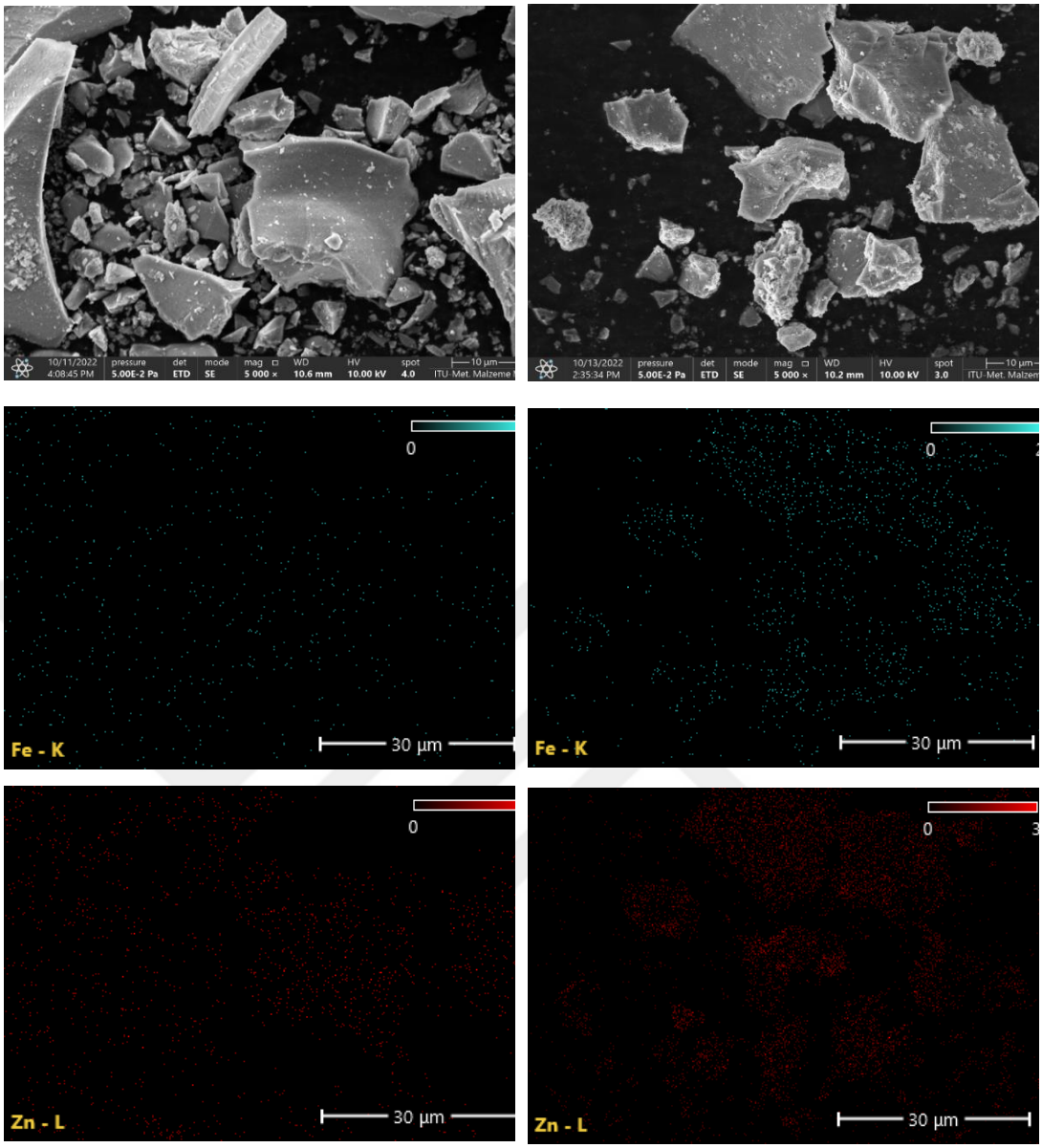

Figure 5.2 : SEM micrographs of S1: 2Fe.Zn (AH) and S6: 2Fe.Zn (SC) catalysts together with elemental mappings for iron and zinc. On the left: 2Fe.Zn (AH) and on the right: 2Fe.Zn (SC).

The results of TPR analysis of catalysts are presented in Figure 5.3 which shows the removal profile of lattice oxygen atoms from zinc ferrite in sodium free and sodium laden forms using H_2 as the reductant. Three different reduction zones are distinguished in temperature regions of: 300-450 °C, 450-575 °C and 575-800 °C [62]. The peak centered at around 300-450 °C associates with the formation of magnetite phase ($Fe_2O_3 \rightarrow Fe_3O_4$) while the second broad peak extending to 800 °C corresponds to the transition region from Fe_3O_4 to FeO[63] . Since FeO (wustite) is known to be unstable below 570 °C, α-Fe and Fe_3O_4 phases may also exist due to FeO disproportionation reaction. 2Fe.Zn(SC), 2Fe.Zn(AH), 2Fe.Zn0.2Na (AH), and

2Fe.Zn0.4Na (AH) had very similar TPR profiles. It was clear that their poor TPR peaks indicate that $ZnFe_2O_4$ was much more persistent to reduction compared to Fe_2O_3. Changing the ionic strength in the precipitation bath by incorporating sodium and ammonium ions together as for 2Fe.Zn0.2Na (AH), and 2Fe.Zn0.4Na (AH) samples, a slight decrease in the initial reduction temperature of Fe_2O_3 to Fe_3O_4 was seen as compared to 2Fe.Zn(AH). Since there is a significant difference between the solubility constant of $Fe(OH)_3$ and that of $Zn(OH)_2$, some $Zn(OH)_2$ could partially be in dissolved phase while all Fe^{3+} ions were completely precipitated in the alkaline environment. Change in ionic strength may have an impact on this phenomenon.

Therefore, we can consider the purity of $ZnFe_2O_4$ nanoparticles would be affected as noticed from altered TPR profile with changing alkaline environment. So dopant material i.e. an alkali metal added by impregnation, can significantly modify the reduction behavior of the catalysts. This was observed in patterns of 2Fe.Zn (SC), 2Fe.Zn0.2Na $(SC\text{-}I)_1$, 2Fe.Zn0.2Na $(SC\text{-}I)_2$, and 2Fe.Zn0.2Na $(SC\text{-}I)_3$ catalysts all precipitated with sodium carbonate but containing different amounts of sodium. In the profile of 2Fe.Zn (SC) catalyst with least amount of sodium and the smallest iron oxide crystal size, the first peak is indistinct and its maximum occurred at around 330 °C. Similarly, the first peaks of 2Fe.Zn0.2Na $(SC\text{-}I)_1$, 2Fe.Zn0.2Na $(SC\text{-}I)_2$, and 2Fe.Zn0.2Na $(SC\text{-}I)_3$ catalysts shifted to the right with their maximums displayed at 380 °C, 390 °C and 420 °C, respectively, in accordance with their increasing sodium content.

These results are in agreement with that of An et al.[64] who investigated the effect of the residual sodium on the reduction and carburization behavior of iron based catalysts and observed that the first stage reduction peak shifted to higher temperature with increasing the residual sodium content. This was claimed to be associated with the textural properties of the catalyst and was attributed to the changing iron oxide crystallite size in the presence of sodium. They also reported that surface areas of the catalysts decreased and the crystal size increased with increasing sodium concentration as a result of the poor dispersion. Since the reduction sequence can depend on the crystallite size and the crystallographic form for a given oxide, iron oxides in close contact with sodium may have different chemisorptive properties that may induce the reduction sequence. Therefore, the presence of three peaks observed in the TPR profile of 2Fe.Zn0.2Na $(SC\text{-}I)_3$ seems reasonable, which has the largest crystal size among

the catalysts compared. Finally, the completion of the reduction reactions at a lower temperature in 2Fe.Zn (AH) catalyst prepared with ammonium hydroxide (sodium-free precipitant) than in the 2Fe.Zn (SC) catalyst prepared with sodium carbonate supports this argument. This may be due to sodium ions remained in the catalyst as previously discussed. These finding are in line with previous studies declaring that the preparation method of iron oxide catalysts can considerably affect their reduction behavior due to the different structural properties and morphologies [65].

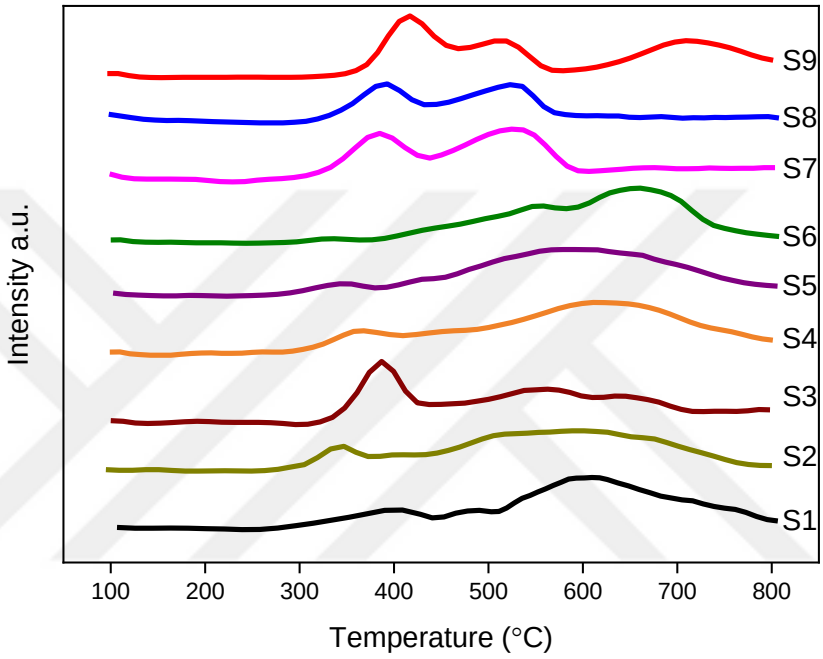

Figure 5.3 : H_2-TPR profile of Na- promoted calcined catalysts. S1= 2Fe.Zn (AH), S2= 2Fe.Zn0.1Na (AH-I), S3= 2Fe.Zn0.2Na (AH-I), S4= 2Fe.Zn0.2Na (AH), S5= 2Fe.Zn0.4Na (AH), S6= 2Fe.Zn (SC), S7= 2Fe.Zn0.2Na (SC-I)$_1$, S8= 2Fe.Zn0.2Na (SC-I)$_2$, S9= 2Fe.Zn0.2Na (SC-I)$_3$.

The surface basicity exhibited by zinc ferrites with or without sodium impregnation was studied by CO_2-TPD. The results are shown in Figure 5.4. TPD peaks were observed in three different temperature zones: 100-150 °C, 350-525 °C, and 550-800 °C. Since the surface basicity of the catalysts mainly comes from Na_2O over the catalyst surface, all sodium-impregnated catalysts appear to have an overall surface basicity.

It is noteworthy that the zinc ferrite catalyst precipitated with ammonium hydroxide in the absence of sodium, 2Fe.Zn (AH), has shown slight surface basicity. Therefore, it would be helpful to discuss first from where the basicity of the catalysts without sodium comes. As discussed by Yang et al.[22], the addition of Zn might bring some

basicity due to the strong interaction between Zn and Fe in the lattice spinel structure as with 2Fe.Zn (AH). On the other hand, the addition of sodium nitrate to the ammonium hydroxide precipitation bath did not increase the surface basicity, and even led to a lesser surface basicity. Less basicity over 2Fe.Zn0.2Na (AH) and 2Fe.Zn0.4Na (AH) compared to 2Fe.Zn (AH) may have been observed due to the altered precipitation equilibria in the presence of additional sodium and nitrate ions.

TPD peaks are more visible for sodium impregnated catalysts, 2Fe.Zn0.1Na (AH-I), 2Fe.Zn0.2Na (AH-I), 2Fe.Zn0.2Na $(SC\text{-}I)_1$, 2Fe.Zn0.2Na $(SC\text{-}I)_2$ and 2Fe.Zn0.2Na $(SC\text{-}I)_3$. As reported in the literature[66], CO_2-TPD desorption profiles of most basic metal oxides, such as magnesium or aluminum oxide, consist of three distinct basic groups: the weak basic surface OH groups, Lewis acid–base sites of medium strength, and low-coordination oxygen anions of strong basicity. The first groups are a kind of quite labile bicarbonate surface species formed on the surface hydroxyl groups [67]. The second groups may be ascribed to CO_2 interaction with the surface basic sites likely through a variety of bidentate carbonates. They might display stability of different degrees due to the oxygen exchange between adsorbed carbon dioxide and the surface of metal oxides[62, 63]. Therefore, they may produce more than one peak. The third class might be unidentate carbonates requiring low-coordination O_2^- anions as argued by Di Cosimo et al.[67] and Aziz et al.[66].

Evaluation of Figure 5.4, noticeably indicates the surface basicity for all sodium-impregnated catalysts in all groups. A weak peak at around 100-150 °C is common for all catalysts and may be simply assigned to the labile bicarbonate species. As the amount of impregnated sodium increases, the high temperature peak, which is the indicator of the strongest surface basic sites, shifts to the right irrespective of the precipitating agent. As the number and strength of the surface basicity increases, the coke formation during FT reaction increases as well. In this regard, it is of interest to compare the results of catalysts 2Fe.Zn0.2Na (AH-I) and 2Fe.Zn0.2Na$(SC\text{-}I)_1$ prepared with different precipitants but having nearly the same bulk sodium content. 2Fe.Zn0.2Na (AH-I) has produced more intense peak in the high temperature zone as seen in Figure 5.4. Its peak temperature is 690 °C while that of 2Fe.Zn0.2Na$(SC\text{-}I)_1$ is about 633 °C. These differences may be attributed to differences in the dispersion degrees of sodium species in the catalysts. Dispersions of the alkali metals seem to be influenced by the surface basicity [22]. The results suggest that 2Fe.Zn0.2Na (AH-I)

has a better sodium dispersion than 2Fe.Zn0.2Na(SC-I)$_1$. Although these two catalyst have similar chemical compositions, the amount of carbon formed during their FT reactions was significantly different, 15.7% for 2Fe.Zn0.2Na (AH-I) and 2.2% for 2Fe.Zn0.2Na(SC-I)$_1$ as reported in Table 5.1. Much higher coking tendency of 2Fe.Zn0.2Na (AH-I) upon FT reaction supports the argument that both the number of basic sites and strength impact the coke formation.

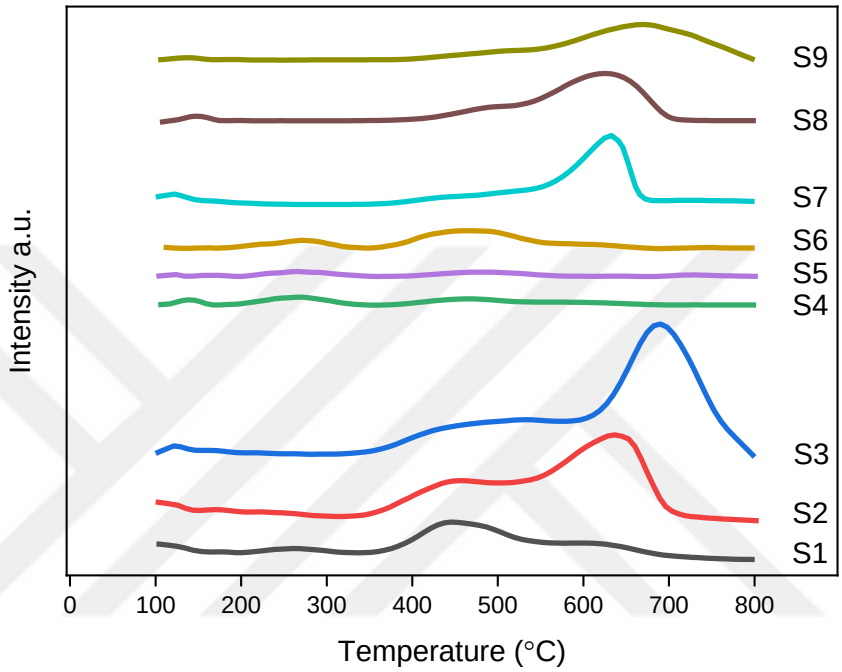

Figure 5.4 : CO_2-TPD profile of reduced Na-promoted catalysts.S1= 2Fe.Zn (AH), S2= 2Fe.Zn0.1Na (AH-I), S3= 2Fe.Zn0.2Na (AH-I), S4= 2Fe.Zn0.2Na (AH), S5= 2Fe.Zn0.4Na (AH), S6= 2Fe.Zn (SC), S7= 2Fe.Zn0.2Na (SC-I)$_1$, S8= 2Fe.Zn0.2Na (SC-I)$_2$, S9= 2Fe.Zn0.2Na (SC-I)$_3$.

5.1.1.2 Characterization of K- and Cu- promoted bulk catalysts

In this part of the study the results of the K- and Cu-promoted catalysts will be presented and discussed. Copper, potassium and sodium content of K and Cu promoted bulk catalysts are given in Table 5.3. Besides, iron and zinc content of Fe.Zn (AH) catalyst were checked by chemical analysis to determine the actual iron to zinc molar ratio. Although all catalysts were initially prepared with the same synthesis batch having stoichiometric amounts of iron and zinc salts to obtain catalysts with a molar Fe/Zn = 2, the resulting base catalyst Fe.Zn (AH) was found containing 37.8 wt% Fe and 16.6 wt% Zn. This composition fit to a final Fe/Zn molar ratio of ~2.6. The higher Fe content was the indicative of the coexistence of different iron oxide phases alongside of $ZnFe_2O_4$. From examination of Na contents of the catalysts precipitated

with sodium carbonate(SC), it was noticed that ~0.5% of sodium in the final base 2Fe.Zn (SC) catalyst resulted from sodium carbonate precipitant (SC). It appears that potassium promoter led severe coking compared to sodium. Moreover, copper seemed to have a stabilization effect giving the least coke among them.

Table 5.3 : Cu, K, and Na content of fresh catalysts and carbon content of spent catalysts.

Code	Catalyst	Cu(%)	Na(%)	K(%)	C(%)
S1	2Fe.Zn (AH)	0	0	0	2.2
L1	2Fe.Zn0.2Cu (AH-I)	6.8	0	0	1.7
L2	2Fe.Zn0.2K (AH-I)	0	0	4.1	20.1
L3	2Fe.Zn0.2Cu0.05K (AH-I)	9.5	0	1.4	17
S6	2Fe.Zn (SC)	0	0.5	0	3.5
L4	2Fe.Zn0.2K (SC-I)	0	0.3	3.1	16.3

XRD patterns of calcined fresh K- and Cu- promoted catalysts are given in Figure 5.5. Their crystal sizes calculated by Scherer equation are reported in Table 5.4. Diffraction peaks at $2\theta = 30.37^{o}$, 35.5^{o}, 42.9^{o}, 53.6^{o}, 57.09^{o}, and 62.62^{o}, in XRD patterns of calcined catalyst assigned to a cubic spinel phase of $ZnFe_2O_4$ (JCPDS card No. 22-1012), were observed for all catalysts [55] .

The formation of $ZnFe_2O_4$ phase with a cubic franklinite spinel-type structure for Fe_2O_3–ZnO precursors with Zn/Fe atomic ratios of > 0.2 has been reported by Li et al.[26]. XRD patterns of all samples displayed broad peaks due to small crystallite size except 2Fe.Zn0.2K (SC-I) with relatively narrower peaks. It is noteworthy that the precipitation agent has a significant effect on the crystal size of zinc ferrite. As previously mentioned (in part 5.1.1.1.) and the comparative evaluation of XRD patterns of base 2Fe.Zn(AH) and 2Fe.Zn(SC) catalysts, the synthesis with sodium carbonate (SC) gives structures with smaller crystal size than that by ammonium hydroxide. It is well known that the crystal growth can be induced by the precipitation agent in the solution where the size of nanoparticles can be manipulated by alkali concentration and ionic strength of aqueous medium [61]. In 2Fe.Zn0.2K (SC-I) catalyst, high alkali strength of the catalyst comes from both precipitation agent (SC) and impregnated potassium and leads to the growth of crystallites (9.4 nm). In XRD pattern, any peak that is indicative of K or Cu oxide was not detected probably due to trace amount of these promoters.

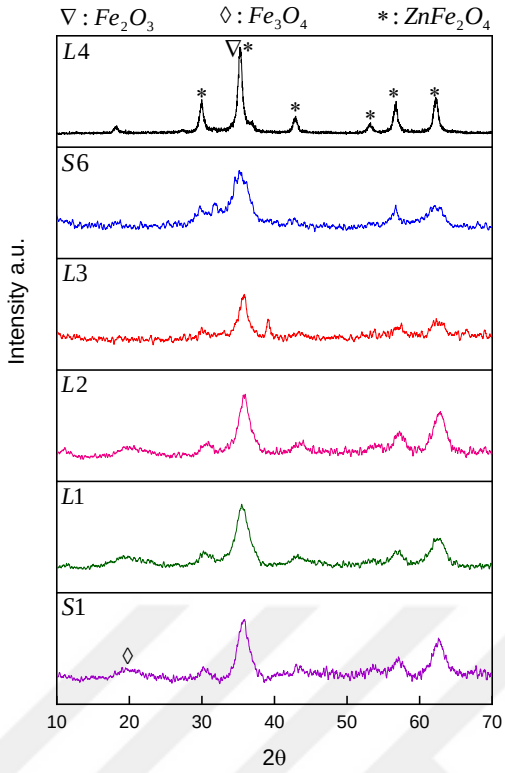

Figure 5.5 : XRD patterns of unpromoted and K- and Cu-promoted fresh bulk 2Fe.Zn (AH) and 2Fe.Zn(SC) catalysts. S1: 2Fe.Zn (AH), L1: 2Fe.Zn0.2Cu (AH-I), L2: 2Fe.Zn0.2K (AH-I), L3: 2Fe.Zn0.2Cu0.05K (AH-I), S6: 2Fe.Zn (SC), L4: 2Fe.Zn0.2K (SC-I).

It is also reported by Farias et al. [70] that as the potassium content in the catalyst increased, BET surface area decreased. This may be caused by the formation of larger hematite crystallites that are promoted by potassium. Dry and Oosthuizen [71] had similar conclusion that increase in the Fe crystallite size may result in a decrease in the BET surface area due to the presence of strong bases like potassium.

XRD patterns of spent catalysts were also evaluated and are given in Appendix B2. The peaks at $2\theta = 20.82^o$, 26.62^o, 36.52^o, 50.1^o and 60^o were the main peaks coming from the used samples contaminated with significant amount of quartz since quartz was used for the dilution of the catalyst to prevent hot spots [72] . It was observed that XRD peaks of zinc ferrite became weaken upon reaction. The presence of Fe_2O_3 and Fe_3O_4 peaks were checked in order to understand if there had been any change in the crystal phase. The most intense peak of α-Fe_2O_3 phase at 33.29^o corresponding to (104) plane was barely noticeable. On the other hand, the peak of Fe_3O_4 phase at 35.6^o corresponding to 311 plane was hard to be distinguished since it overlapped with the characteristic peak of zinc ferrite at the same crystal plane. The characteristic peaks in the range of $2\theta = 43^o - 45^o$ assigned to iron carbide phases of both Fe_3C and Fe_5C_2, were not clearly visible in the XRD patters except for that of 2Fe.Zn0.2K (AH-I),

2Fe.Zn0.2Cu0.05K (AH-I), and 2Fe.Zn0.2K (SC-I). Sharper carbide peaks exist in XRD patterns of these three catalysts were probably due to the effect of their potassium concentration. This effect was not observed for the potassium-free samples. It has been suggested that potassium promotes the CO activation and the rate of carburization of Fe_3O_4 [26] which leads to higher iron carbide formation. For all these samples, namely 2Fe.Zn0.2K (AH-I), 2Fe.Zn0.2Cu0.05K (AH-I), and 2Fe.Zn0.2K (SC-I), potassium was post impregnated and all have shown the highest olefin selectivity up to 45% (Table 5.9). This potassium promoted catalysts were the samples which were much heavily fouled by carbon deposition as it is apparent from their high carbon content given in Table 5.3. However, the Cu- promoted catalyst, 2Fe.Zn0.2Cu (AH-I), has shown very low olefin selectivity (5.6%) but attained the highest stability (93.7 % CO Conversion). The high stability is compatible with subtle deactivation and low carbon content (1.7%) of the spent catalyst.

2Fe.Zn0.2Cu0.05K (AH-I) was the catalyst simultaneously promoted with both K and Cu in order to observe the effect of co-existence of K and Cu promoter. High olefin selectivity of 45% was preserved by only 0.05 mole ratio of potassium in relation to 2Fe.Zn0.2Cu(AH-I). This has shown the effect of alkalinity strength on olefin selectivity.

Textural properties of promoted catalysts alongside with that of the two base catalyst, 2Fe.Zn(AH) and 2Fe.Zn(SC), are presented in Table 5.4. The type of the precipitant and ionic medium of hydrolysis appeared to be effective on the total surface area of zinc ferrite samples.

Potassium incorporation has decreased the surface areas and increased the crystal sizes of both base catalysts, 2Fe.Zn(AH) and 2Fe.Zn (SC), as seen in Table 5.4. Changes in the textural properties were larger for catalyst prepared with ammonium hydroxide, 2Fe.Zn(AH). Its surface area decreased 54% and pore volume decreased 40% on addition of K. The simultaneous presence of K and Cu, however, induced a lower drop in surface area (28%) while similar drop (40%) in pore volume. On the other hand, 31% and 22% drops were observed in the surface area and pore volume of 2Fe.Zn (SC), respectively, as its alkali content (sodium+ potassium) increased from 0.5% to 3.4% via impregnation. Adding of Cu did not cause any noticeable change in the surface area and pore volume of 2Fe.Zn(AH) catalyst but slightly decreased its crystallite size.

Table 5.4 : Textural properties and crystallite size of unpromoted and K- and Cu-promoted fresh bulk 2Fe.Zn (AH) and 2Fe.Zn(SC) catalysts.

Code	Catalyst	Surface area (m^2/g)	Pore volume (cm^3/g)	Average pore diameter (A)	Crystallite size(nm)[a]
S1	2Fe.Zn (AH)	77.0	0.10	52.3	4.7
L1	2Fe.Zn0.2Cu (AH-I)	77.6	0.11	57.0	3.9
L2	2Fe.Zn0.2K (AH-I)	35.4	0.06	70.4	4.3
L3	2Fe.Zn0.2Cu0.05K (AH-I)	55.5	0.06	50.0	5.7
S6	2Fe.Zn (SC)	102.0	0.18	71. 4	2.9
L4	2Fe.Zn0.2K (SC-I)	70.6	0.14	54.3	9.4

[a] : Crystallite size of calcined catalysts from XRD data estimated by Scherrer equation, $2\theta=35.6^o$.

Figure 5.6 shows the H_2-TPR profiles of K- and Cu- promoted catalysts in sodium free and sodium laden forms. Three different reduction zones are noteworthy with a rough estimation: 300-450 °C, 450-600 °C and 600-800 °C [73]. As widely reported in the literature, the peak centered at around 300-450 °C can be attributed to the formation of magnetite phase ($Fe_2O_3 \rightarrow Fe_3O_4$) while the second peak extending to 600 °C corresponds to the region where the Fe_3O_4 to FeO transformation takes place [63]. The TPR analysis has been performed up to 850 ^oC. The third peak at temperatures 600 - 800 °C may be assigned to the transition of FeO to Fe^o. Base catalysts prepared with sodium carbonate, 2Fe.Zn(SC), and ammonium hydroxide, 2Fe.Zn(AH), displayed similar TPR profiles.

The second peak assigned to the reduction of Fe_3O_4 to FeO occurred at 600 ^oC for the base 2Fe.Zn (AH) catalyst while it moved to a lower temperature, 435 ^oC, on Cu inclusion as seen in the profile of 2Fe.Zn0.2Cu (AH-I). This results indicate that the presence of Cu facilitated the reduction of Fe_3O_4 to FeO in the catalyst. This was also reported by O. James et al. that the first stage reduction temperature lowers by adding Cu to Fe.Zn catalysts [74]. The presence of Cu appeared to considerably enhance the reduction reaction of FeO to $Fe^{o.}$ as· by the reduction temperature decreased from ~ 850 ^oC in 2Fe.Zn (AH) to 750 ^oC in 2Fe.Zn0.2Cu (AH-I) catalyst. This change in the reduction behavior of Fe.Zn catalysts by addition of Cu may results from the nucleation of Cu crystallites formed through CuO to Cu process which provides dissociation sides for H_2. So-formed reactive hydrogen species, on the other hand, are able to reduce iron oxide at lower temperatures [26].

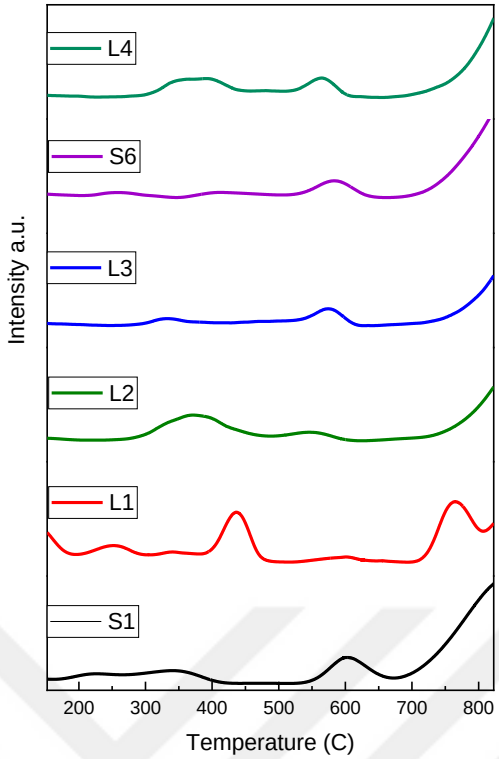

Figure 5.6 : H_2-TPR profile of unpromoted and K- and Cu-promoted fresh bulk 2Fe.Zn (AH) and 2Fe.Zn(SC) catalysts. S1: 2Fe.Zn (AH), L1: 2Fe.Zn0.2Cu (AH-I), L2: 2Fe.Zn0.2K (AH-I), L3: 2Fe.Zn0.2Cu0.05K (AH-I), S6: 2Fe.Zn (SC), L4: 2Fe.Zn0.2K (SC-I).

The TPR pattern of 2Fe.Zn0.2K (AH-I) catalyst indicated that addition of K delayed the reduction of Fe_2O_3 to Fe_3O_4 in the base 2Fe.Zn (AH) catalyst. The temperature of peak represented this reaction shifted from 350 ^oC to 375 ^oC after K was included. It also seemed to weakly inhibits the reduction of FeO to Fe^o at higher temperatures. These results are in line with the study of Li et al. [26].

The pattern of simultaneously K-and Cu-promoted 2Fe.Zn0.2Cu0.05K (AH-I) catalyst, is similar to that of the base catalyst 2Fe.Zn (AH). Although Cu has facilitating effect on the reduction of iron oxides species [74], it seems that its effect was largely counterbalanced by the retarding effect of K, resulting in no visible change in the TPR pattern of the catalyst.

Comparison of the patterns of the base 2Fe.Zn (SC) and the K-promoted in 2Fe.Zn0.2K (SC-I) catalyst, revealed that K has slightly retarded the reduction of the Fe_2O_3 to Fe_3O_4 as indicated by the maximum peak temperature of 2Fe.Zn (SC) increased from ~350 ^oC to ~380 ^oC. Similar to the case of base catalyst prepared with AH, the reduction of FeO to Fe^o seemed to be also slightly inhibited by K. The

maximum peak temperatures in last reduction stage, however, were not reached up to 850 ^{o}C for both 2Fe.Zn (SC) and 2Fe.Zn0.2K (SC-I) catalysts.

2Fe.Zn0.2K (AH-I) and 2Fe.Zn0.2K (SC-I) catalyst obtained by potassium impregnation of 2Fe.Zn (AH) and 2Fe.Zn (SC) base catalysts, respectively, have similar TPR profiles although their total alkalinity is slightly different, the former with 4.1% and the later with 3.4%.

Overall evaluation of H_2-TPR profiles of the Cu and K promoted bulk catalysts indicates that presence of copper can facilitate the reduction of iron oxides while potassium with its strong alkali nature may retard these reduction reactions.

The results of TPR and textural analyses of catalysts appeared to be in agreement. Addition of potassium increased the surface area and crystallite size of the base catalyst prepared with sodium carbonate, 2Fe.Zn(SC), ~ 30% and ~3 times, respectively. Since the reduction sequence can depend on the crystallite size and the crystallographic form for a given oxide, iron oxides in close contact with K may have different chemisorptive properties that may induce the reduction sequence.

5.1.2 Characterization of activated carbon and modified activated carbon supported catalysts

In the other part of this study, activated carbon supported iron catalysts have been synthesized, characterized and tested. Commercial activated carbon and its modified form by nitrogen doping (AC and N-doped AC) have been used as the catalyst support. HNO_3, NH_3, and urea were used as N source (dopants) for modification of AC. N-doped carbon might contribute to the catalytic performance since nitrogen content of the catalyst may act as an electron donor and induce interaction between iron-zinc nanoparticles and N-doped carbon towards improving the final textural properties of the catalyst [31, 57]. The supported catalysts have been characterized both before and after FT reaction as explained in section 5.1.1.

5.1.2.1 Characterization of supports (AC and N-doped AC)

In order to investigate the effect of nitrogen addition to the activated carbon supports, characterization has been performed on the supports before metal loading. The results obtained have been evaluated below. By using elemental analysis, % N content of each N-doped support has been determined. Brunauer-Emmett-Teller analysis (BET) to

have total surface areas have been determined by N_2-adsorption. The pore volume and average pore size distribution were calculated by Barret–Joyner–Hallender (BJH) method. Results of nitrogen and BET surface areas analyses of AC and modified AC are given in Table 5.5.

The original AC has 0.74 %N. After nitrogen doping by HNO_3, NH_3, and Urea, the amount of nitrogen in AC increased to 1.15%,1.16%, and 2.02%, respectively. The surface area (S_{BET}) of AC (702.4 m^2/g) increased 12.9%, 4.4%, and 4.9% after N-doping in AC-N_1, AC-N_2, and AC-N_3, respectively. Nitrogen doping, however, did not significantly change the pore volume and average pore diameter of AC. It can be said that nitrogen was introduced into AC matrix although not to a high extend.

Table 5.5 : Amount of nitrogen and textural properties of activated carbon (AC) and the nitrogen-doped activated carbon (N-doped AC).

Catalyst support	N (%)	Surface area (m^2/g)	Pore volume (cm^3/g)	Average pore diameter (A^o)
AC	0.74	702.4	0.73	41.3
AC-N_1	1.15	793.1	0.76	38.5
AC-N_2	1.16	734.9	0.75	41.2
AC-N_3	2.02	738.8	0.74	40.2

Figure 5.7 illustrates the results of thermogravimetric (TG) and derivative thermogravimetric (DTG) analyses of support materials. The figure also includes all TGA data in a single graph for comparison. In order to assure the changes are assigned to the effect of N-doping not only due to high temperatures, AC was heat treated under N_2 (0.3 L/h) atmosphere at 500 °C by heating ramp of 6 °C.min^{-1} and kept at 600 °C for 2 h followed. As the catalysts would work at 400 ^oC, TG analyses of catalyst supports were conducted till 750-800 ^oC in order to investigate their thermal stability. Higher temperatures beyond 800°C were not investigated.

Three steps of weight loss were observed in almost all samples though the third stage was not completed till investigated temperature range was up to 800 ^oC. The first weight change was ascribed to physically adsorbed moisture in between 30 and 130 °C. The weight loss in this region in AC-N_1, AC-N_2, AC-N_3, and AC, graph was 0.8%, 3.7%, 2.4%, and 6% respectively.

The initial temperature is known as the temperature which material starts to decompose. The maximum weight loss point defines the oxidation temperature (Peak

in DTG vs. T). In all TGA graphs of this work, oxidation temperature supposedly occurs in higher temperatures beyond 800-850 °C.

In the TG graph of AC-N_1 (Figure 5.7a), upon moisture removal completed at 125°C, a second region with a weight loss of 2% has been observed as in plateau laying from 130 to 630 °C. Then an accelerated weight loss region starting from 630 °C has been noticed with a narrow temperature band which was up to 843 °C. The initial temperature of this final stage has been known as the decomposition temperature and here a 2.5% of weight loss has been recorded. In the TG graph of AC-N_2 (Figure 5.7b), upon completion of the initial moisture removal, there was 2% weight loss in the temperature ranging from 130 to 730°C. The decomposition temperature was 730 °C. In its decomposition region up to 830 °C, only 0.5% weight loss has been observed. In the last case for AC-N_3(Figure 5.7c), a similar TGA profile with those of AC-N_1 and AC-N_2 has been received. In the second weight loss plateau of this sample, a weight loss of 2.5% has been noticed in between 130 °C and 530 °C. However, its decomposition temperature was quite low as of 530 °C in comparison with the others. Its weight loss in the decomposition region has been extended to 740 °C with a weight loss of just 0.7%. For the base case, the TG graph of virgin AC (Figure 5.7d) has been evaluated for comparison under the same conditions. It means, AC has been thermally pretreated at 500 °C for 2 hours under N_2 atmosphere. The main point was that AC had the highest moisture content. Moreover, in spite of the fact that it had similar second weight loss and decomposition regions as between 130-530°C and from 530 to 793°C, respectively, remarkably much higher decomposition weight loss from 530 °C to 793° C has been observed as 24%. The weight loss of 4% before the main decomposition region as in between 130 and 530°C were also higher. Test results of TGA analyses of support materials are compared in Figure 5.7e. As seen in the figure, all modified AC have a lower weight loss than that of original AC in the temperature range applied. All this has shown that AC treated with a nitrogen agent gained thermal stability probably due to the modification of its surface functional groups. Nitrogen doping seems substituting surface carboxylic and phenolic groups with nitrogen containing ones such amides, or amines etc. This might lead to stabilize the surface functional groups towards its thermal decomposition [10]. On the other hand, the measurements on FT-IR did not gave interpretable result, therefore this potential

surface modification has not been supported with spectroscopic surface characterizations.

According to Rehman et al [44], different functional groups might be added to the surface of AC by acid treatment including by using carboxyl, lactone, phenol, and by base treatment by using ketone, chromene, and pyrones. In this study, the modification of AC done by HNO_3, NH_3 and urea addition may be considered as acid, base, and a weak base treatment. It can be elucidated that these nitrogen-enriched functionalities at the surface enhanced stability and retarded decomposition. These results are in line of that of Li et al. [39] who modified the surface of carbon Nano tubes (CNT's) by using nitric acid of different concentrations.

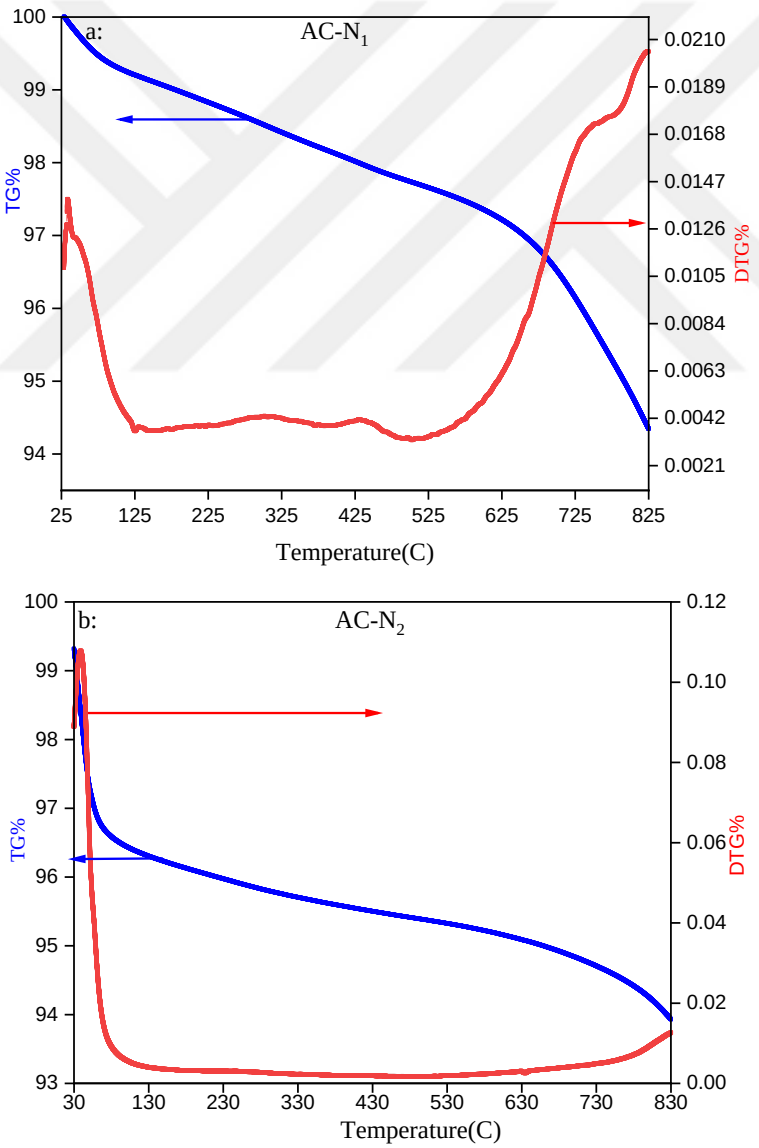

Figure 5.7 : TG % and DTG % curves of a: AC-N_1, b: AC-N_2, c: AC-N_3, and d: AC, e: TG of all supports in a single graph.

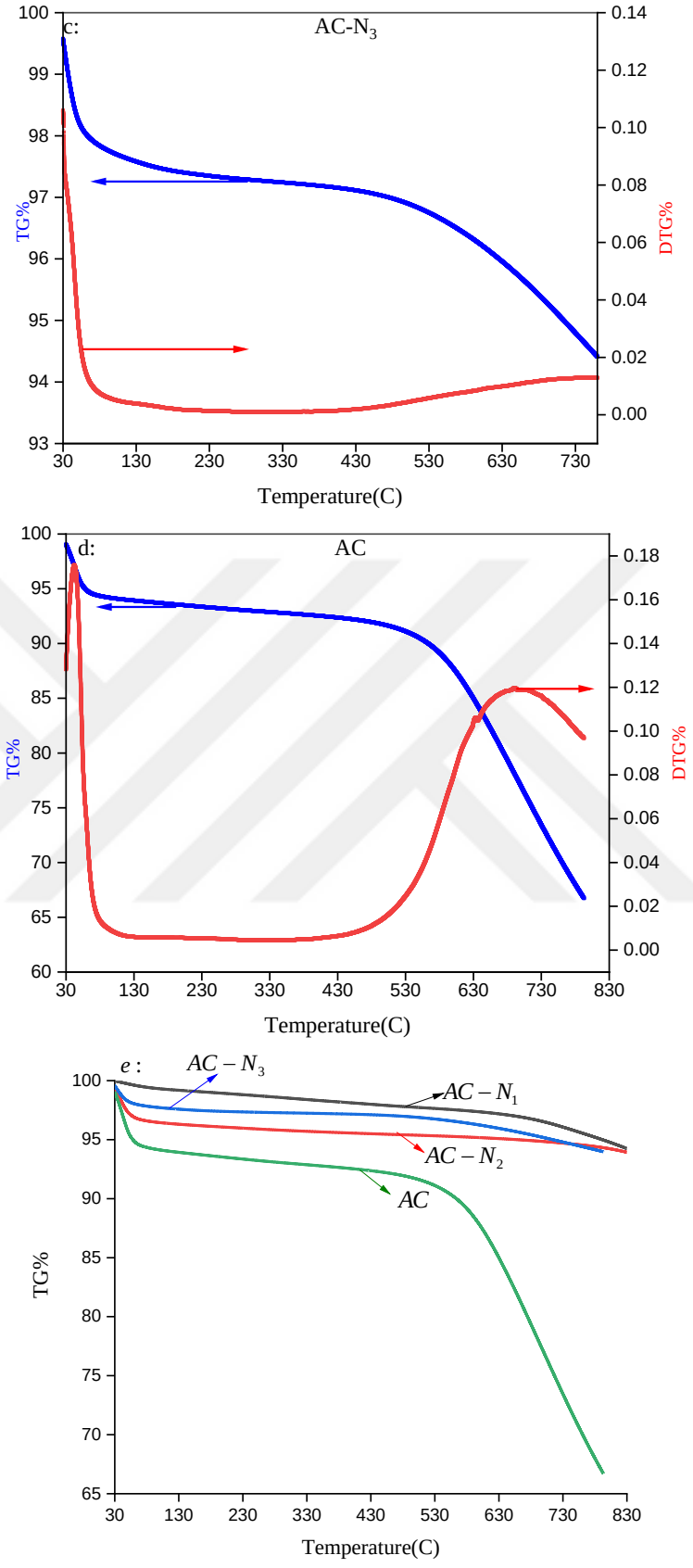

Figure 5.7 (continued) : TG % and DTG % curves of a: AC-N_1, b: AC-N_2, c: AC-N_3, and d: AC, e: TG of all supports in a single graph.

5.1.2.2 Characterization of supported catalysts

In this section, same characterization technique as section 5.1.1 was applied. The characterization of 7 supported catalysts were discussed in the following part.

ICP-OES

Iron and zinc content of the catalyst Fe.Zn.Na/AC-N_1 were checked by chemical analysis to see the actual iron to zinc molar ratio. All the catalysts were precipitated initially with the same synthesis batch in which iron and zinc salts existed in stoichiometric amounts for zinc ferrite structure (Fe to Zn molar ratio of 2). The ultimate composition for Fe.Zn.Na/ AC-N_1 catalyst was found to be 15.45 (% wt) iron and 8.83 (% wt) zinc which fit to a final Fe/Zn molar ratio of ~2.04. This is indicative of the formation of $ZnFe_2O_4$. The weight percent of promoters(Na/K) of the Fe.Zn.Na/ AC-N_1 and Fe.Zn.K/AC-N_1 catalysts is given in Table 5.6.

Table 5.6 : Na and K content of catalysts A1 and A2.

Code	Catalyst	Na/K(wt%)
A1	Fe.Zn.Na/ AC-N_1	Na: 0.67
A2	Fe.Zn.K/AC-N_1	K:0.86

XRD

The diffraction patterns (XRD) of the fresh and spent catalysts are shown in Figure 5.8 and Figure B.3 in Appendix B, respectively. In the pattern of fresh catalysts, diffraction peaks at 2θ= 30.2° , 35.4° ,43 °, 53.5°, 56.9°, and 62.4° are assigned to a cubic phase of spinel $ZnFe_2O_4$ (JCPDS card No. 22-1012)[55]. The peak at 2θ=25.9° is related to graphitic carbon [76]. Peaks at 2θ =34.62° and 36.36° that observed only in A1 catalyst are associated to ZnO [77]. The presence of the iron oxide phase, which does not take part in the zinc ferrite structure, was proved by the peaks occurred at 2θ=31.78^o and 35.34^o [21, 39]. As the peaks at 35.5° ascribed to Fe_2O_3 and $ZnFe_2O_4$ are very similar, therefore they may be assigned to both crystal phases.

Some low intensity peaks in the XRD patterns of the spent catalysts Figure B.3 in Appendix B that might be attributed to carbide species have been noticed. As frequently reported in the literature, iron carbide may be characterized by many peaks of low intensity in range of 37.76°- 49.13°[52, 53]. XRD pattern of spent catalysts showed low intense peaks at 2θ=42 – 45 ^{o} that are assigned to iron carbides. The main peaks at 2θ =20.82^o, 26.62^o, 36.52^o, 50.1^o and 60^o are attached to quartz. Quartz was

used for the dilution of the catalyst loaded to reactor to increase heat distribution[72]. Beside iron carbide, there is a diffraction peak of 55° that might be ascribed to a pure rhombohedral phase of α-Fe_2O_3 [26].The peak at 67.8º is assigned to Fe_2O_3 [59, 69]. Iron oxide is observable in spent catalysts. During reduction , addition of sodium probably preserves the iron oxide phases in the bulk of catalysts [22]. Furthermore, it may be the result of re-oxidation of the iron carbide phase [63]. XRD, however, did not seem an adequate technique for the accurate identification of iron carbide compounds in none of the spent catalysts of this study. Supplementary surface or in-situ characterization techniques like XPS, Mossbauer spectroscopy or in-situ XRD are needed to resolve this matter.

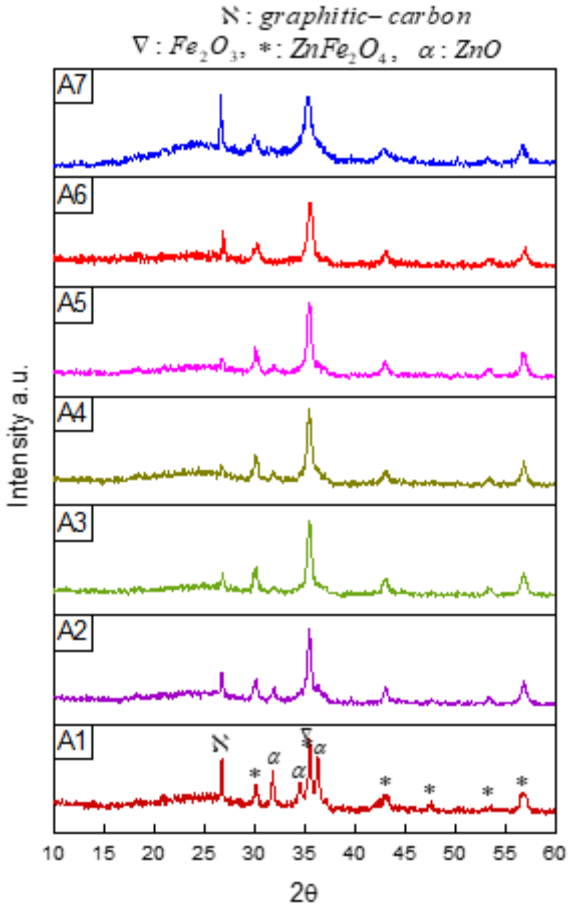

Figure 5.8 : XRD patterns of fresh calcined A1-A7 catalysts.A1=Fe.Zn. Na/AC-N_1, A2=Fe.Zn.K/ AC-N_1, A3=Fe.Zn.Na/ AC-N_2, A4=Fe.Zn.K/ AC-N_2, A5=Fe.Zn.K/ AC-N_3, A6=Fe.Zn.Na/AC, A7=Fe.Zn.K/AC.

BET

The textural properties of supported catalysts, A1-A7, are listed in Table 5.7. When metals are co-impregnated to the supports, the surface areas of the supports decreased

in all of the catalysts A1-A7. The surface areas of the supports varied in the range of 700-800 m^2/g. As seen in the table, surface areas of catalysts (Table 5.7) are smaller than that of their support materials (Table 5.5). After metal loading the surface areas of supports decreased to about 400-500 m^2/g. Obviously impregnation of metals blocks a part of pores and led to decrease in surface area. Similar results are reported in the literature[39].The extent of reduction in surface area, pore volume, and average pore size after metal impregnation was in a similar range for all of the catalysts.

Table 5.7 : Textural characteristics of AC and N-doped AC supported catalysts.

Code	Catalyst	Surface area (m^2/g)	Pore volume (cm^3/g)	Average pore diameter(A)
A1	Fe.Zn.Na/ AC-N_1	493.8	0.43	35.5
A2	Fe.Zn.K/AC-N_1	494.1	0.43	35.4
A3	Fe.Zn.Na/AC-N_2	479.6	0.43	35.9
A4	Fe.Zn.K/AC-N_2	494.1	0.44	36.3
A5	Fe.Zn.K/AC-N_3	489.7	0.44	36.4
A6	Fe.Zn.Na/AC	435.4	0.42	39.2
A7	Fe.Zn.K/AC	442.7	0.37	33.9

Since all catalysts have similar pore distribution profiles, only the pore distribution of Fe.Zn.K/AC catalyst has been given in Figure 5.9. As seen in the figure, the catalyst is mesoporous material. Most of the pores have radius in range of 5-15 nm.

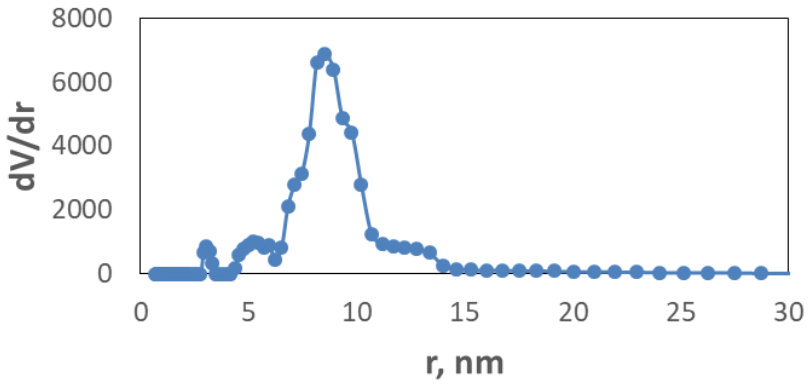

Figure 5.9 : Pore distribution of Fe.Zn.K/AC catalyst.

H_2-TPR

The reduction behavior of supported catalysts is given in Figure 5.10. As reported by Oschatz et al. [79] , it is difficult to extract quantitative information on Fischer-Tropsch to olefin performance of supported catalyst from their H_2-TPR curves due to the overlapping contributions of Fe reduction reactions and the release of surface groups

upon heating. Generally, three reduction zones have been observed in bulk Fe.Zn catalysts in the temperature ranges of 300-400 ^{o}C, 480-600 ^{o}C, and 600-750 ^{o}C. These reduction steps were ascribed to: $Fe_2O_3 \rightarrow Fe_3O_4$, $Fe_3O_4 \rightarrow FeO$, and $FeO \rightarrow Fe^{o}$, respectively[29]. In the H_2-TPR patterns of the supported catalyst three reduction zones have been observed: 1- a slight shoulder at about 300-400 ^{o}C that was assigned to the reduction of hematite to magnetite ($Fe_2O_3 \rightarrow Fe_3O_4$), 2- a peak at 500-680 ^{o}C that was ascribed to the reduction of magnetite to iron oxide ($Fe_3O_4 \rightarrow FeO$) and 3- a low intensity peak at 700-800 ^{o}C that was assigned to the reduction of iron oxide to metallic iron ($FeO \rightarrow Fe^{o}$). Low intensity of the third peak at high temperatures ($FeO \rightarrow Fe^{o}$) can be interpreted as hard reducibility of FeO to metallic Fe.

There seems additional peak at temperatures higher than 800 ^{o}C that could be the result of carbon(support) methanation as also reported by Oschatz et al. and Tang et al.[72,73] . Fe.Zn.Na/AC-N_1 and Fe.Zn.K/AC-N_2 supported catalysts, have very similar TPR patterns. The pattern of Fe.Zn.K/AC-N_3 catalyst was a bit different. In the pattern of this catalyst, the first and second peaks were observed at 530 ^{o}C and 650 ^{o}C, respectively. The third zone peak that could be ascribed to the reduction of ($FeO \rightarrow Fe^{o}$) or methanation of carbon support, occurred at higher temperatures (> 800 ^{o}C) which may show the harder reduction of $FeO \rightarrow Fe^{o}$. These results may indicate different effect of dopants on the reduction behavior of the catalysts.

In Fe.Zn.Na/AC and Fe.Zn.K/AC in which both are AC supported catalysts without chemical modification, similar behavior was observed in the reduction zones of the catalysts as A1-A5. In Fe.Zn.K/AC, the first peaks exists in the form of a shoulder at ~ 300 ^{o}C while it occurred at higher temperatures in K promoted N-doped supported catalysts Fe.Zn.K/AC-N_1 , Fe.Zn.K/AC-N_2 , and Fe.Zn.K/ AC-N_3. It seems that doping has retarded the reduction of $Fe_2O_3 \rightarrow Fe_3O_4$. As the total metal loading of the supported catalysts is 25 %, compared with that of bulk catalysts with 100% metal, the reduction peaks exhibit in lower intensities in Figure 5.10 compared to Figure 5.3.

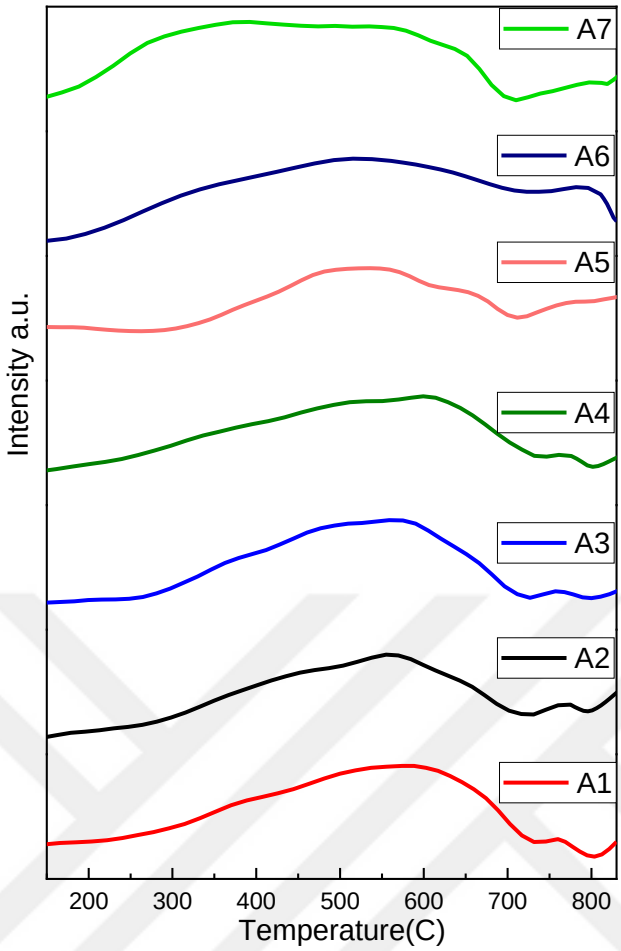

Figure 5.10 : H_2-TPR patterns of AC- and modified AC-supported calcined catalysts.A1=Fe.Zn. Na/AC-N1, A2=Fe.Zn.K/ AC-N1, A3=Fe.Zn.Na/ AC-N2, A4=Fe.Zn.K/ AC-N2, A5=Fe.Zn.K/ AC-N3, A6=Fe.Zn.Na/AC, A7=Fe.Zn.K/AC.

SEM-EDS

The scanning electron microscope images of Fe.Zn.Na/AC-N_2 catalyst as a representative of supported catalysts and its elemental mapping of Fe and Zn is given in Figure 5.11. The points marked in green in Figure 5.11a have been elementally mapped. For comparison, SEM image with elemental mapping has been given for unsupported 2Fe.Zn0.2Na (AH-I) bulk catalyst as well in Figure 5.11f. Elemental mapping of each element, namely, Fe, Zn, and O is also given in Figure 5.11c, Figure 5.11d, and Figure 5.11e, respectively. In Figure 5.11, finer particles and an even distribution of metals on the surface are seen on Fe.Zn.Na/AC-N_2 catalyst due to the use of porous support. Using support in catalyst Fe.Zn.Na/AC-N_2 has provided small particles on the surface which leads to high surface area. More discussion is available in FT performance part.

a b

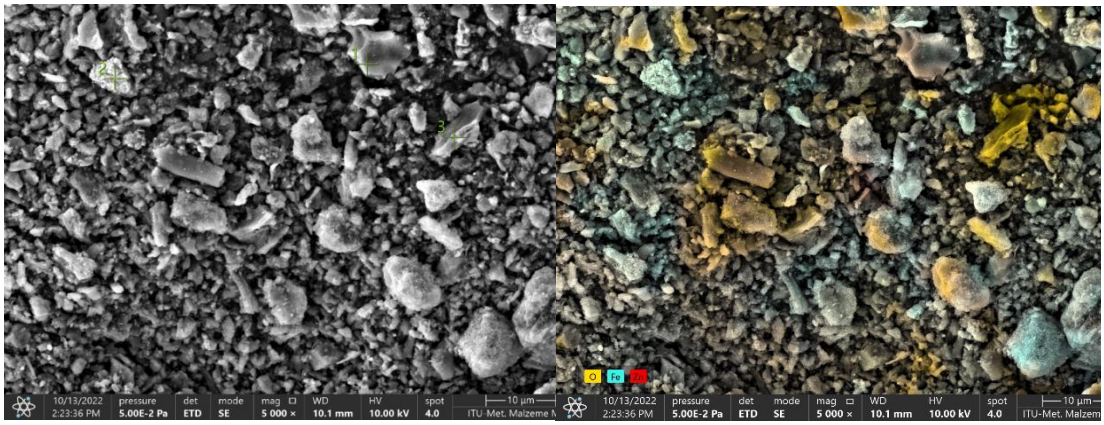

c d

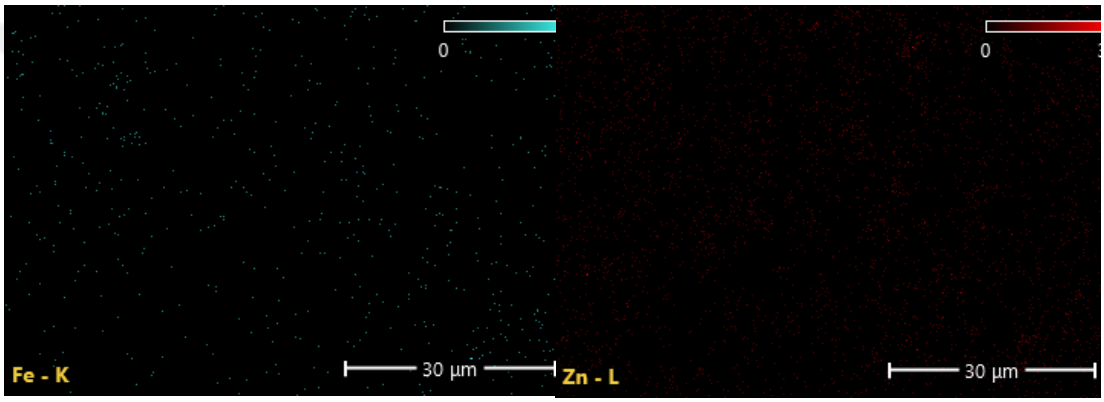

e f

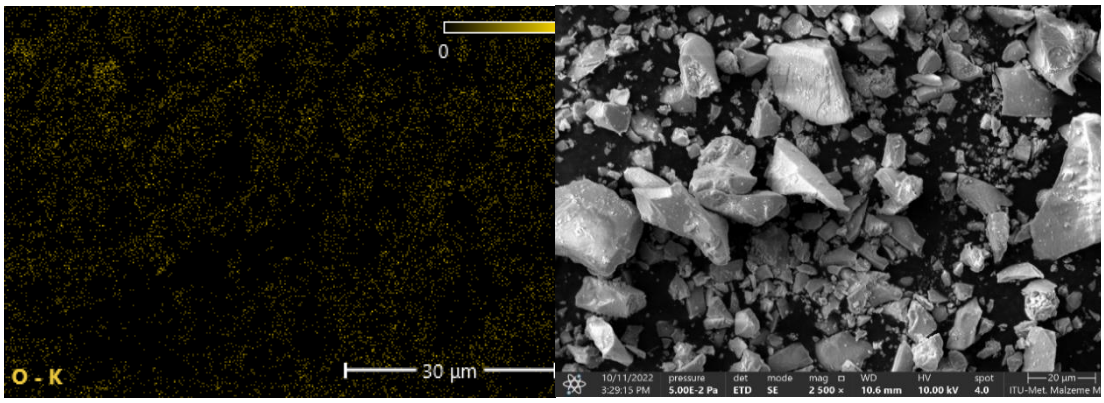

Figure 5.11 : a: SEM-EDS image of Fe.Zn.Na/AC-N_2 catalyst with investigated 3 points, b: Fe and Zn mapping in image a, c: Fe distribution in image a, d: Zn distribution in image a, e: O distribution in image a, , f: SEM-EDS image of 2Fe.Zn0.2Na (AH-I) bulk catalyst.

5.2 Fischer-Tropsch to Olefin Performance of Catalysts

All catalyst synthesized, both bulk and supported, were tested for their performance in the Fischer-Tropsch synthesis with particular focus for producing light olefins:

ethylene, propylene and butylene. Tests were conducted in a high pressure fixed-bed reactor with continuous flow of H_2/CO =2/1 at 310 ^oC temperature and 10 bar pressure. The gas hourly space velocity was GHSV=2580 h^{-1} and GHSV=516 h^{-1} for bulk and supported catalysts, respectively. The effects of promoter, synthesis method, precipitants, and catalyst support on FTS activity, selectivity and stability of the catalyst were investigated in this part of the work.

5.2.1 Fischer-Tropsch to olefin performance of Na-promoted bulk catalysts

The results obtained from Fisher-Tropsch to olefin (FTO) tests of Na-promoted catalysts are presented in Figure 5.12, Figure 5.13, Figure 5.14, Figure 5.15 and Table 5.8. Table 5.8 shows the average selectivity of catalysts over a time on stream (TOS) period of 30 hours and CO conversion at 30^{th} hour of reaction. Figure 5.12 and Figure 5.13 show the variation of the CO conversion with time on stream (TOS) for the catalysts synthesized by ammonium hydroxide (AH) and sodium carbonate (SC) precipitants, respectively. As seen in the figures the CO conversion initially is high for both type catalyst, 91-96% for catalysts prepared with AH and 87-97% for catalysts prepared with SC. CO conversion generally decreased however, with time, for all. Catalysts displayed different extents of loss in CO conversion as a measure of their stability. These results indicate that the stability of catalysts are affected by both the type of precipitant and synthesis method. All catalysts, except 2FeZn0.1Na (AH-I) and 2Fe.Zn0.2Na $(SC\text{-}I)_3$, still maintained their CO conversions higher than 80% at the end of 30 hours-long time period. The CO conversion of 2Fe.Zn0.1Na (AH-I) and 2Fe.Zn0.2Na $(SC\text{-}I)_3$, on the other hand, steadily and much rapidly deteriorated with time. Alkalinity of the synthesis batch appeared to enhanced the stability of the base catalyst as prepared by AH, 2Fe.Zn(AH) as seen in Figure 5.12 but residual sodium content of precipitate diversely affected the stability of the base catalyst as prepared with SC, 2Fe.Zn(SC), Figure 5.13. 2Fe.ZnNa type catalysts prepared by AH synthesis method with increased synthesis batch alkalinity appeared to display better stability than the base catalyst, 2Fe.Zn (AH). Catalysts prepared with AH-I method, however, had diverse performances. A similar trend was observed for the catalysts prepared with SC through SC and SC-I methods. These results suggest that the stability of the catalysts is exposed to the combined effect of the amount of Na in and the addition way of Na to catalyst and synthesis method.

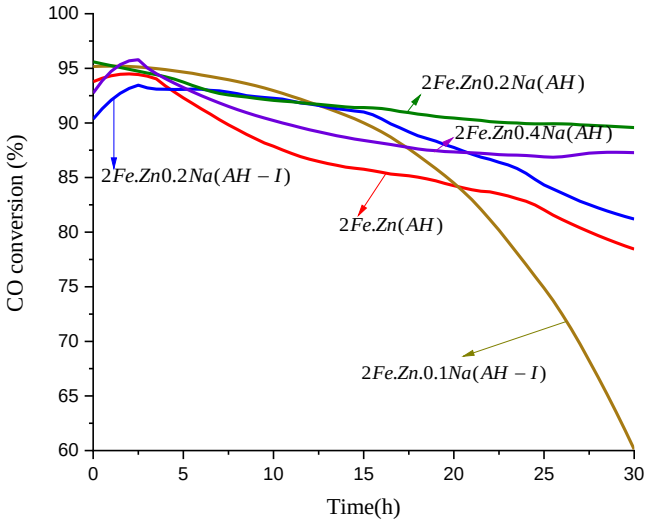

Figure 5.12 : CO conversion of the Na-promoted bulk catalysts synthesized by ammonium hydroxide versus TOS.

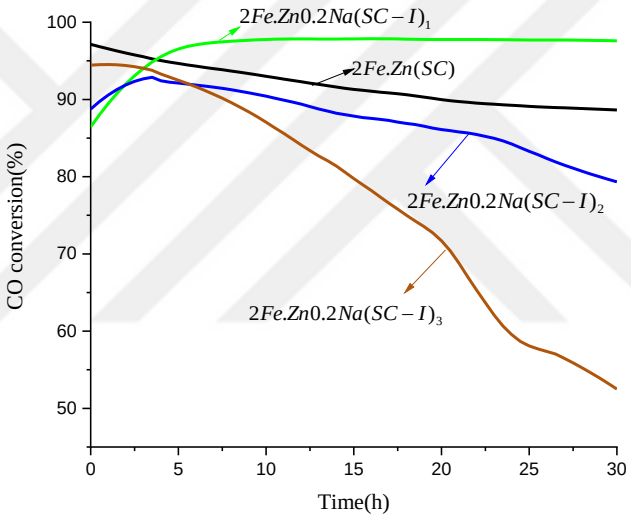

Figure 5.13 : CO conversion of the Na-promoted bulk catalysts synthesized by sodium carbonate versus TOS.

Olefin, paraffin, methane, and C_{5+} selectivity of the catalysts precipitated with AH (S1-S5) and the catalysts precipitated with SC (S6-S9) versus time on stream are illustrated in Figure 5.14 and Figure 5.15. Investigating hydrocarbon selectivity of the Na promoted bulk catalysts(S1-S9), as is obvious from Figure 5.14 and Figure 5.15, by Na addition to the Fe.Zn structure, especially when the Na is added by post impregnation to the base catalysts, 2Fe.Zn(AH) and 2Fe.Zn(SC), and Na content is approximately higher than ~1.5 wt% as in 2Fe.Zn0.1Na(AH-I) , 2Fe.Zn0.2Na(AH-I), $2Fe.Zn0.2Na(SC\text{-}I)_1$, $2Fe.Zn0.2Na(SC\text{-}I)_2$, and $2Fe.Zn0.2Na(SC\text{-}I)_3$, Na donates electron to the surface, strengthen the CO adsorption and its dissociation, provides a relatively high coverage of carbon on the surface in relation to hydrogen. As a result

of deficiency of surface hydrogen, decrease in the paraffin and methane selectivity is observed. The chain growth and termination occurs in a way that C_2-C_4 olefins are formed. As a result, light olefin selectivity increases. Presence of alkali contributes to increase in CO adsorption and dissociation provided that the presence of alkali content does not exceed optimum level. In addition, in the presence of alkali, the chain growth rate increases and longer hydrocarbons are formed on re-adsorbed olefin intermediate compounds. As a result of this, C_{5+} selectivity increases as well in Na impregnated catalysts in comparison with that of base catalysts, 2Fe.Zn(AH) and 2Fe.Zn(SC), from ~11% to ~25%. Olefin selectivity increases from ~20% to ~50 %, methane selectivity decreases from 32% to 20% and paraffin selectivity from ~37% to ~8%, respectively.

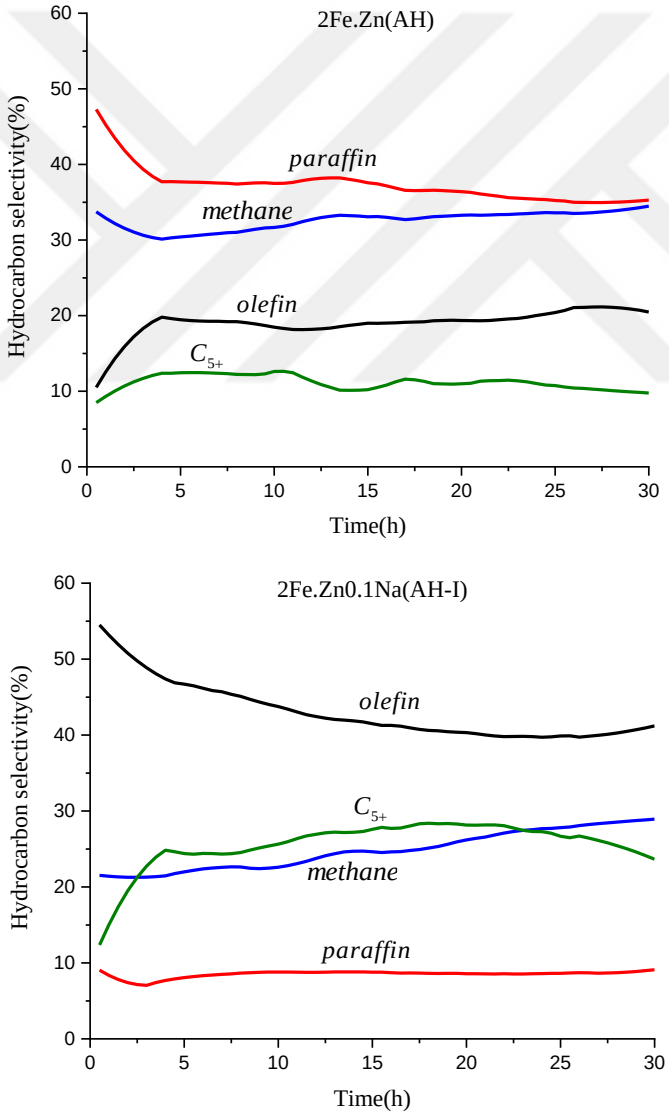

Figure 5.14 : Olefin, paraffin, methane, and C_{5+} selectivity of the catalysts precipitated with AH.

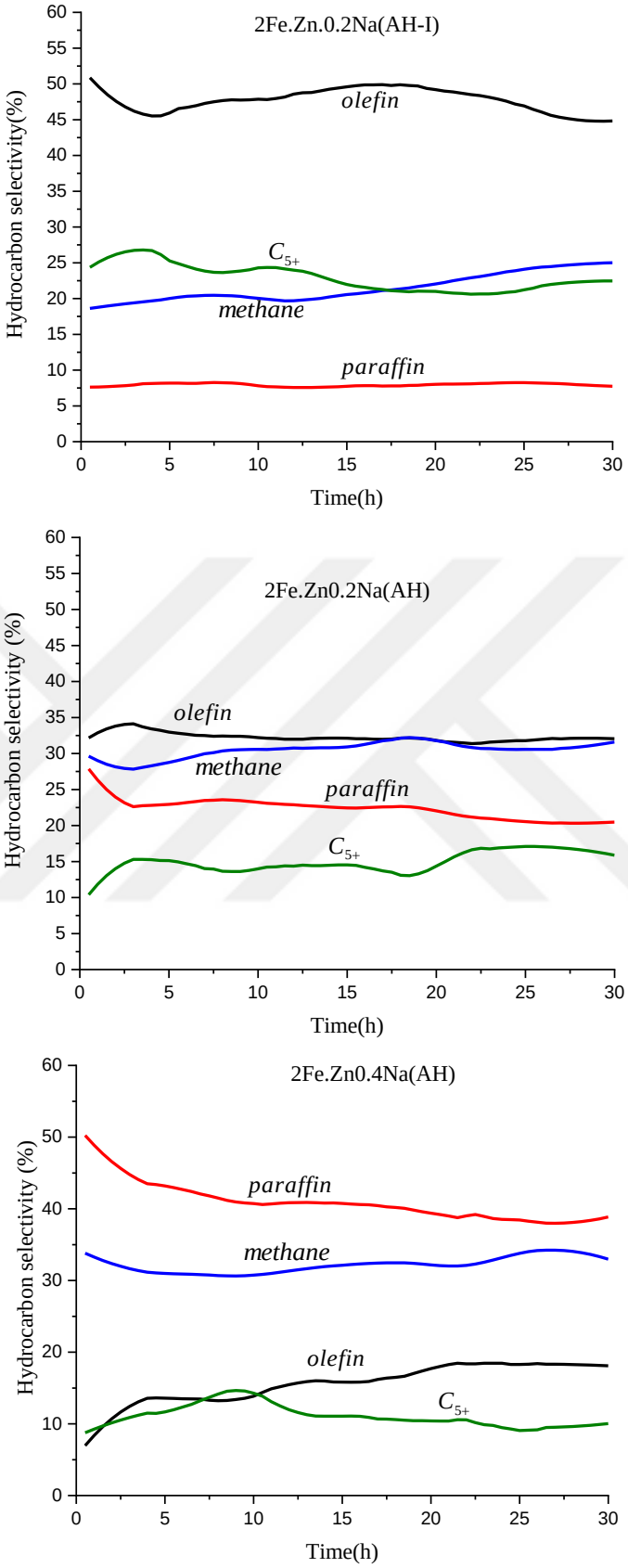

Figure 5.14 (continued) : Olefin, paraffin, methane, and C_{5+} selectivity of the catalysts precipitated with AH.

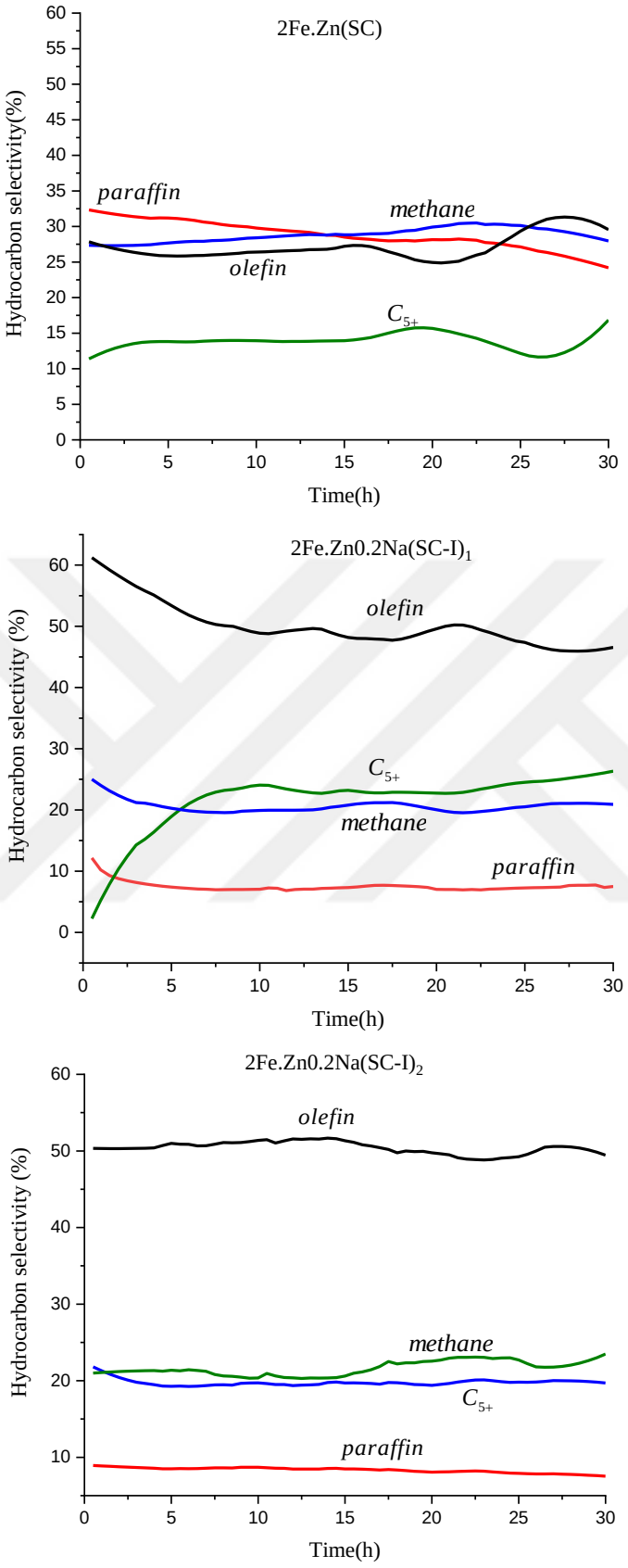

Figure 5.15 : Olefin, paraffin, methane, and C_{5+} selectivity of the catalysts precipitated with SC.

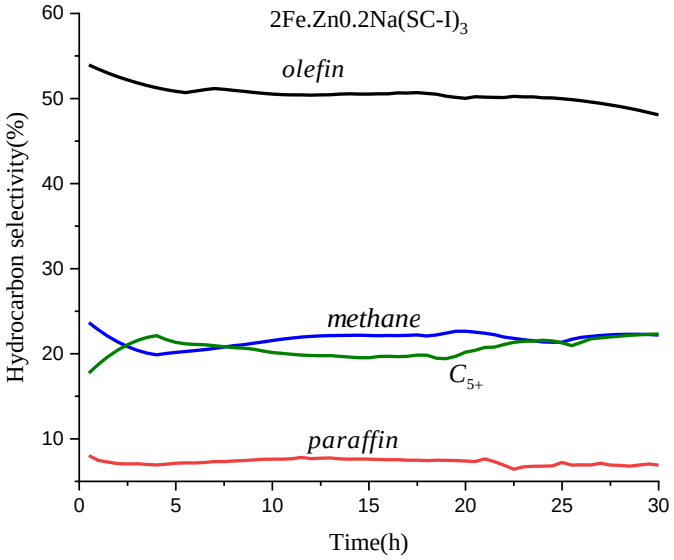

Figure 5.15 (continued) : Olefin, paraffin, methane, and C_{5+} selectivity of the catalysts precipitated with SC.

As can be seen in Table 5.8, CO conversion of 88.6% was achieved with a C_2-C_4 olefin selectivity of 27.1%, C_{5+} selectivity of 13.8% and methane selectivity of 28.7% for 2Fe.Zn(SC) having the sodium content of 0.5%. An olefin to paraffin ratio of 0.9 was calculated over 2Fe.Zn(SC). On the other hand, with increasing the sodium content, CO conversion was first increased to 97.4% for 2Fe.Zn0.2Na $(SC\text{-}I)_1$ and then a rapid decrease was recorded to 70.3% and 52.3% for the samples 2Fe.Zn0.2Na $(SC\text{-}I)_2$ and 2Fe.Zn0.2Na $(SC\text{-}I)_3$, respectively. However, their selectivity profiles come to a common point for all, namely higher light olefin and C_{5+} selectivity at around ~50% and ~21% and lower methane selectivity of ~21%. As a result of improved olefin selectivity, olefin to paraffin ratio of the product stream was increased to around 6-7. It is reasonable to explain the decrease in the CO conversion with the concomitant increase in the coke formation as a measure of improved CO dissociation activity coming from the sodium content of the catalyst. Deactivation caused by levels of alkali content beyond an optimum point was proved for K promoted catalysts which is in line with the study of An et al.[81]. There are studies reporting that alkali cations suppress the secondary olefin hydrogenation and increase the chain growth probability. As explained by Herzog and Gaube [82], the strength of carbon monoxide adsorption is enhanced by the alkali compounds. This causes facilitated 1-alkene desorption and reduced rate of consecutive hydrogenation and of isomerization of 1-alkenes into 2-alkenes. As widely reported in the literature, alkali cations act as an electron donor providing an iron surface with high electron density. This strengthens

the CO adsorption and its dissociation. Inhibited re-adsorption of olefins and relatively lowered rate of hydrogen transfer are responsible for the observed high olefin selectivity [74,75] .

Although the effects of structural promoters like zinc on the catalytic performance of iron catalysts were reported for the direct synthesis of light olefins, e.g. by Zhao et al.[34] no systematic study, however, has not been reported on relationship between sodium content of zinc ferrite catalysts and their basicity and FT activity. In the study of Zhao et al, FeZn type catalysts with a molar ratio of 1/1 were precipitated with the precipitants, K_2CO_3, Na_2CO_3, $(NH_4)_2CO_3$, and $CO(NH_2)_2$ in order to see the effect of alkali content left over the precipitate on the product selectivity. However, our study differs from their study as we used a Fe/Zn atomic ratio of 2 to end up with a spinel zinc ferrite crystal structure. Moreover, the effect of ionic strength was evaluated for 2Fe.Zn precipitation in the presence of NH_4OH, NH_4OH plus $NaNO_3$ and Na_2CO_3 precipitation agents in an effort to understand the effect of ionic strength on the catalyst basicity and on its catalytic performance. We also investigate the effect of precipitation agent on FT activity in terms of solid basicity. As can be seen from the CO_2-TPD graph in Figure 5.4, the number of sites with moderate and strong basicity increases with sodium content in the sequence of 2Fe.Zn (SC) < 2Fe.Zn0.2Na $(SC\text{-}I)_1$ < 2Fe.Zn0.2Na $(SC\text{-}I)_3$. Since all these catalysts were prepared with the same precipitation agent, namely sodium carbonate, linearly varying basicity with the sodium content was expected. However, despite the increased basicity of 2Fe.Zn0.2Na $(SC\text{-}I)_1$ compared to 2Fe.Zn (SC), less coking and a higher and more stable CO conversion over 2Fe.Zn0.2Na $(SC\text{-}I)_1$ needs to be argued. Normally facilitated CO dissociation over basic sites provides a relatively high coverage of carbon species on the surface in relation to hydrogen. This leads to a decrease in the paraffin selectivity and/or chain termination rates due to deficiency of surface hydrogen [85]. Therefore, more favorable conditions were established for carbon formation. As discussed by van Santen et al.[14], catalytic surface becomes blocked with the accumulation of growing hydrocarbon chains due to the decreased hydrogen atom transfer in the chain growth termination reaction. Under this condition, CO conversion decreases as well since the lack of surface vacancies suppresses the rate of CO dissociation with time on stream. Therefore, there should be an optimum interaction strength of the surface where the rate of CO to CH_x becomes balanced with the rates of chain growth and chain growth

termination. As a plausible explanation, 2FeZn0.2Na $(SC\text{-}I)_1$ might have an optimum amount of basicity and basic strength that ensures this balance.

To highlight the importance of surface basicity, FT activity of 2Fe.Zn0.2Na (AH-I) and 2Fe.Zn0.2Na $(SC\text{-}I)_1$ catalysts with the same sodium content but different basicity was compared in Table 5.8, much lower CO conversion of 60.2% over 2Fe.Zn0.2Na (AH-I) was recorded compared to the value of ~97.4% for 2Fe.Zn0.2Na $(SC\text{-}I)_1$ catalyst. However, selectivity and the calculated olefin to paraffin ratio values for these two catalysts were quite similar. Light olefin and C_{5+} selectivity at around ~ (47-50) % and ~22% and low methane selectivity of ~21% was obtained. Olefin to paraffin ratio of the product was ~ 6.

Although 2Fe.Zn0.2Na (AH-I) and 2Fe.Zn0.2Na $(SC\text{-}I)_1$ contain nearly the same amount of sodium, it is not easy to explain why the basic site density of zinc ferrite precipitated with ammonium hydroxide, 2Fe.Zn0.2Na (AH-I), was much higher compared to the one, 2Fe.Zn0.2Na $(SC\text{-}I)_1$. Since the increase in the number of basic centers also affects the catalytic activity and stability, it is important to examine this effect. In a study by Dry and Oosthuizen[71] , catalysts promoted with oxides of Li, Na, K, Ca, and Ba were studied and surface basicity were correlated with hydrocarbon selectivity in the Fischer-Tropsch synthesis. They have argued that there was no such a relationship between the actual K_2O content of the catalyst and its selectivity but there was a clear relationship between surface basicity and methane selectivity. They concluded that the surface basicity and hence the hydrocarbon selectivity depended not only on the amount of alkali but also on how well it is distributed over the catalyst surface. In our study, the higher number of basic sites for 2Fe.Zn0.2Na (AH-I) compared to 2Fe.Zn0.2Na $(SC\text{-}I)_1$ was apparent from their CO_2-TPD profiles even though both of them had the same amount of alkali content. This can be interpreted as the basic sites would be more dispersed over 2Fe.Zn0.2Na (AH-I) surface. So the stronger interaction of 2Fe.Zn0.2Na (AH-I) catalyst surface towards CO dissociation may be expected due to the more basic sites available at the surface. As a result of this, much higher carbon content of the spent catalyst, 2Fe.Zn0.2Na (AH-I) and its poor stability may be ascribed to its higher number of basic sites compared to 2Fe.Zn0.2Na $(SC\text{-}I)_1$ catalyst. This catalyst has shown the best FTO performance among bulk catalysts of this work and the performance was related to the optimum basicity of the catalyst that may make a balance in CO dissociation to CH_x, chain propagation and

termination. Here, it can be added that this optimum basicity may affect H_2 conversion as well. Low number of active sites are covered with deposited carbon, resulting in high stability in CO and H_2 dissociation and deriving the product chain into favorable direction. In 2Fe.Zn0.2Na(SC-I)$_2$ and 2Fe.Zn0.2Na(SC-I)$_3$, H_2 consumption at 30th hour of reaction is ~30% and ~17 %, respectively. High alkali content of these catalysts led to high coke deposition, carbon covered the active sites and led to decrease in CO and H_2 conversion.

H_2 consumption and CO_2 selectivity versus TOS of all catalysts is available at Appendix D, Na-promoted bulk catalysts in Figure D.1. Due to WGS reaction, there is a general trend in the changing behavior of H_2 conversion and CO_2 selectivity. In general, close to 40% CO_2 selectivity was observed. H_2 conversion was always lower than CO conversion due to its secondarily formation over WGS. Its decreasing trend due to coking follows the same manner as with CO conversion loss with time on stream.

Table 5.8 : FTO performance of Na-promoted bulk catalysts over 30 hours[a].

Code	Catalyst	CO Conv. (%).	CO_2 Sel.	Hydrocarbon Sel. %					$C^{=}_2$-$C^{=}_4$ yield (g C/g Fe.s)
				CH_4	$C^{=}_2$-$C^{=}_4$	C^0_2-C^0_4	O/P	C_{5+}	
S1	2Fe.Zn (AH)	77.8	38	32.5	19.9	37.2	0.5	11.5	1.6E-05
S2	2Fe.Zn0.1Na (AH-I)	81.1	39.2	21.5	42.8	8.5	5	25.6	2.4E-05
S3	2Fe.Zn0.2Na (AH-I)	60.2	39.1	21.4	47.7	7.9	5.9	22.9	2.9E-05
S4	2Fe.Zn0.2Na (AH)	89.5	39.8	30.4	32.2	22.3	1.3	14.9	2.7E-05
S5	2Fe.Zn0.4Na (AH)	87.1	38.3	32.1	15.5	40.9	0.3	11	1.4E-05
S6	2Fe.Zn (SC)	88.6	36.6	28.7	27.1	28.7	0.9	13.8	2.1E-05
S7	2Fe.Zn0.2Na (SC-I)$_1$	97.4	34.4	20.6	50	7.5	6.7	21.9	4.3E-05
S8	2Fe.Zn0.2Na (SC-I)$_2$	79.3	40.6	19.7	50.3	8.3	6	21.5	3.1E-05
S9	2Fe.Zn0.2Na (SC-I)$_3$	52.3	41.9	21.6	50.5	7.2	6.9	20.5	2.6E-05

[a]: reaction conditions: 1 g catalyst, 310 °C, 1.0 MPa, 50 ml min^{-1} syngas (H_2/CO = 2), and reaction time = 30 h; CO conversion at the 30th hour, product selectivity listed is obtained as an average value of analysis result in 30 h.

5.2.2 Fischer-Tropsch to olefin performance of K- and Cu-promoted bulk catalysts

The results obtained from Fisher-Tropsch to olefin (FTO) tests of Cu- and K- promoted catalysts are presented in Figure 5.16 and Table 5.9. Table 5.9 shows the average selectivity of catalysts over a time on stream (TOS) period of 35 hours and CO conversion at 35th hour of reaction. Figure 5.16 shows the CO conversion versus time on stream (TOS) for the catalysts promoted by Cu and K. As seen in Figure 5.16, the CO conversion initially is high above 80% for all catalysts at first 5 hour of reaction.

For both base catalysts 2Fe.Zn(AH) and 2Fe.Zn(SC) and Cu promoted catalyst 2Fe.Zn0.2Cu(AH-I), very low deactivation is observed. At the 35th hour of reaction, the CO conversion for the mentioned catalysts remain above 80 %. For the other catalysts namely, 2Fe.Zn0.2K(AH-I), and 2Fe.Zn0.2Cu0.05K(AH-I), 2Fe.Zn0.2K(SC-I), CO conversion decreased however, with time, down to 10-30%. A highly stable catalyst is obtained by Cu impregnation to the base catalyst 2Fe.Zn(AH), final CO conversion of ~97%. While adding K to the base catalyst 2Fe.Zn(AH), makes a highly deactivated catalyst, leads to a final CO conversion of ~10%. In 2Fe.Zn0.2Cu0.05K(AH-I) in which both Cu and K are used, deactivation of the catalyst is in between the two extends, final CO conversion of ~ 30%. Since it is widely reported that alkali metals higher than an optimum amount cause coke deposition and deactivation of catalyst, this finding is reasonable.

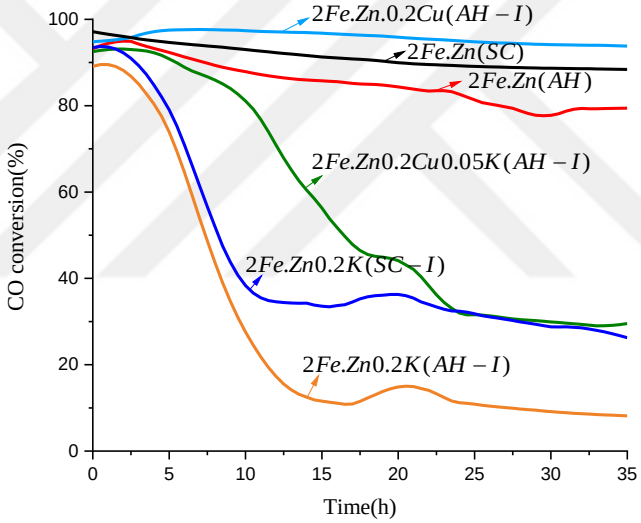

Figure 5.16 : CO conversion of Cu- and K- promoted bulk catalysts versus TOS.

Moreover, investigating the effect of precipitant and alkali content on the stability of the catalyst, when 2Fe.Zn0.2K(AH-I) and 2Fe.Zn0.2K(SC-I), are compared, SC give a more stable catalyst. The CO conversion at 35th hour of reaction is 10% and 30%, and total alkali content is 4.1% and 3.4%, respectively. These results indicate that the stability of catalysts are affected by the promoter, type of precipitant, and alkali content of the catalysts.

Olefin, paraffin, methane, and C_{5+} selectivity of the Cu- and K- promoted Fe.Zn catalysts versus time on stream are illustrated in Figure 5.17.

As discussed by Li et al. [26] , copper provides some sites with low chain growth probability and high olefin hydrogenation activity (high paraffin and methane selectivity). However, potassium titrates acid sites or uncarbided sites and inhibits secondary hydrogenation sites, increases the molecular weight of FTS products and olefin content. Moreover, K increases the rate of secondary water–gas shift reactions. All these effects of copper and potassium addition have been observed in this study and is consistency with the report of Li et al. [26].

In 2Fe.Zn0.2Cu0.05K (AH-I) catalyst, the olefin and C_{5+} selectivity of 2Fe.Zn0.2K (AH-I) catalyst is preserved due to the presence of only 1.4% potassium but methane decreased by 4% and paraffin increased by 2.3%. The sharp deactivation rate with TOS observed in catalyst 2Fe.Zn0.2K (AH-I) has been moderated and CO conversion at 35^{th} hour increased from ~8% to ~40 %. It seems that lower potassium content (1.4%) is sufficient to provide necessary basic sites to promote olefin selectivity. However, there still exists high deactivation with TOS (coke deposition), carbon content of spent catalyst ~ 17% but less than that of 2Fe.Zn0.2K (AH-I). It shows very high alkalinity potential of potassium.

The 2Fe.Zn (SC) base catalyst is synthesized to investigate the effect of precipitant on FTO performance of the catalyst. Comparing 2Fe.Zn (SC) and 2Fe.Zn (AH) base catalysts, hydrocarbon distribution has changed. Comparing 2Fe.Zn (SC) to that of 2Fe.Zn (AH), methane and paraffin decreased by ~4% and ~9%, respectively. Olefin selectivity and C_{5+} selectivity increased by ~7% and ~2%, respectively. The change in hydrocarbon distribution can be ascribed to the residual Na of catalyst 2Fe.Zn (SC) and different ionic strength of precipitation medium as discussed in Na-promoted bulk catalysts.

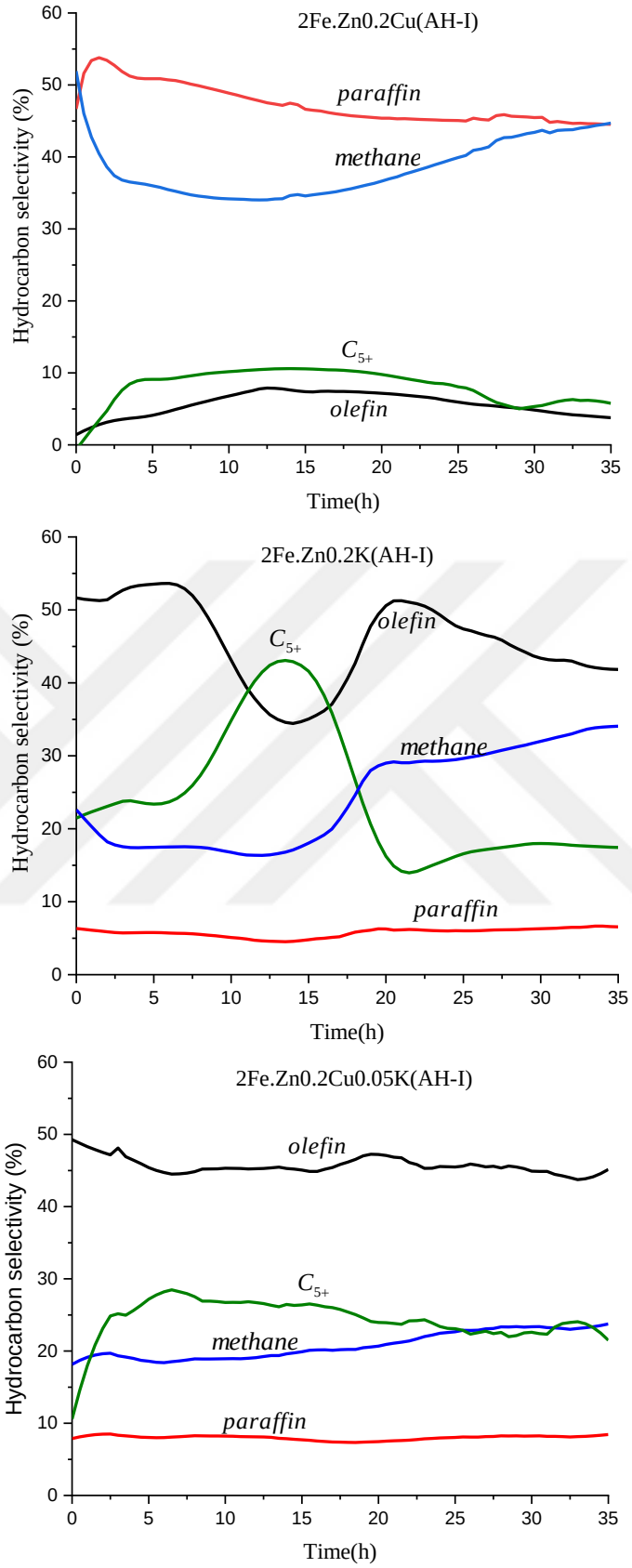

Figure 5.17 : Olefin, paraffin, methane, and C_{5+} selectivity of the K- and Cu-promoted Fe.Zn catalysts.

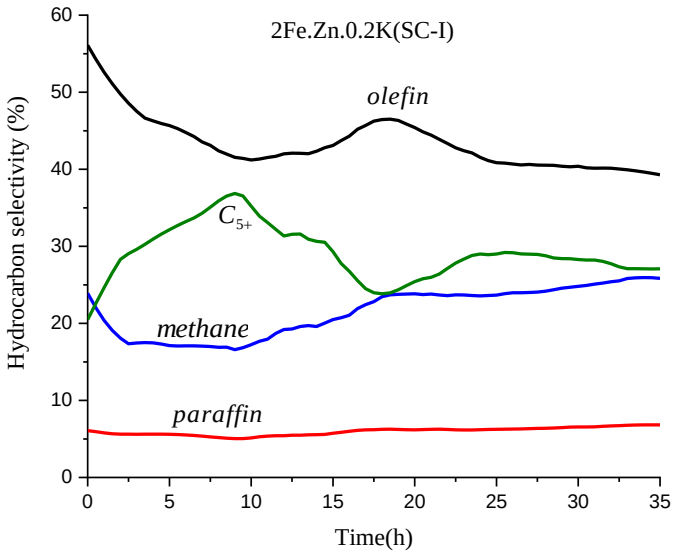

Figure 5.17 (continued) : Olefin, paraffin, methane, and C_{5+} selectivity of the K- and Cu- promoted Fe.Zn catalysts.

In catalysts given in Table 5.9, the effect of K- and Cu- impregnation onto the base catalysts 2Fe.Zn(AH) and 2Fe.Zn(SC) on FTO performance have been investigated. In 2Fe.Zn0.2Cu (AH-I) catalyst in which 6.8% Cu is impregnated onto the base catalyst 2Fe.Zn(AH), O/P decreased from 0.5 to 0.1, olefin selectivity decreased by ~ 14%, C_{5+} decreased by ~ 3%, paraffin selectivity increased by 10%, methane selectivity increased by 6%, and olefin yield decreased from 1.67 ×E-5 to 0.66 ×E-5. No subtle change in CO_2 content was observed. CO conversion increased by 13%. A highly stable catalyst is obtained by Cu impregnation to the base catalyst 2Fe.Zn(AH). The increase in methane and paraffin selectivity and decrease in olefin and C_{5+} selectivity is in agreement with [26] .

However, in 2Fe.Zn0.2K (AH-I) catalyst by adding 4.1% potassium to the base catalyst 2Fe.Zn(AH), much lower CO conversion with the value of 7.9% was recorded compared to that of 79% for 2Fe.Zn (AH) catalyst as it is also clear in Table 5.9. Light olefin selectivity increased significantly from 19.9% to 45.5% and C_{5+} selectivity from 11.5% to 24.2 %. However, methane selectivity decreased from 32.5% to 24.3% and paraffin selectivity from 37.2% to 5.7%. Olefin to paraffin ratio remarkably increased from 0.5 to 7.7. It is reported by [26] that the surface density of promoters (Cu or K) has a threshold value which above that, increasing promoter does not increase the contact with Fe oxide precursors . It seems there is an optimum content for potassium as promoter which provides both high olefin selectivity and also a stable catalyst (low deactivation) in which higher concentrations lead to catalyst deactivation by carbon

deposition. Though this effect was observed for Na in this study but may be presumed to be valid for K too. It is also reported that it is more appropriate to define promoter(potassium) concentration in terms of surface density with optimum content [86]. Deactivation with an amount of alkali content beyond an optimum point was also observed for potassium promoted catalysts as reported by An et al.[81]. In 2Fe.Zn0.2K (AH-I) catalyst, carbon content of the spent catalyst was high ~ 20% and carbon deposition may be considered as the reason of catalyst deactivation versus TOS.

K effect on FTS hydrocarbon distribution which is an increase in light olefin and C_{5+} selectivity with concomitant decrease in paraffin and methane selectivity is similar to the effect of Na as discussed in page 68.

By adding ~3% K to 2Fe.Zn (SC) catalyst via impregnation, 2Fe.Zn0.2K (SC-I) catalyst is obtained with much lower CO conversion of 25.5%. As given in Table 5.3, the carbon content of 2Fe.Zn0.2K (SC-I) spent catalyst is ~ 16% comparing to low content of ~3% in the 2Fe.Zn (SC) spent base catalyst. The methane and paraffin selectivities decreased by ~7% and ~22%, respectively. In contrast, olefin selectivity and C_{5+} increased by ~16% and 15%, respectively. Olefin to paraffin ratio remarkably increased from 0.9 to 7.3. The promotion effect of K is clearly observed here and is the same as 2Fe.Zn0.2K (AH-I) catalyst except deactivation pattern. 2Fe.Zn0.2K (AH-I) catalyst with ~4% alkali metal content had final CO conversion of ~8% while 2Fe.Zn0.2K (SC-I) catalyst with ~3.5 % alkali metal content had final CO conversion of ~ 25.5 %. The higher stability of 2Fe.Zn0.2K (SC-I) can be ascribed to different ionic strength of precipitation medium of the base catalyst, 2Fe.Zn (SC), beside the slightly less alkali metal concentration of 2Fe.Zn0.2K (SC-I).

H_2 conversion and CO_2 selectivity of Cu- and K- promoted catalysts is available in Appendix D, Figure D-2. As in the case of sodium promoted catalysts, due to WGS reaction, there is a general trend in the changing behavior of H_2 conversion and CO_2 selectivity. In general, close to 40% CO_2 selectivity was observed. H_2 conversion was always lower than CO conversion due to its secondarily formation over WGS. Its decreasing trend due to coking follows the same manner as with CO conversion loss with time on stream.

Table 5.9 : FTO performance of Cu- and K- promoted bulk catalysts[a].

Code	Catalyst	CO Conv. (%).	CO_2 Sel.	Hydrocarbon Sel. %					
				CH_4	$C^{=}_2$-$C^{=}_4$	C^{0}_2-C^{0}_4	O/P	C_{5+}	Olefin yield (g C/g Fe.s)
S1	2Fe.Zn (AH)	79	38	32.5	19.9	37.2	0.5	11.5	1.67 E-05
L1	2Fe.Zn0.2Cu (AH-I)	93.7	36.1	38.5	5.6	47.2	0.1	8	0.66 E-05
L2	2Fe.Zn0.2K (AH-I)	7.9	36.5	24.3	45.5	5.7	7.7	24.2	1.41 E-05
L3	2Fe.Zn0.2Cu0.05K(AH-I)	39.5	39.3	20.8	45.5	8	5.6	24.5	1.28 E-05
S6	2Fe.Zn (SC)	88	36.6	28.7	27.1	28.7	0.9	13.8	2.13 E-05
L4	2Fe.Zn0.2K (SC-I)	25.5	40	21.6	43.3	5.9	7.3	29	1.07 E-05

[a]: Reaction conditions: 1 g catalyst, 310 °C, 1.0 MPa, 50 ml min^{-1} syngas (H_2/CO = 2), and reaction time = 35 h; CO conversion at 35th hour and product selectivity listed is obtained as an average value of analysis result in 35 h.

5.2.3 Fischer-Tropsch to olefin performances of AC and N-doped AC supported catalysts

The results obtained from Fisher-Tropsch to olefin (FTO) tests of AC and N-doped AC supported catalysts are presented in Figure 5.18, Figure 5.19 and Table 5.10. The catalysts were exposed to the flow of H_2/CO:2/1 with a gas hourly space velocity (GHSV) of 516 h^{-1} at T=310 °C and P=10 bar in a high pressure fixed-bed reactor to provide the FTS reaction conditions. In Table 5.10, the average selectivity of catalysts over a time on stream (TOS) period of 35 hours and CO conversion at 35th hour of reaction is given.

As shown in Figure 5.18 and Figure 5.19, high CO conversion (~88%-~93%) is obtained. Investigating the effect of nitrogen doping on CO conversion, urea, HNO_3 and NH_3 doping slightly increased the CO conversion (by 4%). CO_2 selectivity did not show considerable change and ranges from 37% to 39%. A straight trend in hydrocarbon distribution is not observed as the effect of nitrogen doping.

In the report of Guoguo Liu a et al. [46], the highest CO conversion of 92.6% and olefin selectivity 33.9% is achieved from 40%Fe /N_2 which N_2 is the nitrogen-rich mesoporous carbon(NMC's) with 16.5 % nitrogen, 786 m^2/g surface area, and 2.76 cm^3/g pore volume. In this thesis, not only Fe, but also Zn and Na/K was impregnated to the support (AC/N-doped AC) and the resulted in 93.6% CO conversion with 50.5% olefin selectivity for Fe-Zn-Na/AC-N_2 catalyst with its support AC-N_2 characteristics including: 734.9 m^2/g surface area, 0.75 cm^3/g pore volume, and 1.16% nitrogen content. AC-N_2 support showed highest stability among AC and other N-doped AC supports with decomposition temperature higher than 730 °C. The thermal stability

confirmed by TGA was consistent with the highest CO conversion in Fe.Zn.Na/ AC-N_2 catalyst. As can be seen in Table 5.10, Fe.Zn.K/AC-N_2 with the same support also has shown high final CO conversion (93%). It can be concluded that the NH_3 modified support as well as presence of Zn as a structural promoter has formed a highly stable catalyst.

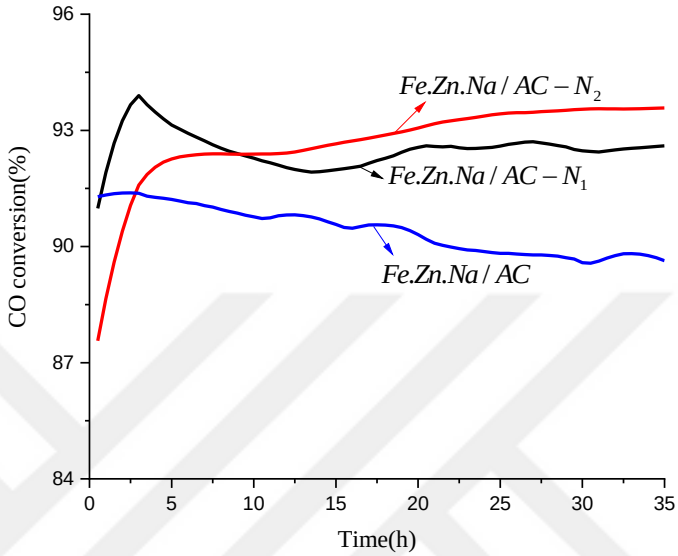

Figure 5.18 : CO conversion of Na promoted supported catalysts versus TOS.

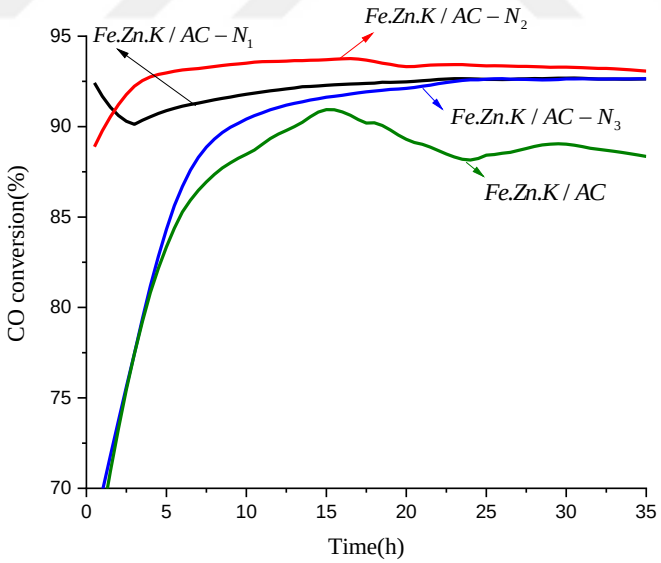

Figure 5.19 : CO conversion of K promoted supported catalysts versus TOS.

As given in Figure 5.20 - Figure 5.26, high olefin selectivity (~45%- ~51%), low methane selectivity (~15%- ~21%), low paraffin selectivity (~7%- ~11%), and high C_{5+} (~18%-~26%) is obtained in all AC and N-doped AC supported catalysts. As discussed in FTO performance of bulk catalysts (Na/K promoted), increase in olefin

selectivity and O/P is concomitant with decrease in in paraffin and methane selectivity at the presence of alkali metals. Na provides a surface with high electron density that leads to intensification of CO adsorption and dissociation. However, although this is a favorable effect, it has limitation in terms of alkali content of the catalyst and its dispersion. As mentioned before, there is an optimum basicity which ensures a balance between CO conversion to CH_x and the rate of hydrocarbon chain growth and its termination. If this balance alters, long chain hydrocarbon may form and cover the catalyst surface which can block the active sites. Lack of surface vacancies suppress the rate of CO dissociation with time on stream and result in high deactivation. In this case, the hydrocarbon distribution does not change significantly but deactivation dominates. When surface is covered with high C content, the C/H ratio increases at the surface. H deficiency may result in a decrease in the paraffin and methane selectivity.

Moreover, alkali metal drives the polymerization reaction in a way that beside increase in C_2-C_4 olefin selectivity, the chain growth increases as well, namely C_{5+} increases. All in all, the general hydrocarbon distribution is as described above. However, comparing light olefin selectivity behavior to that of C_{5+} selectivity apart from general trend that was explained, it is observed that C_2-C_4 olefin peaks change in reverse with C_{5+} peaks. For instance, in supported catalysts, wherever olefin selectivity has a sharp decrease, a sharp increase in C_{5+} is observed which is clearer in Fe.Zn.Na/AC and Fe.Zn.K/AC. In order to justify this behavior in terms of chain growth and termination rates, it can be interpreted as when C_2-C_4 olefin selectivity increases, most of the formed olefins having 2-4 carbon atoms are easily desorbed from the surface without further hydrogenation and further chain growth. It means that the chain growth decreases to some extent. On the other hand, when C_{5+} selectivity has a sharp increase, means that rate of chain growth dominates and get ahead of desorption of the formed light olefins. This internal trend between C_2-C_4 olefins and C_{5+} selectivity is observed in some of the synthesized catalysts.

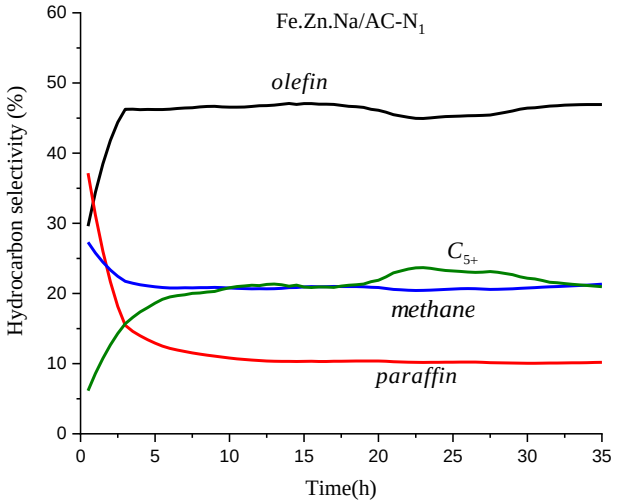

Figure 5.20 : Olefin, paraffin, methane, and C_{5+} selectivity of Fe.Zn.Na/AC-N_1 catalyst.

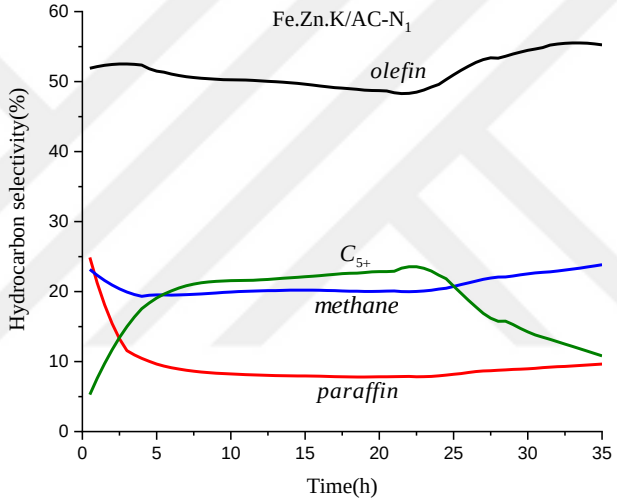

Figure 5.21 : Olefin, paraffin, methane, and C_{5+} selectivity of Fe.Zn.K/AC-N_1 catalyst.

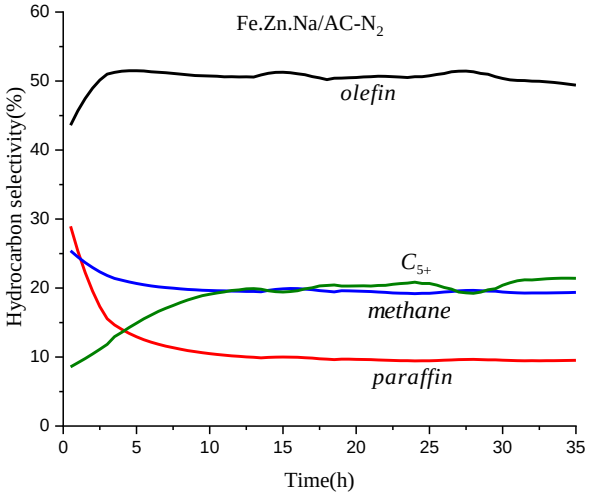

Figure 5.22 : Olefin, paraffin, methane, and C_{5+} selectivity of Fe.Zn.Na/AC-N_2 catalyst.

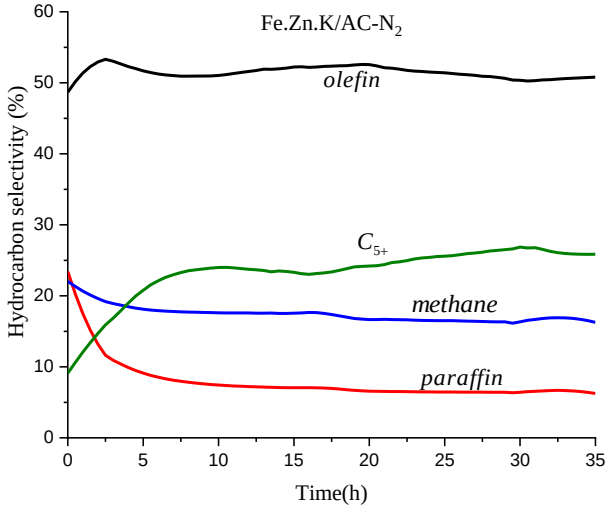

Figure 5.23 : Olefin, paraffin, methane, and C_{5+} selectivity of Fe.Zn.K/AC-N_2 catalyst.

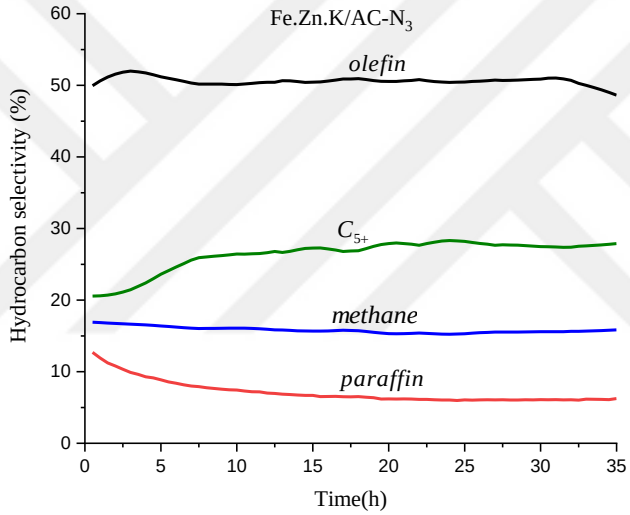

Figure 5.24 : Olefin, paraffin, methane, and C_{5+} selectivity of Fe.Zn.K/AC-N_3 catalyst.

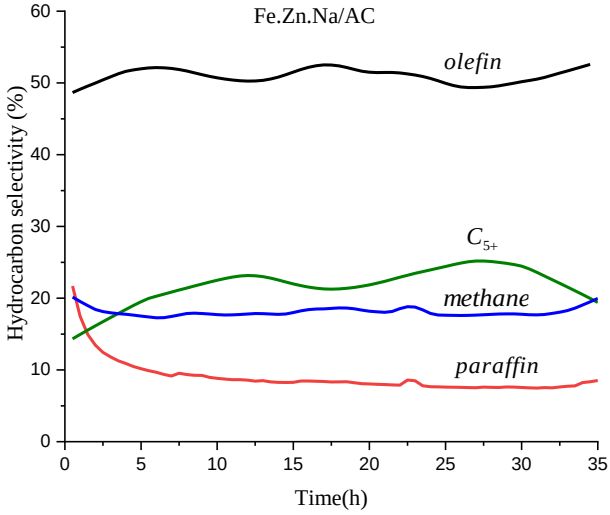

Figure 5.25 : Olefin, paraffin, methane, and C_{5+} selectivity of Fe.Zn.Na/AC catalyst.

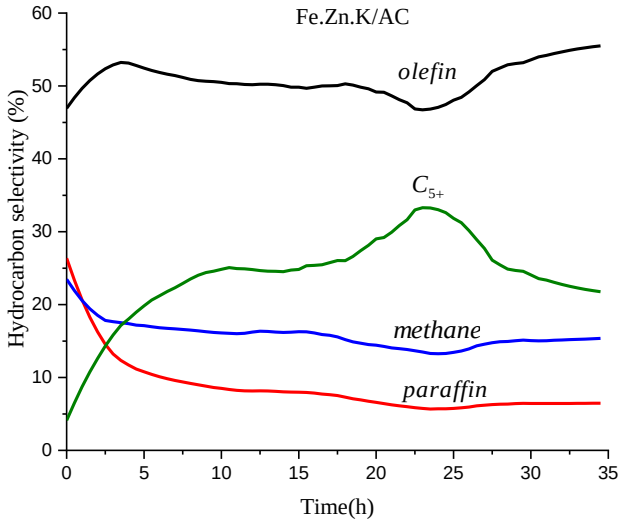

Figure 5.26 : Olefin, paraffin, methane, and C_{5+} selectivity of Fe.Zn.K/AC catalyst.

As given in Table 5.10, potassium as promoter has shown higher O/P and olefin selectivity in comparison with sodium. O/P is 5.7, 6.9, 7.3, and 6.6 and olefin selectivity is 51.3%, 51.4%, 50.6%, and 50.9% in Fe.Zn.K/AC-N_1, Fe.Zn.K/AC-N_2, Fe.Zn.K/AC-N_3, and Fe.Zn.K/AC, respectively.(Figure 5.21, Figure 5.23, Figure 5.24 and Figure 5.26). O/P is 4.2, 4.7, 5.3, and 5.9 and olefin selectivity is 45.9%, 50.5%, 45.2%, and 51% in Fe.Zn.Na/AC-N_1, Fe.Zn.Na/AC-N_2, and Fe.Zn.Na/AC, respectively(Figure 5.20, Figure 5.22 and Figure 5.25).

Olefin yield of bulk catalyst in this study ranged from 1.4×E-5 to 4.3×E-5 in 2Fe.Zn0.4Na (AH) and 2Fe.Zn0.2Na (SC-I)$_1$ catalysts, respectively. However, olefin yield ranges from 1.22×E-4 - 1.62×E-4 in AC and N-doped AC supported catalysts as given in Table 5.10 that are higher than that of bulk catalysts and are generally acceptable compared to literature values. Considerable difference between olefin yields of supported catalysts was not observed.

The aim of using support in this study was to decrease deactivation by providing high surface area and enhancing dispersion. This was achieved by observing FTO results of the bulk and supported catalysts.

In order to figure out the different deactivation behavior of bulk catalysts and supported ones, it is of interest to compare SEM-EDS images of 2Fe.Zn0.2Na (AH-I) with that of Fe.Zn.Na/AC-N_2 (Figure 5.11). These two catalysts have similar metal molar ratio of Fe/Zn/Na =2/1/0.2, the former is bulk catalyst and the later includes 25% metal.

Both available high surface area and even distribution of metals (Fe and Zn) on the surface of the supported Fe.Zn.Na/AC-N_2 catalyst may lead to reduction in coking tendency and deactivation and increase the stability. The CO conversion of the supported catalyst was 93% while that of bulk catalyst was 60% at the end of 30-35 hour reaction period (Table 5.8 and Table 5.10).

Finally, H_2 conversion and CO_2 selectivity of AC and N-doped supported catalysts are available in Appendix D, Figure D.3 for evaluation.

Table 5.10 : FTO performance of AC and N-doped AC supported catalysts.

				Hydrocarbon Sel. %					
Code	Catalyst	CO Conv. (%)	CO_2 Sel.	CH_4	$C^{=}_2$-$C^{=}_4$	C^{0}_2-C^{0}_4	O/P	C_{5+}	Olefin yield (g C/g Fe. s)
A1	Fe.Zn.Na/ AC-N_1	92.5	38.4	21.1	45.9	11.8	4.2	20.5	1.6 E-04
A2	Fe.Zn.K/ AC-N_1	92.5	37.5	20.8	51.3	9.2	5.7	18.6	1.4 E-04
A3	Fe.Zn.Na/ AC-N_2	93.6	37.6	19.9	50.5	11.1	4.7	18.6	1.5 E-04
A4	Fe.Zn.K/ AC-N_2	93.0	38.4	17.4	51.4	7.9	6.9	23.1	1.4 E-04
A5	Fe.Zn.K/ AC-N_3	92.6	38.6	15.8	50.6	7.1	7.3	26.3	1.3 E-04
A6	Fe.Zn.Na/AC	89.6	38.5	18.1	51.0	9.2	5.9	21.6	1.6 E-04
A7	Fe.Zn.K/AC	88.4	38.9	15.8	50.9	8.6	6.6	24.0	1.2 E-04

a: reaction conditions: 1 g catalyst, 310 °C, 1.0 MPa, 50 mL. min^{-1} syngas (H_2/CO = 2), and reaction time = 35 h; CO conversion is reported at 35^{th} hour and product selectivity listed is obtained as an average value of analysis result in 35 h.

6. CONCLUSIONS AND RECOMMENDATIONS

Na-promoted Fe.Zn catalysts in zinc ferrite structure were used to directly get light olefins (C_2-C_4) from syngas. In an effort to understand the effect of precipitant and solid basicity on Fischer-Tropsch activity, different synthesis methods with two different precipitants have been applied. As total alkalinity of precipitation affects hydrolysis and influences the composition of the intermediate hydrolytic complexes, the final features of metal hydroxide precipitates might be induced with the precipitation conditions. This was proved by the observed change on the textural properties of zinc ferrites such as total surface area, crystal size and morphology under different alkaline environment. Different TPR profiles of the catalysts with different basicity might be indicative of changing chemisorption properties depending on the catalyst crystallite size and morphology. Three distinct classes of basic groups affecting the catalytic activity and stability were noticed as well. Improved conversion due to the facilitated CO dissociation over basic sites and concomitant deactivation possibly through fouling might be interpreted as both the number of basic sites and strength were determinant on the final catalytic behavior. For all samples with certain amount of sodium, selectivity profiles come to a common point, namely higher light olefin and C_{5+} selectivity at the expense of methane and paraffin selectivity. However, deactivation in the presence of alkali cations remains an important issue. However, the presence of less-coking catalysts despite basicity, as in 2Fe.Zn0.2Na $(SC\text{-}I)_1$, suggests that there might be an optimum for basicity and its strength. This might ensure a balance between the rate of CO dissociation and the rates of chain growth otherwise coking occurs due to the uncontrolled rate of hydrocarbon chains on the active sites.

Since sodium cation (Na) donates electron to the surface and strengthen the CO adsorption and its dissociation, sodium promotion might provide a relatively high coverage of carbon on the surface in relation to hydrogen. As a result of deficiency in surface hydrogen, decreased paraffin and methane selectivity requiring more hydrogen transfer rates have been observed. The chain growth and termination reactions might occur in a way that C_2-C_4 olefins might be favorably formed at suppressed rate of

hydrogenation reactions of surface species. This might be the reason of high light olefin selectivity when the catalysts have been promoted with an alkali such as sodium or potassium.

In addition to an increase in olefin selectivity, the chain growth rate might increase in the presence of alkali due to the re-adsorption of intermediate olefins and hydrocarbons in longer chains might be formed as apparent from high C_{5+} selectivity in Na impregnated catalysts in comparison with that of base catalysts, 2Fe.Zn(AH) and 2Fe.Zn(SC).

However, although C_2-C_4 olefin and C_{5+} selectivity increases at the expense of C_2-C_4 paraffins and methane, another point that should be mentioned here is that in some cases a local rise in C_2-C_4 olefin selectivity with a concomitant decrease in C_{5+} selectivity has been noticed as well. As a plausible explanation on the mechanism of FT reaction to light olefins and C_{5+} species, upon changing the surface concentration of reaction intermediate species, light olefins might desorb or re-adsorbed onto the surface to proceed the surface polymerization reaction. As a result of this, a concurrent change in light olefin and C_{5+} selectivity might be observed.

Investigating H_2 consumption and CO_2 selectivity, it was believed that there should be a traceable trend in H_2 conversion and CO_2 selectivity due to WGS reaction. In general, CO_2 selectivity, close to 40%, was observed for all samples. Besides, H_2 conversions were always lower than CO conversion proving secondarily hydrogen formation via WGS reaction. Simultaneous decreases in both CO and H_2 conversions due to coking indicated the consecutive occurrence of FT and WGS reactions with time on stream.

In Cu and K promoted bulk catalysts, as it was observed from the H_2-TPR profiles of the catalysts that Cu has facilitated the reduction of iron oxide while K affects retard of reduction. TPR profiles of the catalysts give an idea on their crystallite size and surface areas.

Regarding the change of alkalinity in terms of its cationic nature, the same effect but in different intensities could be expected from potassium and sodium alkali compounds. K seemed to have a slightly stronger effect than sodium since when ~3% of K was added to the base 2Fe.Zn(SC) catalyst it led severe coking tendency (17% C content of spent catalyst) and much loss of CO conversion from 88% to 55%. The same trend was observed for 2Fe.Zn0.2K(AH) catalyst with ~ 4% K content on the

base 2Fe.Zn(AH). The same effect has been observed but in a less intensive way. So the type and amount of alkali in the content of Fe.Zn base catalyst should be decided by considering its ultimate effect on coking and activity loss.

Using AC and N-doped AC as the support of the catalyst in this study showed high and satisfactory FTO performance compared to bulk catalysts. Whereas there seemed a trade off between olefin selectivity and CO conversion when the bulk catalyst was promoted with an alkali compound, high surface area and improved thermal stability as bring with the use of support (AC or N-doped AC) might help in overcoming coking and activity loss problems. It was shown that when these supports have been prepared with metal loading in composition with the bulk catalysts as Fe: Zn: Alkali Promoter=2:1:0.2 in molar ratios, high olefin selectivity together with reasonable CO conversion have been achieved for all these supported catalysts. This improvement in FTO performance of the catalysts were ascribed to the high surface area that was provided by the porous structure of the activated carbon and this was confirmed by SEM-EDS images as well. The relatively less reactive surface of activated carbon is a distinctive feature of it from other kinds of support materials such as metal oxides or acidic or basic micro or mesoporous materials. Its less reactive surface but high surface area with porosity makes advantages over the reactive support surfaces which might otherwise interacts with the active metals and passivates.

In addition, AC might render a higher accessibility to active sites as active sites might be evenly over it in relation to the bulk catalysts. All these may prevent sintering or agglomeration of active metals sites and/or reduce the overall coking tendency of the catalysts due to the uncontrolled rate of hydrocarbon chains on the active sites.

All in all, using AC and N-doped AC had a significant effect on improving CO conversion and stability of the catalyst while preserving its high light olefin selectivity in the presence of alkali promoters. All these seemed closely related to high metal dispersion over the highly porous support surface and its less reactive surface nature. Finally, nitrogen-doping seemed only to be effective to enhance the thermal stability of the catalyst by modifying the surface functional groups.

REFERENCES

[1] **Yahyazadeh, A., Dalai, A. K., Ma, W., & Zhang, L.** (2021). "Fischer–Tropsch Synthesis for Light Olefins from Syngas: A Review of Catalyst Development," *Reactions*, vol. 2, no. 3, pp. 227–257, doi: 10.3390/reactions2030015.

[2] **Gholami, Z.; Gholami, F.; Tišler, Z.; Tomas, M.; Vakili, M.** (2021). "A review on production of light olefins via fluid catalytic cracking," *Energies*, vol. 14, no. 4, pp. 1–36, doi: 10.3390/en14041089.

[3] **Subramanian, R., & Schmidt, L. D.** (2004). "Renewable olefins from biodiesel by autothermal reforming," *Angewandte Chemie - International Edition*, vol. 44, no. 2, pp. 302–305, doi: 10.1002/anie.200460790.

[4] **Torres Galvis, H. M.** (2013). *Direct production of lower olefins from synthesis gas using supported*, (Doctoral dissertation, Utrecht University).

[5] **Statista Research Department,** "Global ethylene demand and capacity 2015-2022." https://www.statista.com/statistics/1246694/ethylene-demand-capacity-forecast-worldwide (accessed Apr. 06, 2023).

[6] **Francis.A.Carey,** "ethylene.". *Encyclopedia Britannica*, 25 Aug. 2023, https://www.britannica.com/science/ethylene. Accessed 6 April 2023

[7] **Li, J. B., Ma, H. F., Zhang, H. T., Sun, Q. W., Ying, W. Y., & Fang, D. Y.** (2014). "Direct production of light olefins from syngas over potassium modified Fe-Mn catalyst," *Reaction Kinetics, Mechanisms and Catalysis*, vol. 112, no. 2, pp. 409–423, doi: 10.1007/s11144-014-0716-0.

[8] **Torres Galvis, H. M., & de Jong, K. P.** (2013). "Catalysts for production of lower olefins from synthesis gas: A review," *ACS Catalysis*, vol. 3, no. 9, pp. 2130–2149, doi: 10.1021/cs4003436.

[9] **Zhang, Q., Deng, W., & Wang, Y.** (2013). "Recent advances in understanding the key catalyst factors for Fischer-Tropsch synthesis," *Journal of Energy Chemistry*, vol. 22, no. 1, pp. 27–38, doi: 10.1016/S2095-4956(13)60003-0.

[10] **Lu, Y., Yan, Q., Han, J., Cao, B., Street, J., & Yu, F.** (2017). "Fischer–Tropsch synthesis of olefin-rich liquid hydrocarbons from biomass-derived syngas over carbon-encapsulated iron carbide/iron nanoparticles catalyst," *Fuel*, vol. 193, pp. 369–384, doi: 10.1016/j.fuel.2016.12.061.

[11] **Lama, S. M., Weber, J. L., Heil, T., Hofmann, J. P., Yan, R., de Jong, K. P., & Oschatz, M.** (2018). "Tandem promotion of iron catalysts by sodium-sulfur and nitrogen-doped carbon layers on carbon nanotube supports for the Fischer-Tropsch to olefins synthesis," *Applied Catalysis A: General*, vol. 568, no. August, pp. 213–220, doi: 10.1016/ j.apcata.2018.09.016.

[12] **Saib, A. M., Moodley, D. J., Ciobîcă, I. M., Hauman, M. M., Sigwebela, B. H., Weststrate, C. J., ... & Van de Loosdrecht, J.** (2010). "Fundamental understanding of deactivation and regeneration of cobalt Fischer-Tropsch synthesis catalysts," *Catalysis Today*, vol. 154, no. 3–4, pp. 271–282, doi: 10.1016/j.cattod. 2010.02.008.

[13] **Jahangiri, H., Bennett, J., Mahjoubi, P., Wilson, K., & Gu, S.** (2014). "A review of advanced catalyst development for Fischer-Tropsch synthesis of hydrocarbons from biomass derived syn-gas," *Catalysis Science and Technology*, vol. 4, no. 8, pp. 2210–2229, doi: 10.1039/c4cy00327f.

[14] **Van Santen, R. A., Markvoort, A. J., Filot, I. A. W., Ghouri, M. M., & Hensen, E.** (2013). "Mechanism and microkinetics of the Fischer-Tropsch reaction," *Physical Chemistry Chemical Physics*, vol. 15, no. 40, pp. 17038–17063, doi: 10.1039/c3cp52506f.

[15] **Wang C., Xu L., and Wang Q.** (2003). "Review of Directly Producing Light Olefins via CO Hydrogenation," *Journal of Natural Gas Chemistry*, vol. 12, no. 1, pp. 10–16, doi: 10.1016/S1003-9953-2003-12-1-10-16.

[16] **Van den Berg, F. R., Crajé, M. W. J., Kooyman, P. J., Van der Kraan, A. M., & Geus, J. W.** (2002). "Synthesis of highly dispersed zirconia-supported iron-based catalysts for Fischer – Tropsch synthesis," vol. 235, pp. 217–224, doi: doi.org/10.1016/S0926-860X(02)00270-3.

[17] **Sun, J., Chen, Y., & Chen, J.** (2017). "Towards stable Fe-based catalysts with suitable active phase for Fischer-Tropsch synthesis to lower olefins," *Catalysis Communications*, vol. 91, pp. 34–37, doi: 10.1016/ j.catcom.2016.12.008.

[18] **Xu-Yide, H. J., & Xu-Longya, W. Q.** (1994). "A new supported Fe-MnO catalyst for the production of light olefins from syngas. II. Effect of support on the secondary reactions of C_2H_4," *Catalysis Letters*, vol. 24, no. 1–2, pp. 187–195, doi: 10.1007/ BF00807389.

[19] **Gaube, J., & Klein, H. F.** "The promoter effect of alkali in Fischer-Tropsch iron and cobalt catalysts(2008), *Applied Catalysis A: General*, vol. 350, no. 1, pp. 126–132, doi: 10.1016/j.apcata.2008.08.007.

[20] **Xiong, H., Motchelaho, M. A., Moyo, M., Jewell, L. L., & Coville, N. J.** (2015). "Effect of Group i alkali metal promoters on Fe/CNT catalysts in Fischer-Tropsch synthesis," *Fuel*, vol. 150, pp. 687–696, doi: 10.1016/j.fuel.2015.02.099.

[21] **Cheng, Y., Lin, J., Xu, K., Wang, H., Yao, X., Pei, Y., ... & Zong, B.** (2016). "Fischer-Tropsch Synthesis to Lower Olefins over Potassium-Promoted Reduced Graphene Oxide Supported Iron Catalysts " *ACS Catalysis*, vol. 6, no. 1, pp. 389–399, doi: 10.1021/ acscatal.5b02024.

[22] **Yang, S., Chun, H. J., Lee, S., Han, S. J., Lee, K. Y., & Kim, Y. T.** (2020). "Comparative Study of Olefin Production from CO and CO_2Using Na-And K-Promoted Zinc Ferrite," *ACS Catalysis*, vol. 10, no. 18, pp. 10742–10759, doi: 10.1021/acscatal.0c02429.

[23] **Zhai, P., Xu, C., Gao, R., Liu, X., Li, M., Li, W., ... & Ma, D.** (2016). " Highly Tunable Selectivity for Syngas-Derived Alkenes over Zinc and Sodium-Modulated Fe_5C_2 Catalyst ," *Angewandte Chemie*, vol. 128, no. 34, pp. 10056–10061, doi: 10.1002/ange. 201603556.

[24] **Li, J. B., Ma, H. F., Zhang, H. T., Sun, Q. W., Ying, W. Y., & Fang, D. Y.** (2014). "Sodium promoter on iron-based catalyst for direct catalytic synthesis of light alkenes from syngas," *Fuel Processing Technology*, vol. 125, pp. 119–124, doi: 10.1016/j.fuproc.2014.03.017.

[25] **Cheng, K., Ordomsky, V. V., Legras, B., Virginie, M., Paul, S., Wang, Y., & Khodakov, A. Y.** (2015). "Sodium-promoted iron catalysts prepared on different supports for high temperature Fischer-Tropsch synthesis," *Applied Catalysis A: General*, vol. 502, pp. 204–214, doi: 10.1016/j.apcata. 2015.06.010.

[26] **Li, S., Li, A., Krishnamoorthy, S., & Iglesia, E.** (2001). "Effects of Zn, Cu, and K promoters on the structure and on the reduction, carburization, and catalytic behavior of iron-based Fischer-Tropsch synthesis catalysts," *Catalysis Letters*, vol. 77, no. 4, pp. 197–205, doi: 10.1023/A: 1013284217689.

[27] **Choi, Y. H., Ra, E. C., Kim, E. H., Kim, K. Y., Jang, Y. J., Kang, K. N., ... & Lee, J. S.** (2017). "Sodium-Containing Spinel Zinc Ferrite as a Catalyst Precursor for the Selective Synthesis of Liquid Hydrocarbon Fuels," *ChemSusChem*, vol. 10, no. 23, pp. 4764–4770, doi: 10.1002/cssc. 201701437.

[28] **Falbo, L., Martinelli, M., Visconti, C. G., Lietti, L., Forzatti, P., Bassano, C., & Deiana, P.** (2017). "Effects of Zn and Mn Promotion in Fe-Based Catalysts Used for CO_x Hydrogenation to Long-Chain Hydrocarbons," *Industrial and Engineering Chemistry Research*, vol. 56, no. 45, pp. 13146–13156, doi: 10.1021/acs.iecr.7b01494.

[29] **Liang, M., Kang, W., & Xie, K.** (2009). "Comparison of reduction behavior of Fe_2O_3, ZnO and $ZnFe_2O_4$ by TPR technique," *Journal of Natural Gas Chemistry*, vol. 18, no. 1, pp. 110–113, doi: 10.1016/S1003-9953 (08)60073-0.

[30] **Yang, S., Lee, S., Kang, S. C., Han, S. J., Jun, K. W., Lee, K. Y., & Kim, Y. T.** (2019). "Linear α-olefin production with Na-promoted Fe-Zn catalysts via Fischer-Tropsch synthesis," *RSC Advances*, vol. 9, no. 25, pp. 14176–14187, doi: 10.1039/c9ra02471a.

[31] **Soled, S. L., Iglesia, E., Miseo, S., DeRites, B. A., & Fiato, R. A.** (1995). "Selective synthesis of α-olefins on Fe-Zn Fischer-Tropsch catalysts," *Topics in Catalysis*, vol. 2, no. 1–4, pp. 193–205, doi: 10.1007/ BF01491967.

[32] **Wang, H., Yang, Y., Xu, J., Wang, H., Ding, M., & Li, Y.** (2010). "Study of bimetallic interactions and promoter effects of FeZn, FeMn and FeCr Fischer-Tropsch synthesis catalysts," *Journal of Molecular Catalysis A: Chemical*, vol. 326, no. 1–2, pp. 29–40, doi: 10.1016/j.molcata. 2010.04.009.

[33] **Posey-Dowty, J., Moskowitz, B., Crerar, D., Hargraves, R., Tanenbaum, L., & Dowty, E.** (1986). "Iron oxide and hydroxide precipitation from ferrous solutions and its relevance to Martian surface mineralogy," *Icarus*, vol. 66, no. 1, pp. 105–116, doi: 10.1016/0019-1035(86)90010-2.

[34] **Zhao, M., Yan, C., Jinchang, S., & Qianwen, Z.** (2018). "Modified iron catalyst for direct synthesis of light olefin from syngas," *Catalysis Today*, vol. 316, no. February, pp. 142–148, doi: 10.1016/j.cattod.2018.05.018.

[35] **Barrientos, J., Garcilaso, V., Venezia, B., Aho, A., Odriozola, J. A., Boutonnet, M., & Järås, S.** (2017). "Fischer–Tropsch Synthesis Over Zr-Promoted Co/Γ-Al_2O_3 Catalysts," *Topics in Catalysis*, vol. 60, no. 17–18, pp. 1285–1298, doi: 10.1007/s11244-017-0813-1.

[36] **Zhang, Y., Yang, X., Yang, X., Duan, H., Qi, H., Su, Y., ... & Zhang, T.** (2020). "Tuning reactivity of Fischer–Tropsch synthesis by regulating TiO_x overlayer over Ru/TiO_2 nanocatalysts," *Nature Communications*, vol. 11, no. 1, doi: 10.1038/s41467-020-17044-4.

[37] **Astruc, D., Lu, F., & Aranzaes, J. R.** (2005). "Nanoparticles as recyclable catalysts: The frontier between homogeneous and heterogeneous catalysis," *Angewandte Chemie - International Edition*, vol. 44, no. 48, pp. 7852–7872, doi: 10.1002/anie.200500766.

[38] **Li, M., Xu, F., Li, H., & Wang, Y.** (2016). "Nitrogen-doped porous carbon materials: Promising catalysts or catalyst supports for heterogeneous hydrogenation and oxidation," *Catalysis Science and Technology*, vol. 6, no. 11, pp. 3670–3693, doi: 10.1039/c6cy00544f.

[39] **Li, Z., Liu, R., Xu, Y., & Ma, X.** (2015). "Enhanced Fischer-Tropsch synthesis performance of iron-based catalysts supported on nitric acid treated N-doped CNTs," *Applied Surface Science*, vol. 347, pp. 643–650, doi: 10.1016/j.apsusc.2015.04.169.

[40] **Dhakshinamoorthy, A., & Garcia, H.** (2012). "Catalysis by metal nanoparticles embedded on metal–organic frameworks," *Chemical Society Reviews*, vol. 41, no. 15, pp. 5262–5284, doi: 10.1039/ c2cs35047e.

[41] **Su, D. S., Perathoner, S., & Centi, G.** (2013). "Nanocarbons for the development of advanced catalysts," *Chemical Reviews*, vol. 113, no. 8, pp. 5782–5816, doi: 10.1021/cr300367d.

[42] **Valero-Romero, M. J., Rodríguez-Cano, M. Á., Palomo, J., Rodríguez-Mirasol, J., & Cordero, T.** (2021). "Carbon-Based Materials as Catalyst Supports for Fischer–Tropsch Synthesis: A Review," *Frontiers in Materials*, vol. 7, no. February, pp. 1–27, doi: 10.3389/fmats.2020.617432.

[43] **Petrova, T., Velinov, N., Filkova, D., Ivanova, I., Ivanov, I., Yordanova, I., ... & Mitov, I.** (2018). "Synthesis and characterization of supported spinel ferrite catalysts," *Journal of Chemical Technology and Metallurgy*, vol. 53, no. 6, pp. 1186–1194.

[44] **Rehman, A., Park, M., & Park, S. J.** (2019), "Current progress on the surface chemical modification of carbonaceous materials," *Coatings*, vol. 9, no. 2, pp. 1–21, doi: 10.3390/COATINGS9020103.

[45] **Grzybek, T., Klinik, J., Motak, M., & Papp, H.** (2008). "Nitrogen-promoted active carbons as catalytic supports. 2. The influence of Mn promotion on the structure and catalytic properties in SCR," *Catalysis Today*, vol. 137, no. 2–4, pp. 235–241, doi: 10.1016/j.cattod.2007.11.006.

[46] **Liu, G., Chen, Q., Oyunkhand, E., Ding, S., Yamane, N., Yang, G., ... & Tsubaki, N.** (2018), "Nitrogen-rich mesoporous carbon supported iron catalyst with superior activity for Fischer-Tropsch synthesis," *Carbon*, vol. 130, pp. 304–314, doi: 10.1016/j.carbon.2018.01.015.

[47] **Inagaki, M., Toyoda, M., Soneda, Y., & Morishita, T.** (2018). "Nitrogen-doped carbon materials," *Carbon*, vol. 132, pp. 104–140, doi: 10.1016/j.carbon.2018.02.024.

[48] **He, D., Jiang, Y., Lv, H., Pan, M., & Mu, S.** (2013). "Nitrogen-doped reduced graphene oxide supports for noble metal catalysts with greatly enhanced activity and stability," *Applied Catalysis B: Environmental*, vol. 132–133, pp. 379–388, doi: 10.1016/j.apcatb.2012.12.005.

[49] **Lu, J., Yang, L., Xu, B., Wu, Q., Zhang, D., Yuan, S., ... & Hu, Z.** (2014). "Promotion effects of nitrogen doping into carbon nanotubes on supported iron fischer-tropsch catalysts for lower olefins," *ACS Catalysis*, vol. 4, no. 2, pp. 613–621, doi: 10.1021/cs400931z.

[50] **Li, K., Chen, W., Yang, H., Chen, Y., Xia, S., Xia, M., ... & Chen, H.** (2019). "Mechanism of biomass activation and ammonia modification for nitrogen-doped porous carbon materials," *Bioresource Technology*, vol. 280, no. February, pp. 260–268, doi: 10.1016/ j.biortech.2019.02.039.

[51] **Tian, Z., Wang, C., Si, Z., Wen, C., Xu, Y., Lv, W., ... & Ma, L.** (2019). "Enhancement of light olefins selectivity over ndoped fischer-tropsch synthesis catalyst supported on activated carbon pretreated with $KMnO_4$," *Catalysts*, vol. 9, no. 6, doi: 10.3390/ catal9060505.

[52] **Xiong, H., Motchelaho, M. A., Moyo, M., Jewell, L. L., & Coville, N. J.** (2014). "Fischer-Tropsch synthesis: Iron-based catalysts supported on nitrogen-doped carbon nanotubes synthesized by post-doping," *Applied Catalysis A: General*, vol. 482, pp. 377–386, doi: 10.1016/j.apcata. 2014.06.019.

[53] **Naderi M.** (2015). "Surface Area: Brunauer-Emmett-Teller (BET)," *Progress in Filtration and Separation*, pp. 585–608, doi: 10.1016/B978-0-12-384746-1.00014-8.

[54] **Danesi, P. R, Chiarizia, R., Scibona, G., Riccardi, R.** (1973). "Hydrolytic precipitation of iron(III) in 1 M sodium nitrate medium," *Inorg. Chem*., vol. 12, pp. 2089–2091, doi: 10.1021/ic50127a028.

[55] **Sripriya, R. C., Ezhil, A., Madhavan, J., & Victor, A. R.** (2017). "Synthesis and Characterization studies of $ZnFe_2O_4$ nanoparticles," *Mechanics, Materials Science & Engineering*, no. December, pp. 21–27, doi: 10.2412/mmse.81.85.882.

[56] **Wang, C., Wang, Q., Sun, X., & Xu, L.** (2005). "CO hydrogenation to light alkenes over Mn/Fe catalysts prepared by coprecipitation and sol-gel methods," *Catalysis Letters*, vol. 105, no. 1–2, pp. 93–101, doi: 10.1007/s10562-005-8011-3.

[57] **Alkaim, A. F., Alrobayi, E. M., Algubili, A. M., & Aljeboree, A. M.** (2017). "Synthesis, characterization, and photocatalytic activity of sonochemical/hydration–dehydration prepared ZnO rod-like architecture nano/microstructures assisted by a biotemplate," *Environmental Technology (United Kingdom)*, vol. 38, no. 17, pp. 2119–2129, doi: 10.1080/09593330.2016.1246615.

[58] **Abbas, M., Zhang, J., Mansour, T. S., & Chen, J.** (2020). "Hierarchical porous spinel MFe_2O_4 (M=Fe, Zn, Ni and Co) nanoparticles: Facile synthesis approach and their superb stability and catalytic performance in Fischer-Tropsch synthesis," *International Journal of Hydrogen Energy*, vol. 45, no. 18, pp. 10754–10763, doi: 10.1016/j.ijhydene. 2020.02.044.

[59] **Yang, X., Zhang, H., Liu, Y., Ning, W., Han, W., Liu, H., & Huo, C.** (2019). "Preparation of iron carbides formed by iron oxalate carburization for fischer-tropsch synthesis," *Catalysts*, vol. 9, no. 4, pp. 1–14, doi: 10.3390/catal9040347.

[60] **Janbroers, S., Louwen, J. N., Zandbergen, H. W., & Kooyman, P. J.** (2009). "Insights into the nature of iron-based Fischer-Tropsch catalysts from quasi in situ TEM-EELS and XRD," *Journal of Catalysis*, vol. 268, no. 2, pp. 235–242, doi: 10.1016/j.jcat.2009.09.021.

[61] **Pourbafarani, S.** (2014). "The effect of alkali concentration on the structural and magnetic properties of Mn-Ferrite nanoparticles prepared via the coprecipitation method," *Metallurgical and Materials Transactions A: Physical Metallurgy and Materials Science*, vol. 45, no. 10, pp. 4535–4537, doi: 10.1007/s11661-014-2360-8.

[62] **Gül, Ö. F., Ataç, Ö., Boz, I., & Özkara-Aydınoğlu, Ş.** (2016). "La, Mn and Zn promoted microporous iron catalysts with high productivity and stability for Fischer–Tropsch synthesis," *Reaction Kinetics, Mechanisms and Catalysis*, vol. 117, no. 1, pp. 147–159, doi: 10.1007/ s11144-015-0932-2.

[63] **Tuptup, M., Kayaman-Apohan, N., Özkara-Sarıoğlan, Ş., Ünveren, E., Ataç, Ö., & Sarıoğlan, A.** (2021). "Poly(2,6-diphenyl-p-phenylene oxide) supported iron catalysts for the synthesis of lower olefins via Fischer–Tropsch reaction," *Reaction Kinetics, Mechanisms and Catalysis*, vol. 132, no. 2, pp. 695–715, doi: 10.1007/s11144-021-01964-3.

[64] **An, X., Wu, B., Hou, W., Wan, H., Tao, Z., Li, T., ... & Yi, F.** (2007). "The negative effect of residual sodium on iron-based catalyst for Fischer-Tropsch synthesis," *Journal of Molecular Catalysis A: Chemical*, vol. 263, no. 1–2, pp. 266–272, doi: 10.1016/j.molcata. 2006.09.003.

[65] **Liu, B., Geng, S., Zheng, J., Jia, X., Jiang, F., & Liu, X.** (2018). "Unravelling the New Roles of Na and Mn Promoter in CO_2 Hydrogenation over Fe_3O_4-Based Catalysts for Enhanced Selectivity to Light α-Olefins," *ChemCatChem*, vol. 10, no. 20, pp. 4718–4732, doi: 10.1002/cctc. 201800782.

[66] **Aziz, M. A. A., Jalil, A. A., Wongsakulphasatch, S., & Vo, D. V. N.** (2020). "Understanding the role of surface basic sites of catalysts in CO_2 activation in dry reforming of methane: A short review," *Catalysis Science and Technology*, vol. 10, no. 1, pp. 35–45, doi: 10.1039/c9cy 01519a.

[67] **Di Cosimo, J. I., Díez, V. K., Ferretti, C., & Apesteguía, C. R.** (2014). "Basic catalysis on MgO: Generation, characterization and catalytic properties of active sites," *Catalysis*, vol. 26, no. 3000, pp. 1–28, doi: 10.1039/9781782620037-00001.

[68] **Tsuji, H., Okamura-Yoshida, A., Shishido, T., & Hattori, H.** (2003). "Dynamic Behavior of Carbonate Species on Metal Oxide Surface: Oxygen Scrambling between Adsorbed Carbon Dioxide and Oxide Surface," *Langmuir*, vol. 19, no. 21, pp. 8793–8800, doi: 10.1021/la0342666.

[69] **Montanari, T., Castoldi, L., Lietti, L., & Busca, G.** (2011). "Basic catalysis and catalysis assisted by basicity: FT-IR and TPD characterization of potassium-doped alumina," *Applied Catalysis A: General*, vol. 400, no. 1–2, pp. 61–69, doi: 10.1016/j.apcata.2011.04.016.

[70] **Farias, F. E., Rabelo Neto, R. C., Baldanza, M. A., Schmal, M., & Fernandes, F. A.** (2011). "Effect of K promoter on the structure and catalytic behavior of supported iron-based catalysts in Fischer-Tropsch synthesis," *Brazilian Journal of Chemical Engineering*, vol. 28, no. 3, pp. 495–504, doi: 10.1590/S0104-66322011000300015.

[71] **Dry, M. E., & Oosthuizen, G. J.** (1968). "The correlation between catalyst surface basicity and hydrocarbon selectivity in the Fischer-Tropsch synthesis," *Journal of Catalysis*, vol. 11, no. 1, pp. 18–24, doi: 10.1016/0021-9517(68)90004-3.

[72] **Smyth. J. R.** (2010). "Quartz.", University of Colorado, Adopt-a-Mineral Project.

[73] **Jiang F. , Zhang M., Liu B., Xu Y., and Liu X..** (2017). "Insights into the influence of support and potassium or sulfur promoter on iron-based Fischer-Tropsch synthesis: Understanding the control of catalytic activity, selectivity to lower olefins, and catalyst deactivation," *Catalysis Science and Technology*, vol. 7, no. 5, pp. 1245–1265, doi: 10.1039/c7cy00048k.

[74] **James O. O., Chowdhury B., and Maity S.** (2015). "Comparative TPR and TPD Studies of Cu and Ca Promotion on Fe-Zn- and Fe-Zn-Zr-Based Fischer-Tropsch Catalysts," *Oil & Gas Science and Technology – Revue d'IFP Energies nouvelles*, vol. 70, no. 3, pp. 511–519, doi: 10.2516/ogst/2013114.

[75] **Wang, Z., Zhang, Y., Neyts, E. C., Cao, X., Zhang, X., Jang, B. W. L., & Liu, C. J.** (2018). "Catalyst Preparation with Plasmas: How Does It Work?," *ACS Catalysis*, vol. 8, no. 3, pp. 2093–2110, doi: 10.1021/acscatal. 7b03723.

[76] **Fu T., Liu R., Lv J., and Li Z.** (2014). "Influence of acid treatment on N-doped multi-walled carbon nanotube supports for Fischer-Tropsch performance on cobalt catalyst," *Fuel Processing Technology*, vol. 122, pp. 49–57, doi: 10.1016/j.fuproc.2014.01.016.

[77] **Zhang J., Lu S., Su X., Fan S., Ma Q., and Zhao T.** (2015). "Selective formation of light olefins from CO_2 hydrogenation over Fe-Zn-K catalysts," *Journal of CO_2 Utilization*, vol. 12, pp. 95–100, doi: 10.1016/j.jcou.2015.05.004.

[78] **Blanco-Andujar C., Ortega D., Pankhurst Q. A., and Thanh N. T. K.** (2012). "Elucidating the morphological and structural evolution of iron oxide nanoparticles formed by sodium carbonate in aqueous medium," *Journal of Materials Chemistry*, vol. 22, no. 25, pp. 12498–12506, doi: 10.1039/c2jm31295f.

[79] **Oschatz, M., Hofmann, J. P., van Deelen, T. W., Lamme, W. S., Krans, N. A., Hensen, E. J., & de Jong, K. P.** (2017). "Effects of the Functionalization of the Ordered Mesoporous Carbon Support Surface on Iron Catalysts for the Fischer–Tropsch Synthesis of Lower Olefins," *ChemCatChem*, vol. 9, no. 4, pp. 620–628, doi: 10.1002/cctc.201601228.

[80] **Tang, L., Dong, X. L., Xu, W., He, L., & Lu, A. H.** (2018). "Iron-based catalysts encapsulated by nitrogen-doped graphitic carbon for selective synthesis of liquid fuels through the Fischer-Tropsch process," *Cuihua Xuebao/Chinese Journal of Catalysis*, vol. 39, no. 12, pp. 1971–1979, doi: 10.1016/S1872-2067(18)63158-4.

[81] **An, X., Wu, B. S., Wan, H. J., Li, T. Z., Tao, Z. C., Xiang, H. W., & Li, Y. W.** (2007). "Comparative study of iron-based Fischer-Tropsch synthesis catalyst promoted with potassium or sodium," *Catalysis Communications*, vol. 8, no. 12, pp. 1957–1962, doi: 10.1016/j.catcom. 2007.03.016.

[82] **Herzog K. and Gaube J.** (1989). "Kinetic studies for elucidation of the promoter effect of alkali in Fischer-Tropsch iron catalysts," *Journal of Catalysis*, vol. 115, no. 2, pp. 337–346, doi: 10.1016/0021-9517(89)90038-9.

[83] **Yang, S., Lee, S., Kang, S. C., Han, S. J., Jun, K. W., Lee, K. Y., & Kim, Y. T.** (2019). "Linear α-olefin production with Na-promoted Fe-Zn catalysts via Fischer-Tropsch synthesis," *RSC Advances*, vol. 9, no. 25, pp. 14176–14187, doi: 10.1039/c9ra02471a.

[84] **Jiang F., Zhang M., Liu B., Xu Y., and Liu X.** (2017). "Insights into the influence of support and potassium or sulfur promoter on iron-based Fischer-Tropsch synthesis: Understanding the control of catalytic activity, selectivity to lower olefins, and catalyst deactivation," *Catalysis Science and Technology*, vol. 7, no. 5, pp. 1245–1265, doi: 10.1039/c7cy00048k.

[85] **Zhang, C. H., Yang, Y., Teng, B. T., Li, T. Z., Zheng, H. Y., Xiang, H. W., & Li, Y. W.** (2006). "Study of an iron-manganese Fischer-Tropsch synthesis catalyst promoted with copper," *Journal of Catalysis*, vol. 237, no. 2, pp. 405–415, doi: 10.1016/j.jcat.2005.11.004.

[86] **Li S., Krishnamoorthy S., Li A., Meitzner G. D., and Iglesia E.** (2002). "Promoted iron-based catalysts for the Fischer-Tropsch synthesis: Design, synthesis, site densities, and catalytic properties," *Journal of Catalysis*, vol. 206, no. 2, pp. 202–217, doi: 10.1006/jcat.2001.3506.

APPENDICES

APPENDIX A: SEM-EDS of bulk catalysts S1-S9
APPENDIX B: XRD pattern of all spent catalysts taken with Cu anode
APPENDIX C: XRD of Na-promoted fresh calcined bulk catalysts taken with Co anode
APPENDIX D: H_2 conversion and CO_2 selectivity of the catalysts versus TOS

APPENDIX A: SEM-EDS of bulk catalysts S1-S9

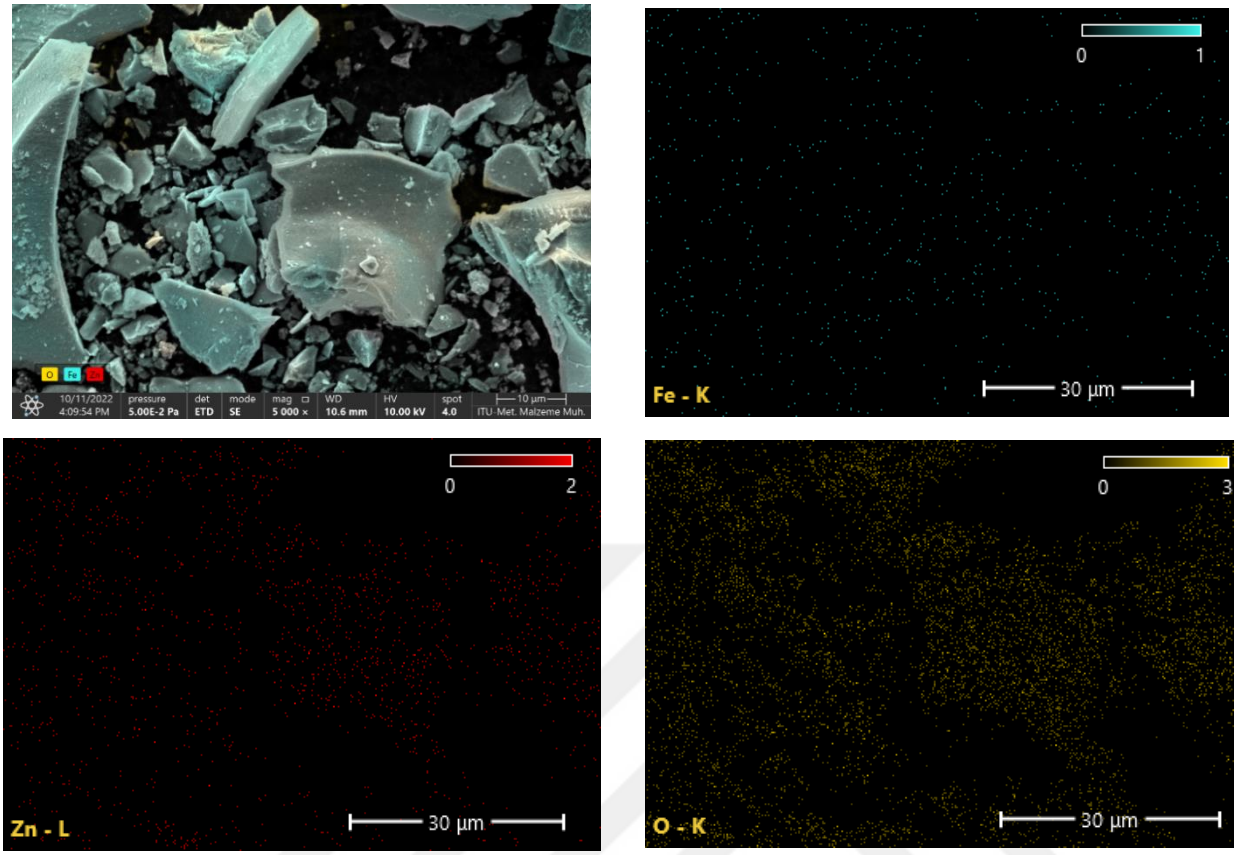

Element	Atomic %	Atomic % Error	Weight %	Weight % Error	Net Counts
Zn	11.0	0.4	20.3	0.7	2 250
O	53.7	0.9	24.2	0.4	6 987
Fe	35.2	2.4	55.4	3.8	957

Figure A.1 : SEM-EDS of 2Fe.Zn (AH) catalyst.

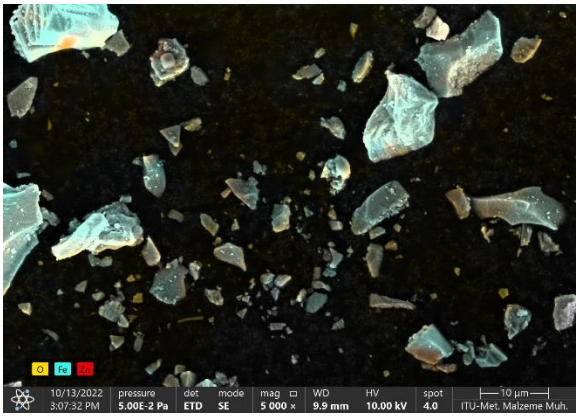

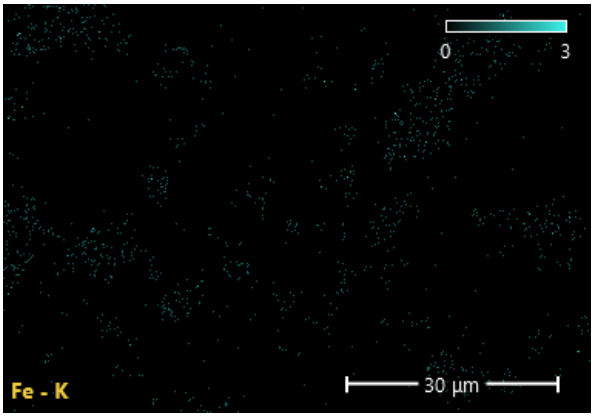

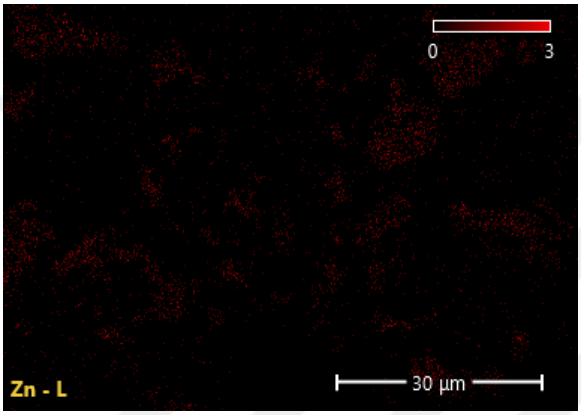

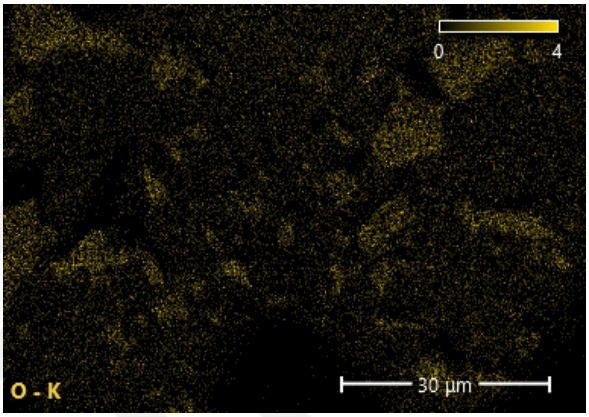

Element	Atomic %	Atomic % Error	Weight %	Weight % Error	Net Counts
Zn	8.8	0.2	19.7	0.5	5 939
O	68.8	0.7	37.6	0.4	29 017
Fe	22.4	1.3	42.7	2.4	1 858

Figure A.2 : SEM-EDS of 2Fe.Zn0.1Na (AH-I) catalyst.

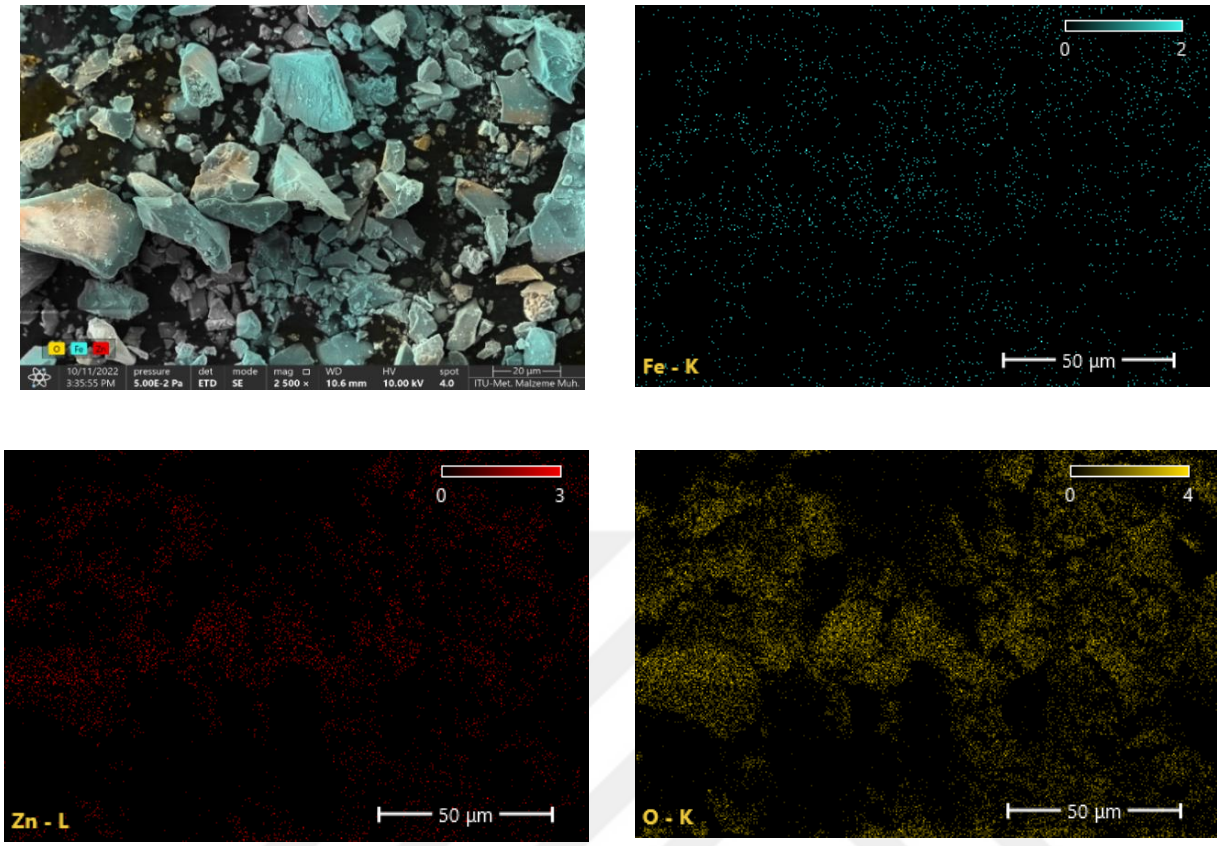

Element	Atomic %	Atomic % Error	Weight %	Weight % Error	Net Counts
Zn	11.3	0.2	21.4	0.3	10 877
O	56.1	0.5	25.9	0.2	33 740
Fe	32.6	1.1	52.6	1.8	4 076

Figure A.3 : SEM-EDS of 2Fe.Zn0.2Na (AH-I) catalyst.

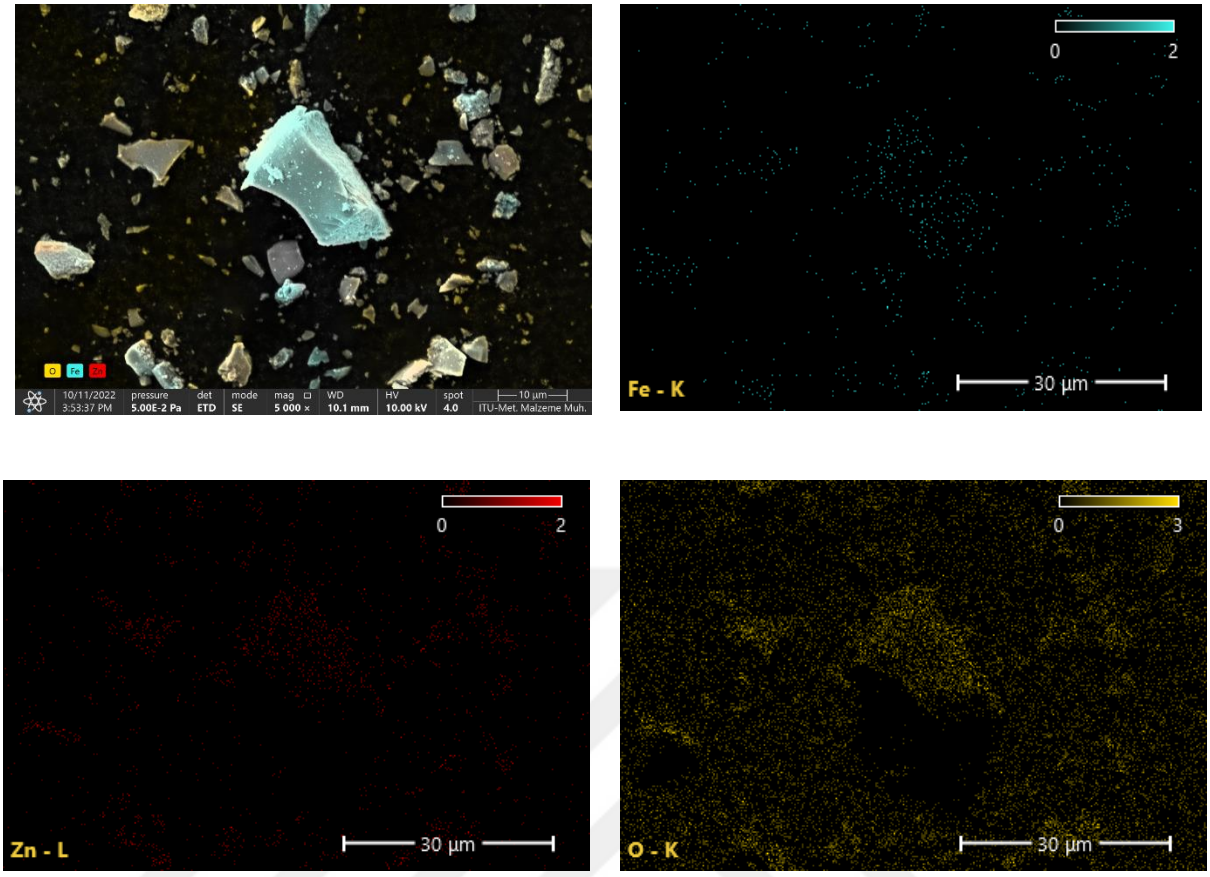

Element	Atomic %	Atomic % Error	Weight %	Weight % Error	Net Counts
Zn	7.1	0.3	17.6	0.7	2 828
O	76.0	0.8	46.4	0.5	19 404
Fe	16.9	1.6	36.0	3.3	817

Figure A.4 : SEM-EDS of 2Fe.Zn0.2Na (AH) catalyst.

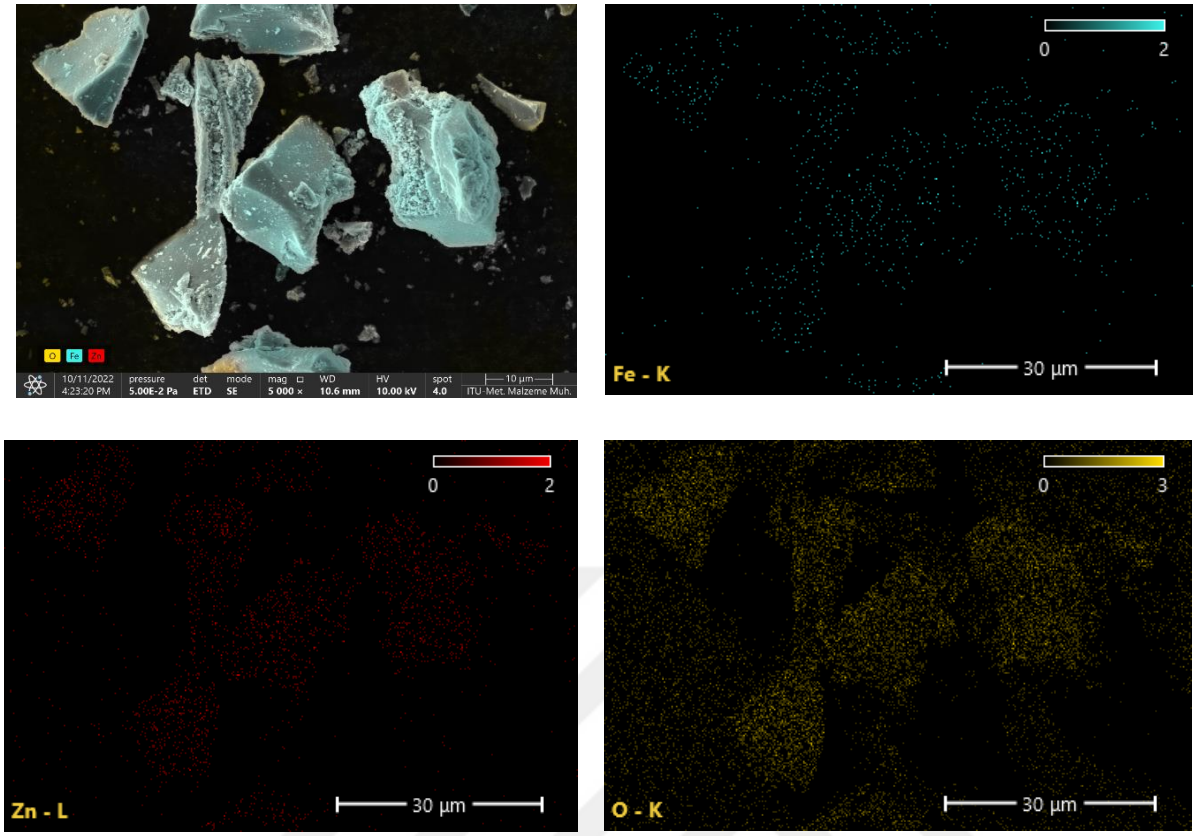

Element	Atomic %	Atomic % Error	Weight %	Weight % Error	Net Counts
Zn	9.2	0.3	19.1	0.6	3 634
O	63.4	0.8	32.2	0.4	16 039
Fe	27.4	1.7	48.7	3.0	1 399

Figure A.5 : SEM-EDS of 2Fe.Zn0.4Na (AH) catalyst.

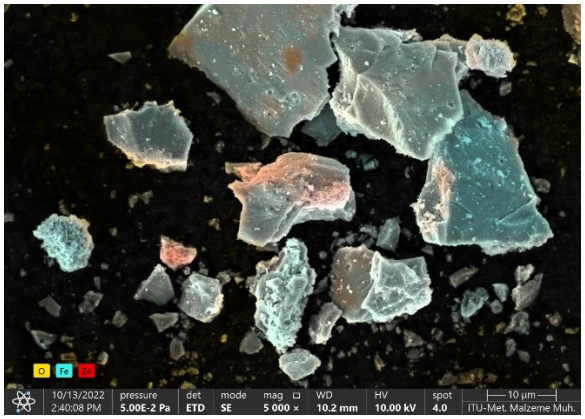

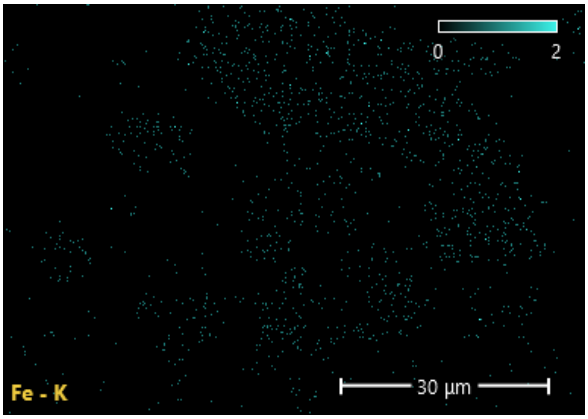

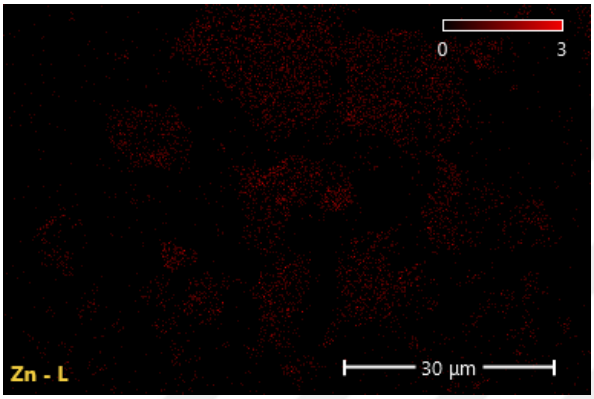

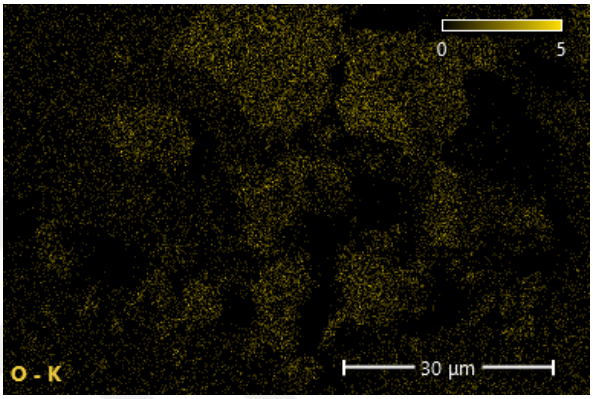

Element	Atomic %	Atomic % Error	Weight %	Weight % Error	Net Counts
Zn	15.0	0.2	28.9	0.5	10 004
O	58.7	0.7	27.7	0.3	22 309
Fe	26.3	1.3	43.3	2.2	2 104

Figure A.6 : SEM-EDS of 2Fe.Zn (SC) catalyst.

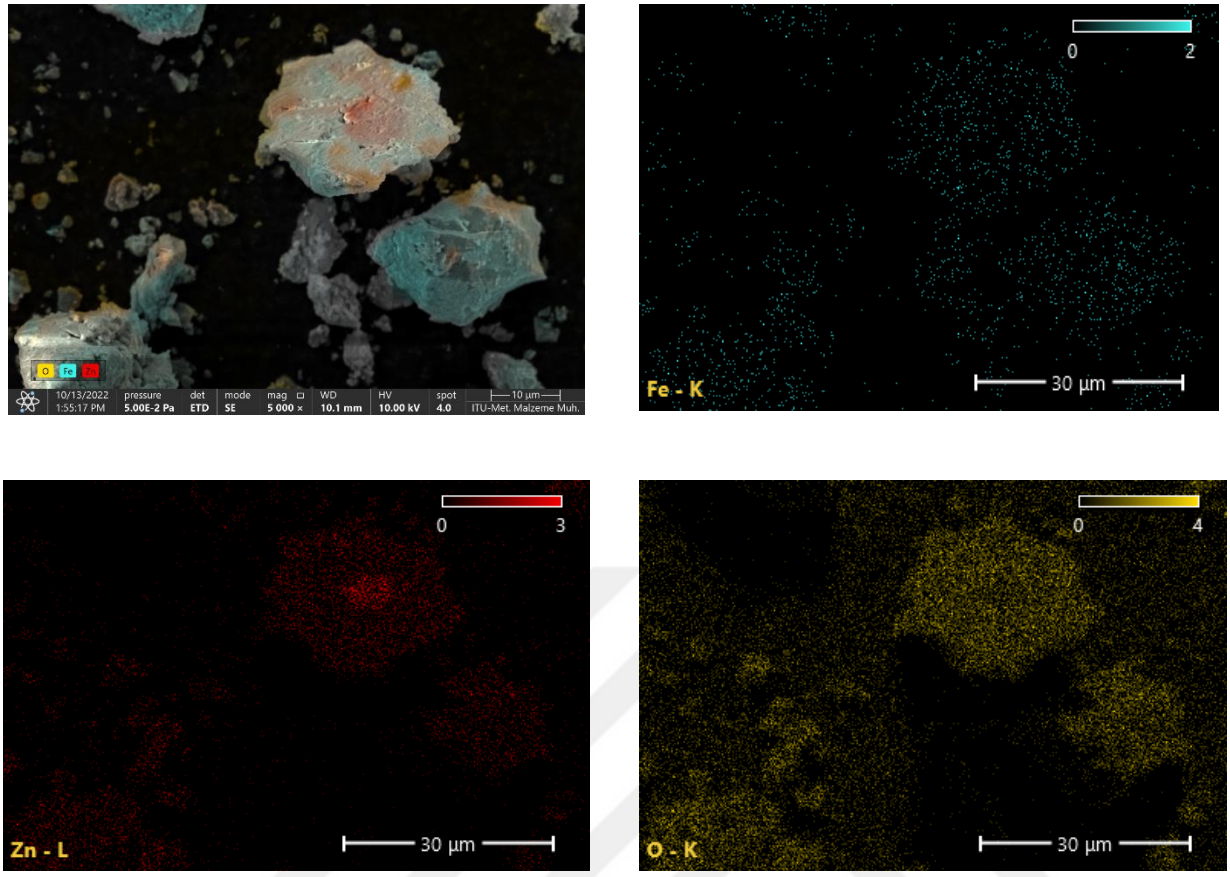

Element	Atomic %	Atomic % Error	Weight %	Weight % Error	Net Counts
Zn	14.7	0.2	28.8	0.4	13 066
O	60.0	0.6	28.8	0.3	30 309
Fe	25.3	1.2	42.4	1.9	2 679

Figure A.7 : SEM-EDS of 2Fe.Zn0.2Na $(SC\text{-}I)_1$ catalyst.

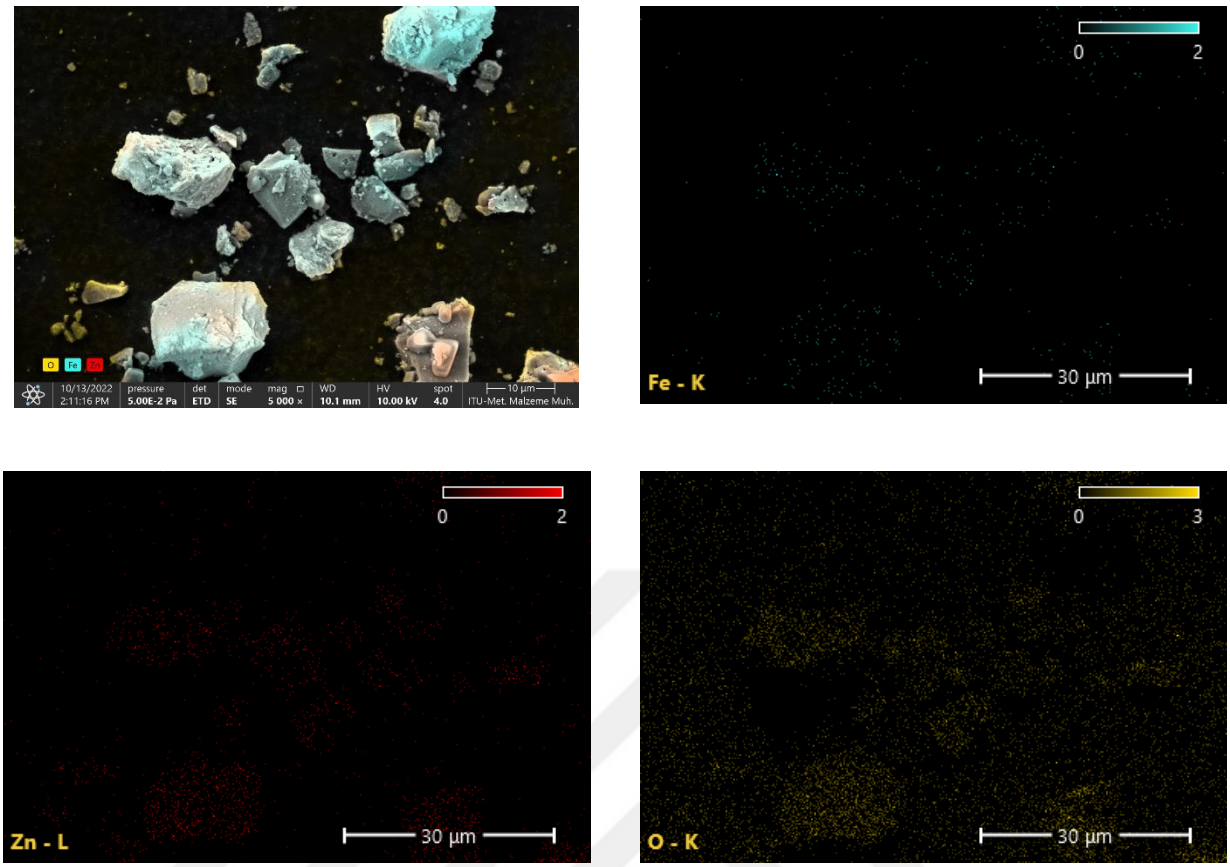

Element	Atomic %	Atomic % Error	Weight %	Weight % Error	Net Counts
Zn	12.8	0.2	27.1	0.5	3 052
O	65.6	1.1	33.9	0.6	8 997
Fe	21.6	2.1	39.0	3.8	607

Figure A.8 : SEM-EDS of 2Fe.Zn0.2Na $(SC\text{-}I)_2$ catalyst.

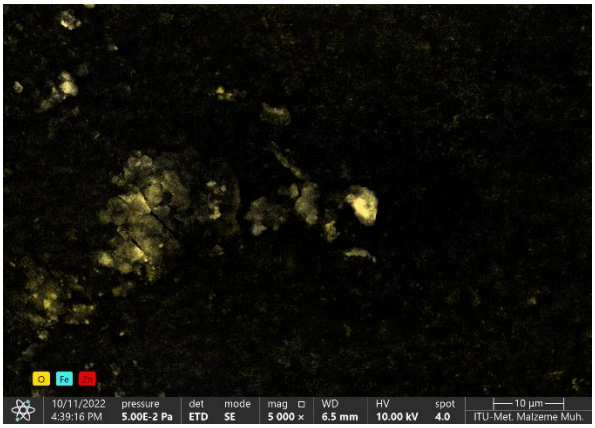

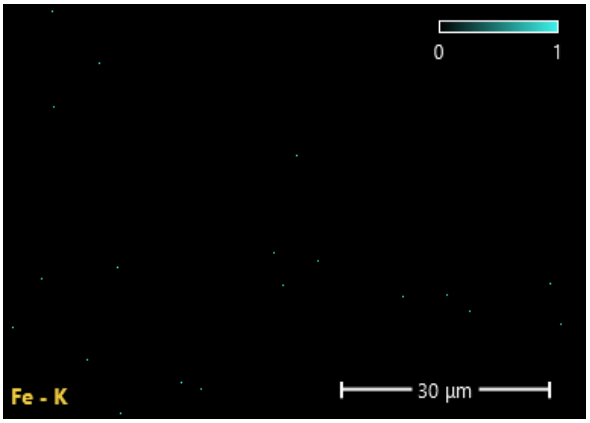

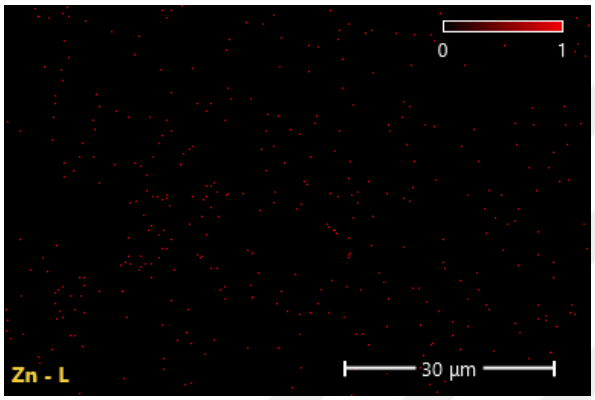

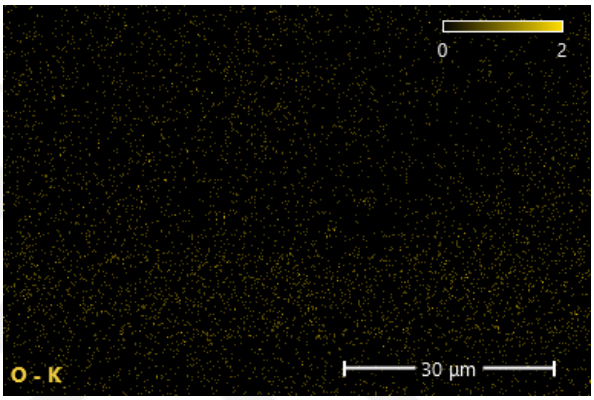

Element	Atomic %	Atomic % Error	Weight %	Weight % Error	Net Counts
Zn	1.3	0.4	5.1	1.4	116
O	98.7	1.5	94.9	1.4	6 544
Fe	0.0	---	0.0	---	0

Figure A.9 : SEM-EDS of 2Fe.Zn0.2Na $(SC\text{-}I)_3$ catalyst.

APPENDIX B: XRD pattern of all spent catalysts taken with Cu anode

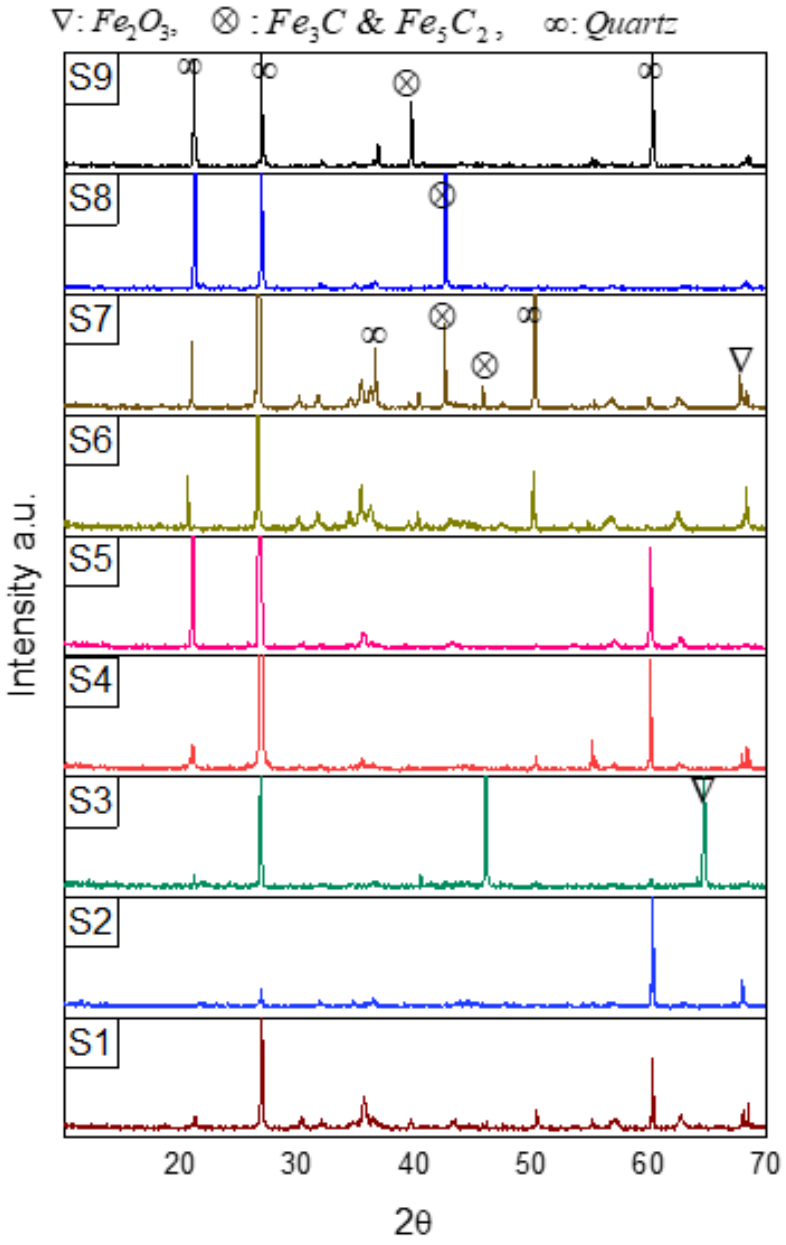

Figure B.1 : XRD of Na-promoted spent catalysts taken with Cu anode. S1= 2Fe.Zn (AH), S2= 2Fe.Zn0.1Na (AH-I), S3= 2Fe.Zn0.2Na (AH-I), S4= 2Fe.Zn0.2Na (AH), S5= 2Fe.Zn0.4Na (AH), S6= 2Fe.Zn (SC), S7= 2Fe.Zn0.2Na (SC-I)$_1$, S8= 2Fe.Zn0.2Na (SC-I)$_2$, S9= 2Fe.Zn0.2Na (SC-I)$_3$.

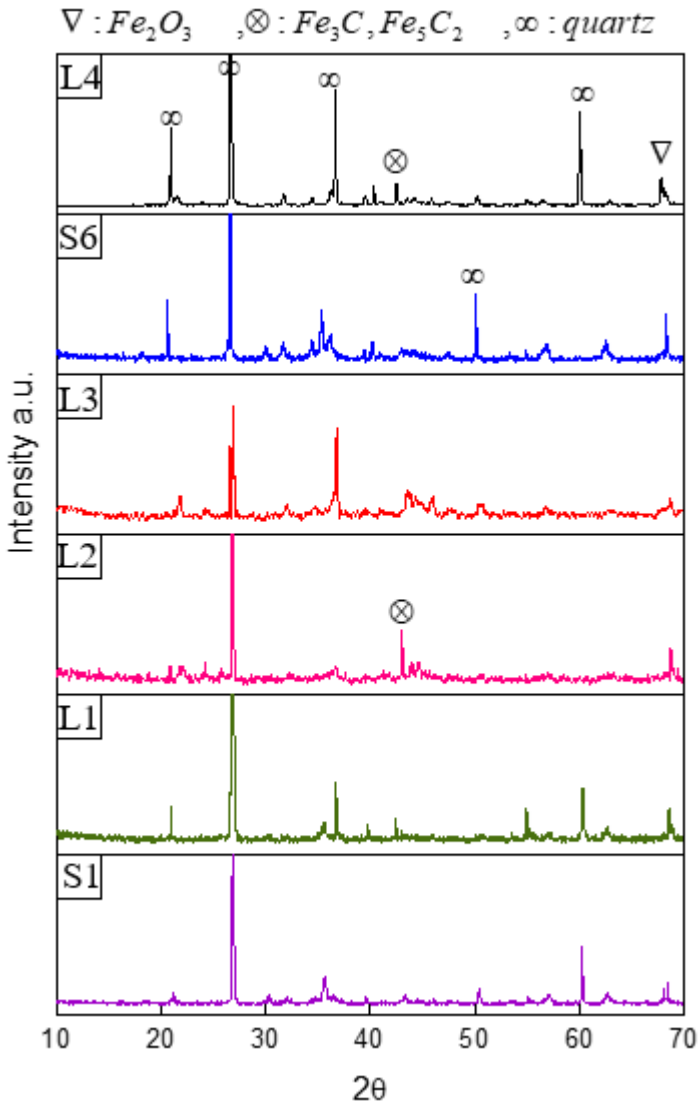

Figure B.2 : XRD of K and Cu-promoted spent catalysts taken with Cu anode. S1: 2Fe.Zn (AH), L1: 2Fe.Zn0.2Cu (AH-I), L2: 2Fe.Zn0.2K (AH-I), L3: 2Fe.Zn0.2Cu0.05K (AH-I), S6: 2Fe.Zn (SC), L4: 2Fe.Zn0.2K (SC-I).

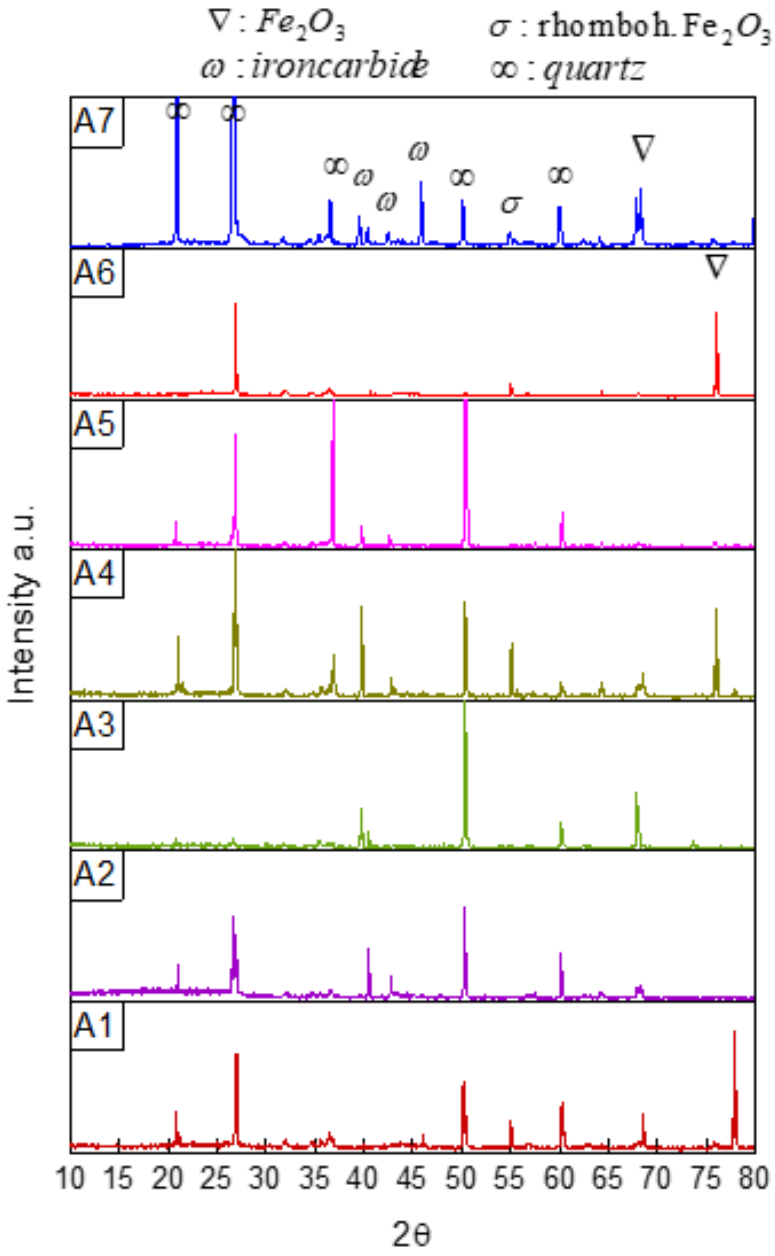

Figure B.3 : XRD of supported spent catalysts, A1-A7 taken with Cu anode. A1=Fe.Zn. Na/AC-N_1, A2=Fe.Zn.K/ AC-N_1, A3=Fe.Zn.Na/ AC-N_2, A4=Fe.Zn.K/ AC-N_2, A5=Fe.Zn.K/ AC-N_3, A6=Fe.Zn.Na/AC, A7=Fe.Zn.K/AC).

APPENDIX C: XRD of Na-promoted fresh calcined bulk catalysts taken with Co anode

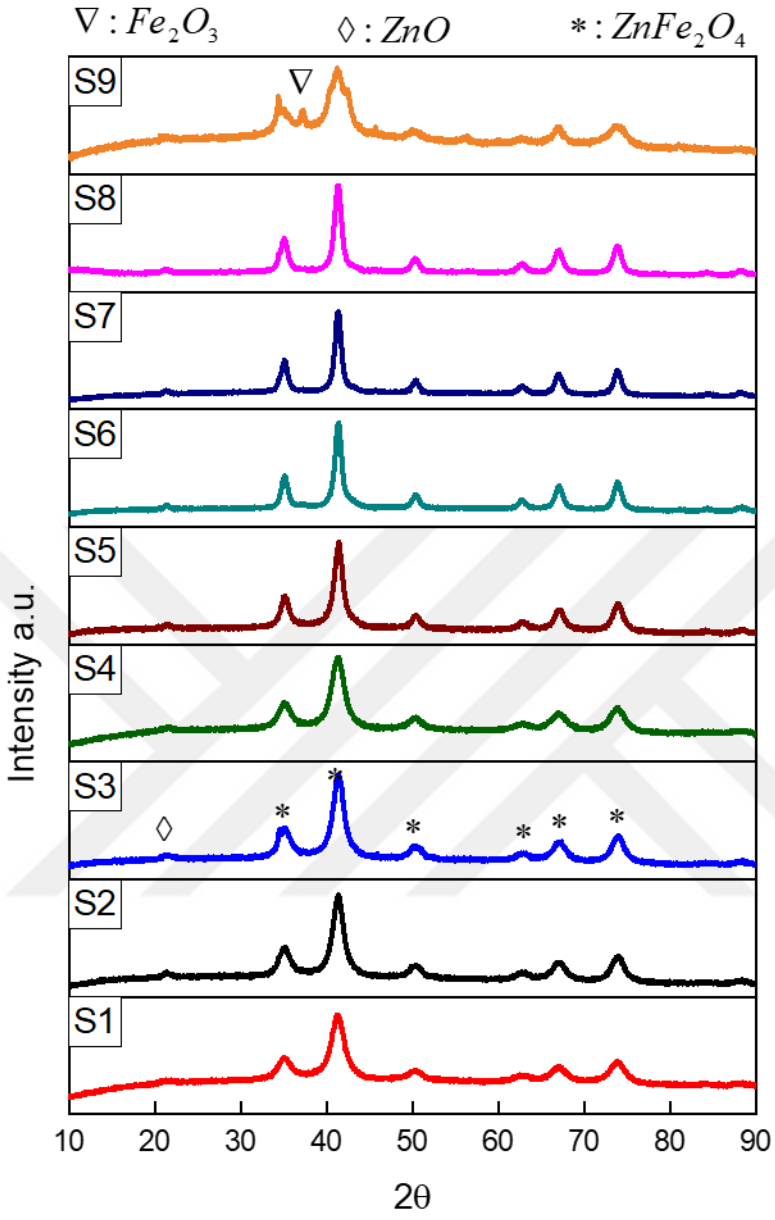

Figure C.1 : XRD of Na-promoted fresh calcined bulk catalysts taken with Co anode. S1= 2Fe.Zn (AH), S2= 2Fe.Zn0.1Na (AH-I), S3= 2Fe.Zn0.2Na (AH-I), S4= 2Fe.Zn0.2Na (AH), S5= 2Fe.Zn0.4Na (AH), S6= 2Fe.Zn (SC), S7= 2Fe.Zn0.2Na $(SC\text{-}I)_1$, S8= 2Fe.Zn0.2Na $(SC\text{-}I)_2$, S9= 2Fe.Zn0.2Na $(SC\text{-}I)_3$.

APPENDIX D: H_2 conversion and CO_2 selectivity of the catalysts versus TOS

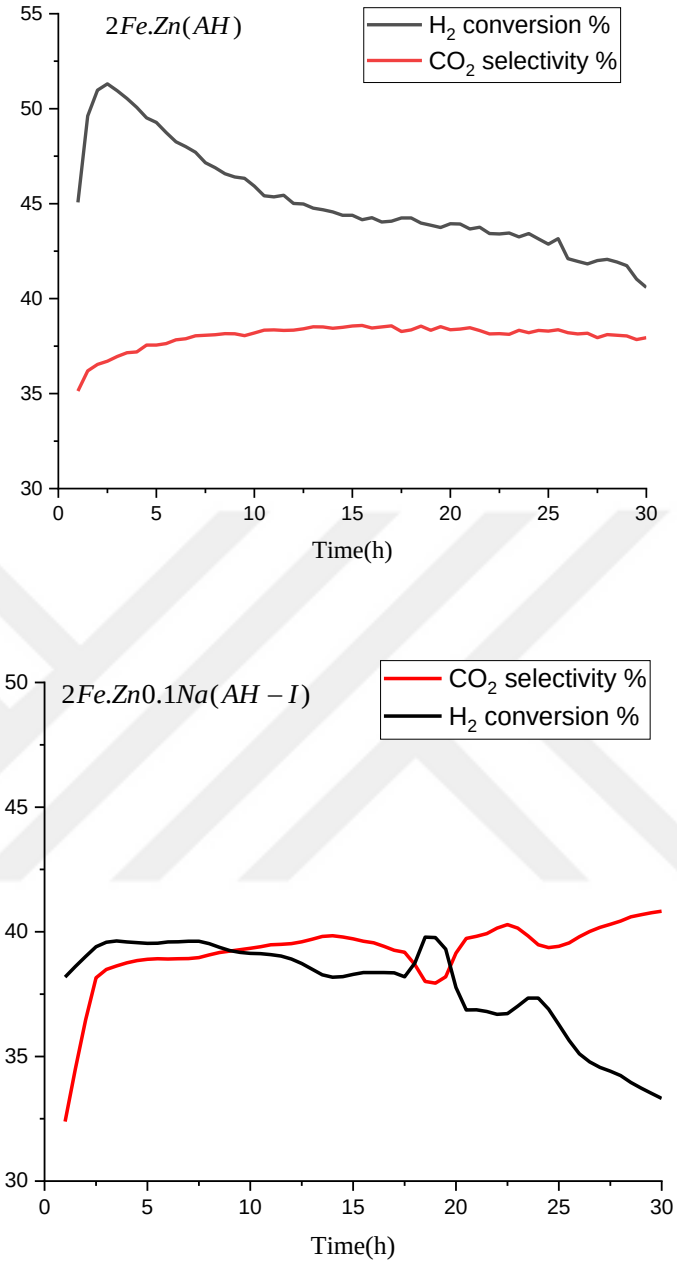

Figure D.1 : H_2 conversion and CO_2 selectivity of Na-promoted bulk catalysts.

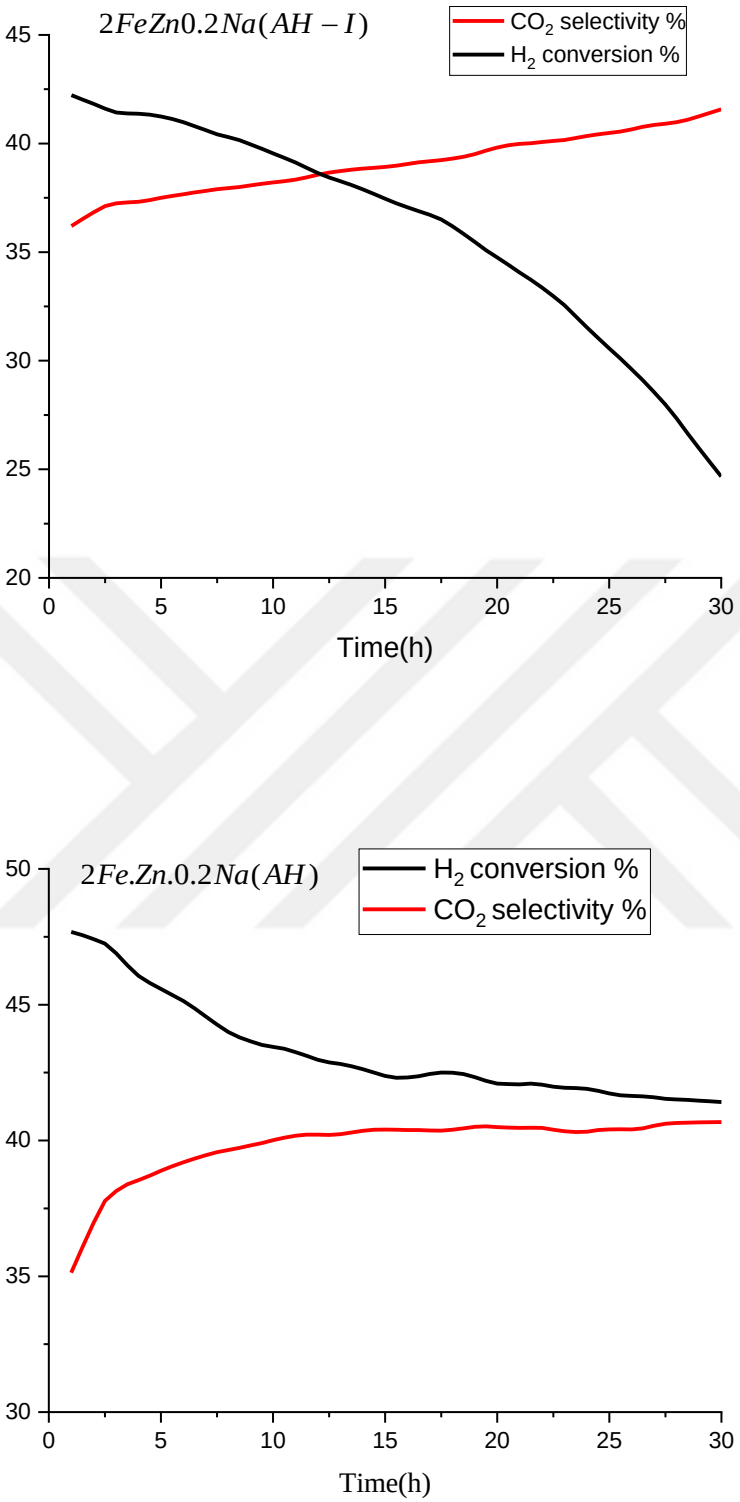

Figure D.1 (continued) : H_2 conversion and CO_2 selectivity of Na-promoted bulk catalysts.

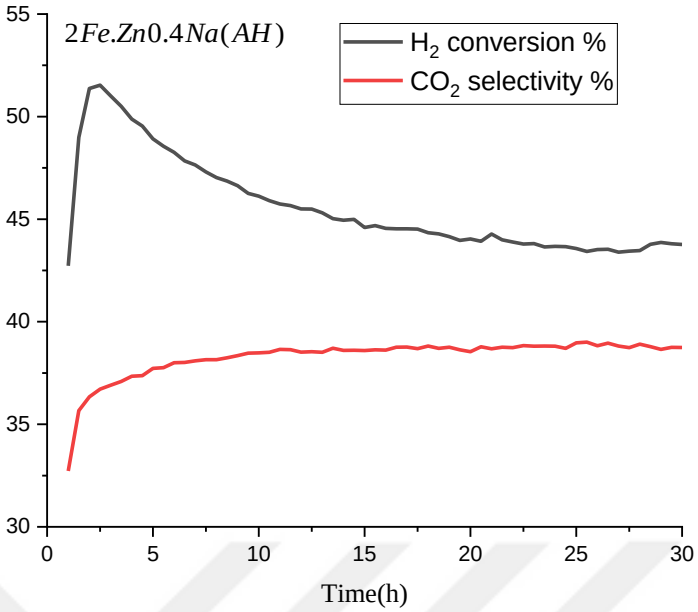

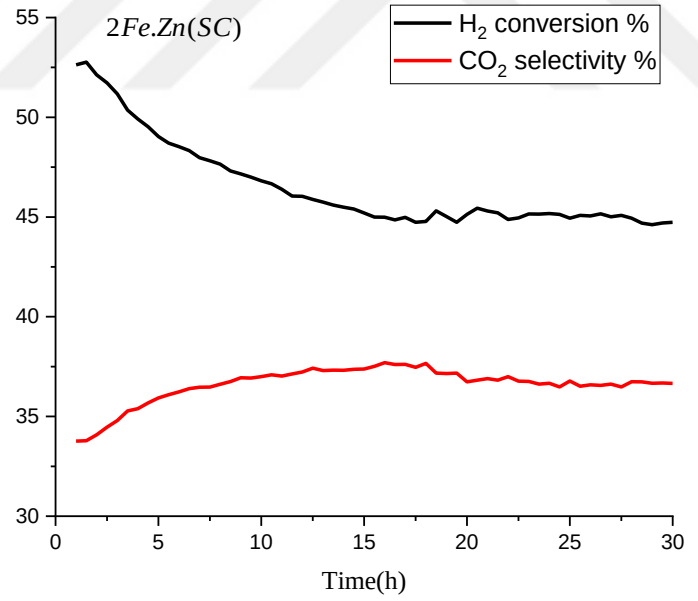

Figure D.1 (continued) : H_2 conversion and CO_2 selectivity of Na-promoted bulk catalysts.

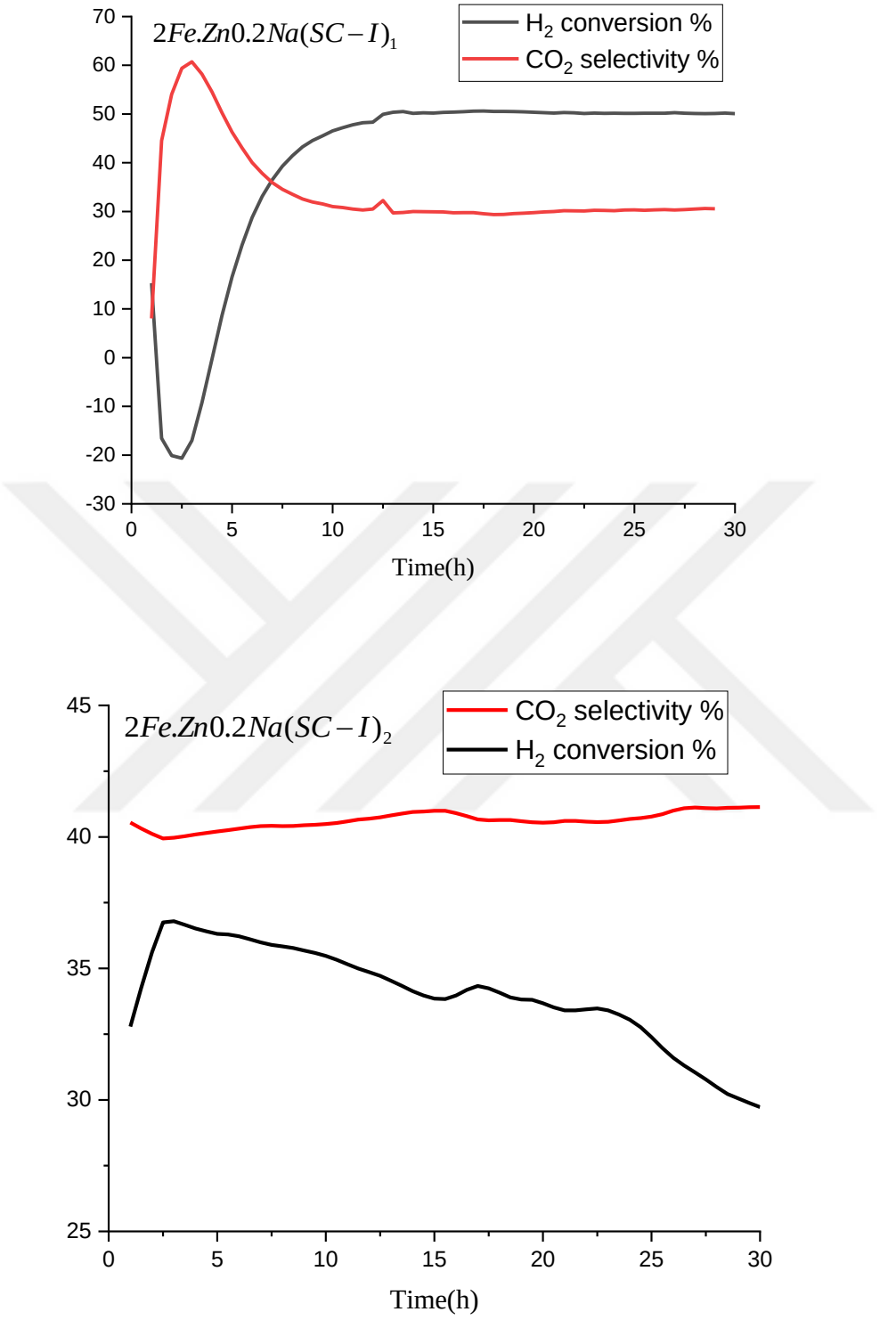

Figure D.1 (continued) : H_2 conversion and CO_2 selectivity of Na-promoted bulk catalysts.

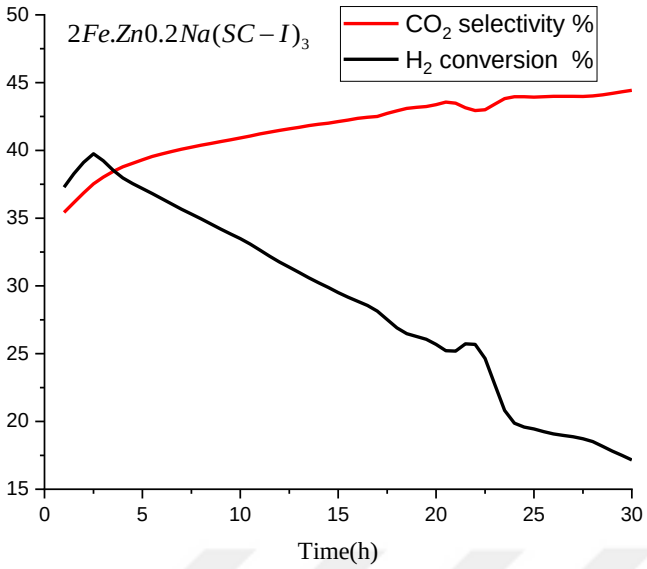

Figure D.1 (continued) : H_2 conversion and CO_2 selectivity of Na-promoted bulk catalysts.

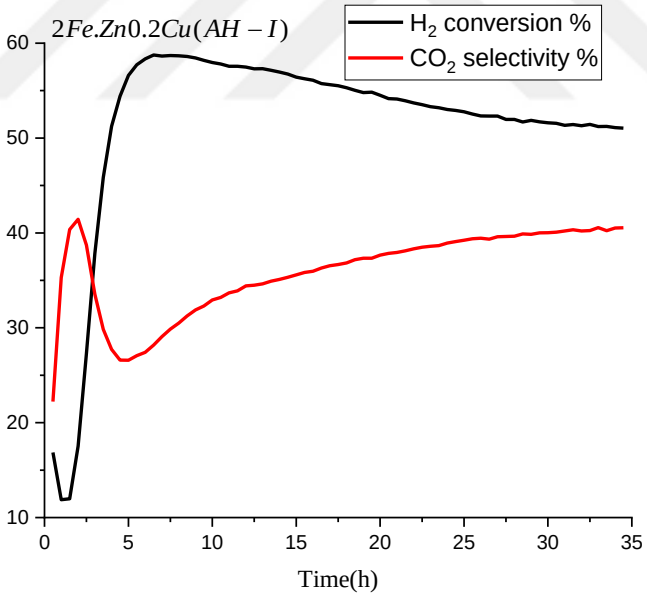

Figure D.2 : H_2 conversion and CO_2 selectivity of Cu-and K-promoted bulk catalysts.

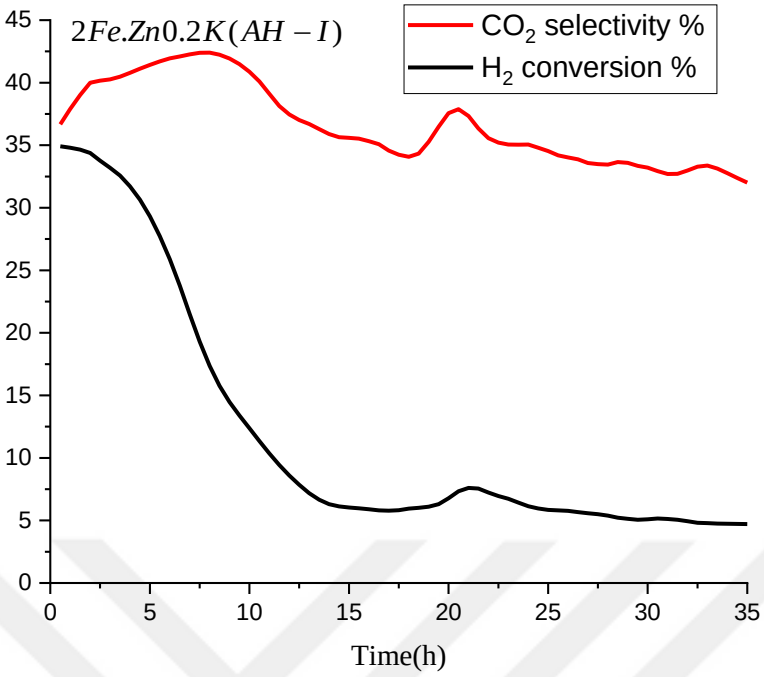

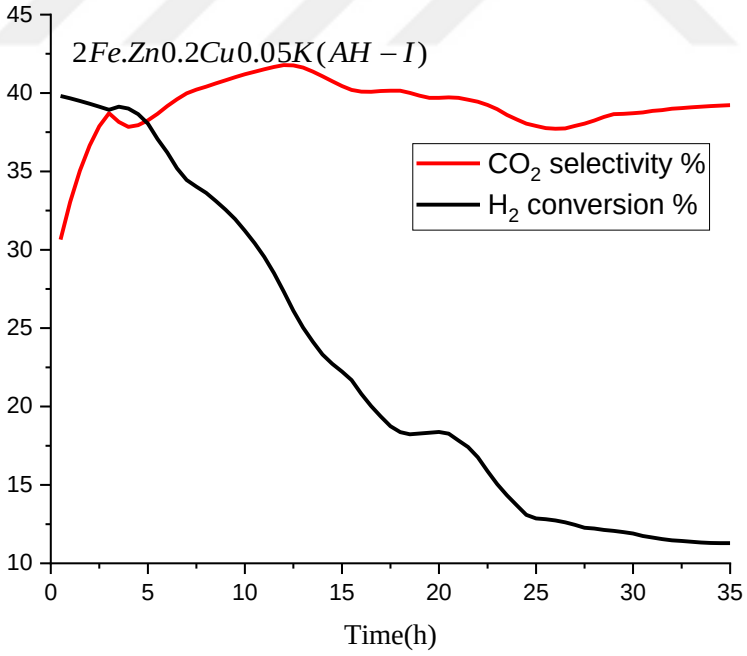

Figure D.2 (continued) : H_2 conversion and CO_2 selectivity of Cu-and K-promoted bulk catalysts

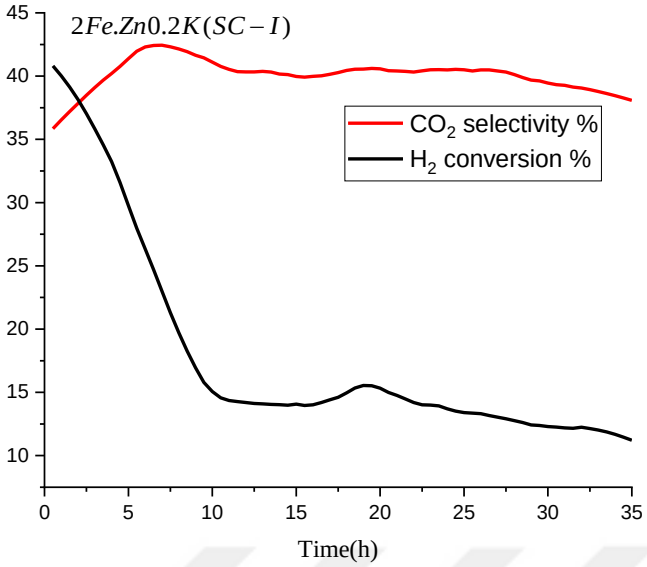

Figure D.2 (continued) : H_2 conversion and CO_2 selectivity of Cu-and K-promoted bulk catalysts

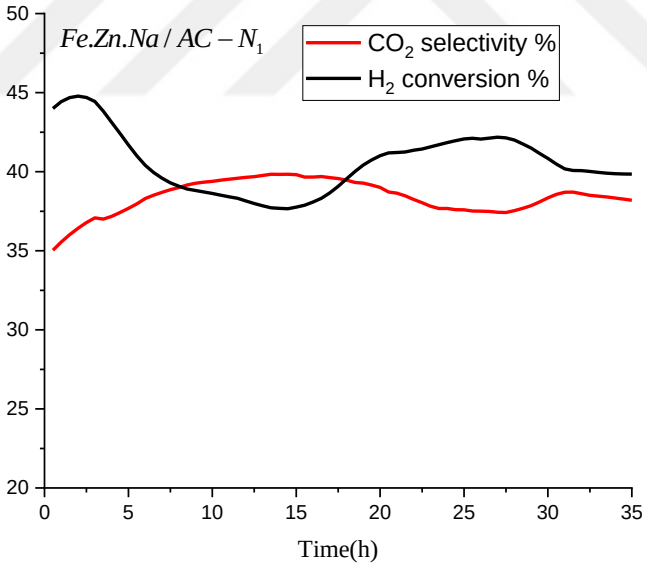

Figure D.3 : H_2 conversion and CO_2 selectivity of AC and N-doped AC supported catalysts.

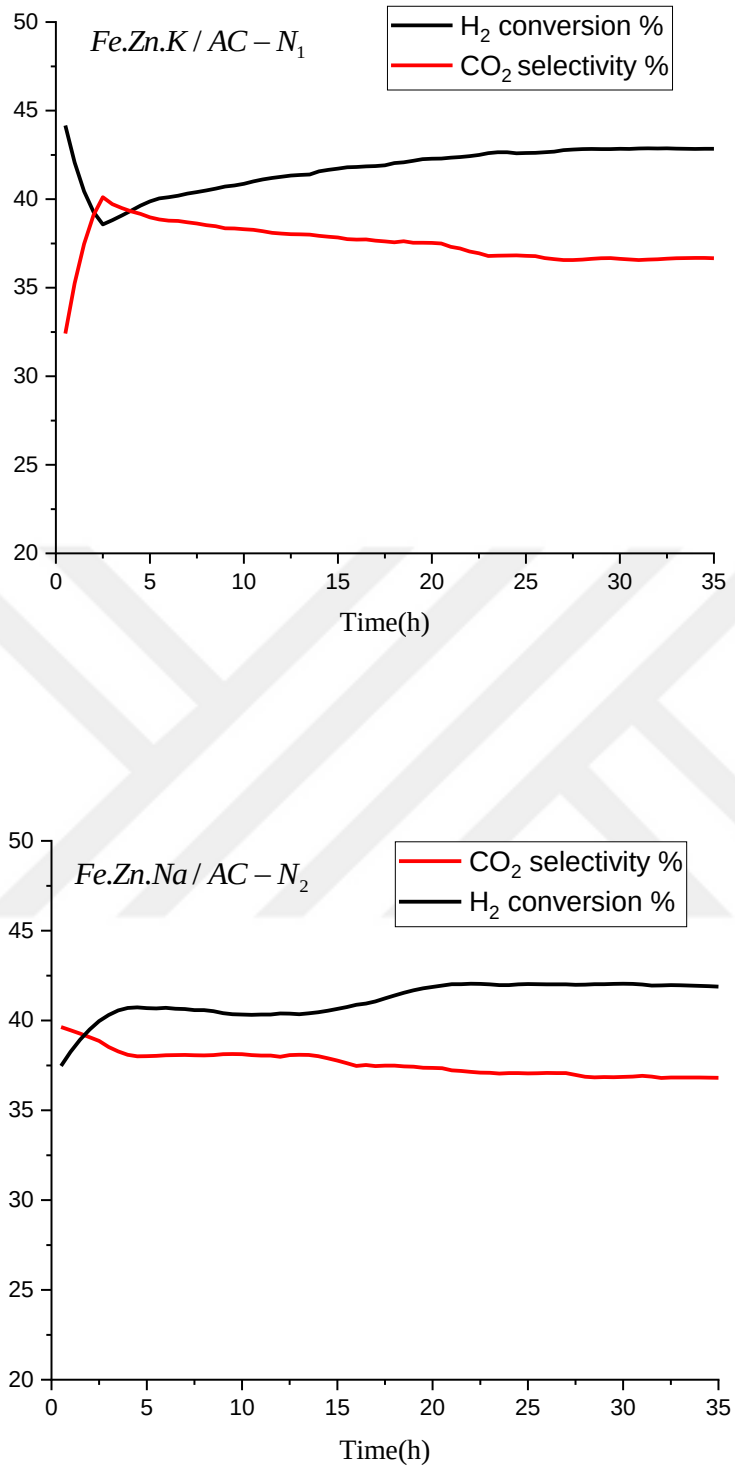

Figure D.3 (continued) : H_2 conversion and CO_2 selectivity of AC and N-doped AC supported catalysts.

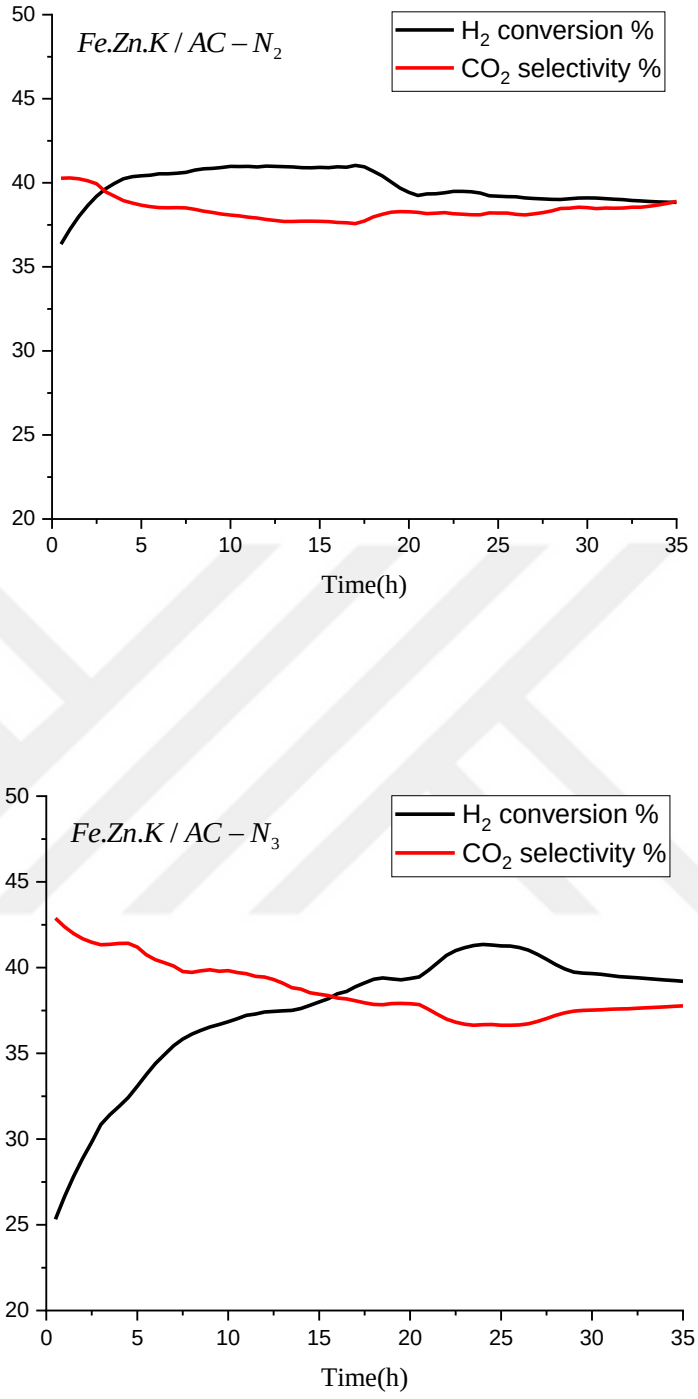

Figure D.3 (continued) : H_2 conversion and CO_2 selectivity of AC and N-doped AC supported catalysts.

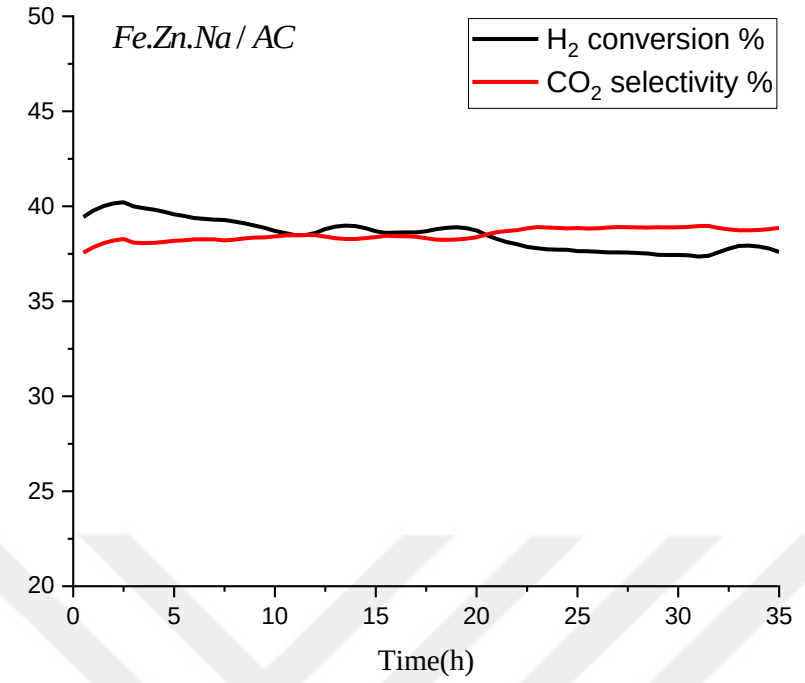

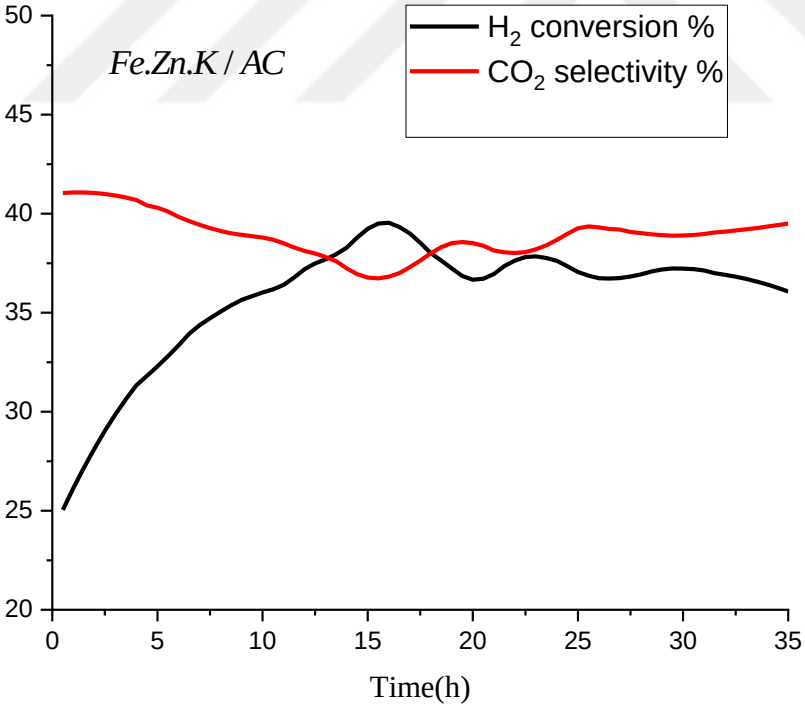

Figure D.3 (continued) : H_2 conversion and CO_2 selectivity of AC and N-doped AC supported catalysts.

CURRICULUM VITAE

Name Surname **:** Yasemin FATİH AGHDAEI (Yasaman FALLAHI)

EDUCATION:

- **B.Sc.** **:** 2006, University of Tehran, College of Engineering, Chemical Engineering Department
- **M.Sc.** **:** 2010, Shahid Beheshti University, College of Engineering, Nuclear Engineering Department
- **M.Sc.** **:** 2016, Istanbul Technical University, Faculty of Chemical and Metallurgical Engineering, Chemical Engineering Department

PUBLICATIONS, PRESENTATIONS AND PATENTS ON THE THESIS:

- **Fatih Y.,** Burgun U., Sarioglan A., Atakul H. 2023: "Effect of Sodium Incorporation into Fe-Zn Catalyst for Fischer- Tropsch Synthesis to Light Olefins" published by *"Molecular catalysis"*, 15 January 2023, https://doi.org/10.1016/j.mcat.2022.112866

OTHER PUBLICATIONS, PRESENTATIONS AND PATENTS:

- **Fallahi Y.,** Aydin A A., Gur M., Okutan H. 2018: An investigation of the pollution risk of residues from a lab-scale Underground Coal Gasification of Malkara (Turkey) lignite" published by "*International Journal of Environmental Science and Technology*", May 2018.

Conferences:

- **Fallahi Y.,** Aydin A A., Gur M., Okutan H. 2017: "Laboratory Studies on Pollution Risk of Ex-Situ Gasification of Malkara Lignite" in INERMA (International Energy Raw Materials and Energy Summit), September 2017.
- Pınar Şakoğlu, **Yasaman Fallahi,** Osman Okur, Alper Sarıoğlan, Hüsnü Atakül, Gamze Gümüşlü Gür. 2022. "Fischer-Tropsch to olefin reaction over carbon supported iron catalysts: Investigation of urea doped activated carbon in the presence of sodium and zinc promoters" in "30th The European Biomass Conference and Exhibition (EUBCE-2022), May 9-12.

- Yavuz AYDEMİR, **Yasaman FALLAHI,** Utku BURGUN, Alper SARIOĞLAN, Gamze GÜMÜŞLÜ GÜR, Sogand AGHAMOHAMMADI 2022, “Fabrication of Enhanced Core-Shell Co-ZIF-67@MOx (M = Zn, Mn and K) Nanocomposites via Intermediate Pyrolysis and Plasma Treatment for Fischer Tropsch Synthesis” in “International Graduate Research Symposium - IGRS'22”, Jun 1-3 , Istanbul, Turkey.